Cairo Air Improvement Project

Air Quality Monitoring Component

Baseline Year Monitoring Report

Volume One

Results and Analysis of

Baseline Year Particulate Matter and Lead Measurements for the Period 1 October 1998 to 30 September 1999

Chemonics International, Inc.

USAID/Egypt, Office of Environment

USAID Contract No. 263-C-00-97-00090-00

June 2000

This report was prepared by:

James E. Howes, AQM Manager, CAIP

Mounir W. Labib, Ph.D., AQM Specialist, CAIP

Noha Samaha, Monitoring Systems Supervisor, CAIP

Marc L. Serre, Ph.D., Statistical & Modeling Analysis Specialist, CH2M HILL

Table of Contents

Page No.

Acronyms and Abbreviations iv

List of Figures v

List of Tables vii

Executive Summary

Chapter 1: Introduction

Chapter 2: Background and Objectives

2-1 CAIP Air Quality Monitoring Program Objectives 2-1

2-2 Monitoring System Design & Implementation Background 2-1

2-3 Egyptian Regulatory Background 2-3

Chapter 3: Monitoring Procedures

3.1 Site Location, Classification, and Sampling Equipment 3-1

3.2 Sampling Procedures 3-7

3.3 Gravimetric and Lead Analysis 3-7

3.4 Quality Control Procedures 3-10

3.4.1 AirMetrics™ Sampler Flow Rate Checks 3-10

3.4.2 Filter Blank Samples 3-10

3.4.3 FAAS Calibration Checks 3-13

3.4.4 Duplicate Mass and Lead Determinations 3-14

3.4.5 Matrix Spiked Samples 3-15

3.4.6 Data Recovery 3-15

3.4.7 Collocated Sampler Data 3-16

3.4.8 Data Validation 3-17

3.4.9 AirMetrics/BGI Sampling Data Comparison 3-18

Chapter 4: Summary of Data

4.1 Ambient Particulate Matter Data 4-1

4.2 Ambient Lead Data 4-14

4.3 Source Site Measurements 4-22

4.4 Meteorological Measurements 4-27

Chapter 5: Data Analysis and Characterization

5.1 Data Analysis Methodology 5-2

5.1.1 The Bayesian Maximum Entropy Framework 5-2

5.1.2 Representation of the Raw Measurements by Means of Hard and Soft Data 5-3

5.1.3 PM and Lead Data Distribution & Transformation 5-3

5.1.4 De-trending of Large-scale Spatial and Temporal Fluctuations 5-4

5.1.5 Modeling the Space/Time Variability by Means of the Covariance Function 5-5

5.1.6 BME Estimation and Confidence Intervals 5-8

5.2 Particulate Matter 5-9

5.2.1 Temporal Characteristics 5-9

5.2.2 Spatial Characteristics 5-15

5.3 Lead 5-26

5.3.1 Temporal Characteristics 5-26

5.3.2 Spatial Characteristics 5-29

Chapter 6: Conclusions

6.1 Particulate Matter 6-1

6.2 Lead 6-2

6.3 Quality of Data 6-2

6.4 Space/Time Mapping using the BME Estimation Method 6-3

6.5 PM and Lead Monitoring Network Optimization 6-3

References

Acronyms and Abbreviations

ºC	Degrees Centigrade
AQM	Air Quality Monitoring
BME	Bayesian Maximum Entropy
CAIP	Cairo Air Improvement Project
CAPMAS	Central Agency for Public Mobilization and Statistics
CCB	Continuing Calibration Blank
CCC	Continuing Calibration Checks
CCS	Continuing Calibration Standard
CNG	Compressed Natural Gas
EEAA	Egyptian Environmental Affairs Agency
EIMP	Environmental Information And Monitoring Program
FAAS	Flame Atomic Absorption Spectrometry
FRM	Federal Reference Method
GIS	Geographical Information Systems
GOE	Government of Egypt
km	Kilometers
lpm	Liters per Minute
m	Meters
µg	Micrograms
µm	Micrometers
MDL	Minimum Detection Limit
NIST	U.S. National Institute of Standards and Technology
Pb	Lead
Pb10	Lead in PM that is equal to or less than 2.5 in aerodynamic diameter
PM	Particulate Matter
PM10	Particulate matter equal to or less than 10 µm in aerodynamic diameter
PM2.5	Particulate matter equal to or less than 2.5 µm in aerodynamic diameter
QC	Quality Control
RH	Relative Humidity
USEPA	United States Environmental Protection Agency

List of Figures

Figure No.	Title	Page No.
3-1	CAIP Monitoring Site Locations	3-2
3-2	10th of Ramadan Residential Site	3-5
3-3	Gomhuriya Street Traffic Site	3-5
3-4	Tebbin South Industrial Site	3-6
3-5	Qaha Background Site	3-6
3-6	Typical Sampler Installation	3-8
3-7	Collocated Sampler Installation	3-8
3-8	Gravimetric Analysis of Filters	3-9
3-9	Lead Analysis by Flame Atomic Absorption Spectrometry	3-9
3-10	Comparison of Measurements with AirMetrics and BGI PM10 Samplers	3-19
4-1	Average PM2.5 and PM10 Concentrations for Sampling Events during Baseline Year	4-4
4-2	Maximum PM10 Concentrations for Sampling Events during Baseline Year	4-5
4-3	Baseline Year Average PM10 Concentrations at Ambient Monitoring Sites	4-7
4-4	Annual Average PM10 Concentrations for Site Classifications	4-10
4-5	Average PM2.5/PM10 Ratios for Sampling Events during Baseline Year	4-11
4-6	Baseline Year Average Pb10 Concentrations at Ambient Monitoring Sites	4-16
4-7	Maximum Lead Concentrations for Sampling Events during Baseline Year	4-17
4-8	Annual Average Lead Concentration for Site Classifications	4-18
4-9	Average Pb2.5/Pb10 Ratios for Sampling Events during Baseline Year	4-19
4-10	Average Monthly PM10 Concentration at Source Site LSA	4-24
4-11	Average Monthly PM10 Concentrations at Source Site LSB	4-25
4-12	Average Monthly Lead Concentrations at Source Site LSA	4-26
4-13	Average Monthly Lead Concentrations at Source Site LSB	4-27
4-14	Windroses of Annual Average Wind Conditions	4-28
5-1	Distribution of Daily Concentrations for PM10 and Pb10	5-4

Figure No.	Title	Page No.
5-2	Spatial and Temporal Covariance for the PM and Pb as a Function of Distance (km) and Time Lag (t)	5-6
5-3	Typical BME Posterior pdf Showing the Probabilistic Distribution of an Estimated Variable (Xk) with Intervals Shown for Different Confidence Levels	5-9
5-4(a)	Estimated Daily PM10 Concentration Profile for CAIP Site #6 in Maadi/Degla	5-10
5-4(b)	Estimated Daily PM2.5 Concentration Profile for CAIP Site #6 in Maadi/Degla	5-10
5-5(a)	Plot of Average of the Logarithm of PM10 Measurements during the Baseline Year	5-12
5-5(b)	Plot of Average of the Logarithm of PM2.5 Measurements during the Baseline Year	5-12
5-6	Plot of Different Percentiles in the Temporal Variations in PM10 Concentration	5-13
5-7	Median PM10 concentration as a function of the day of the week	5-14
5-8	Estimated PM10 Concentrations on 7 October 1998	5-16
5-9	Estimated PM10 Concentrations for 13 October 1988	5-17
5-10	Estimated PM10 Concentrations 28 July 1999	5-18
5-11	Estimated PM2.5 Concentrations on 13 October 1998	5-20
5-12	68% Confidence Interval for PM10 Concentration on 13 October 1998	5-21
5-13	Estimated Average PM10 Concentrations for Baseline Year	5-23
5-14	Estimated Average PM2.5 Concentrations during Baseline Year	5-24
5-15	Estimated PM2.5/PM10 Average Ratio During Baseline Year	5-25
5-16	Estimated Lead Profile for Monitoring Site #6 in Maadi/Degla	5-26
5-17	Temporal Plot of the Average of Logarithm of Lead over Greater Cairo	5-27
5-18	Temporal Plot of Different Percentiles for Lead Concentration	5-28
5-19	Median Lead & PM10 Concentrations over Days of the Week	5-29
5-20	Estimated Pb10 Concentrations on 7 October 1998	5-30
5-21	Estimated Pb10 Concentrations for 13 October 1998	5-31
5-22	Estimated Pb10 Concentrations on 29 January 1999	5-32
5-23	Map of the 68% Confidence Interval for Lead Concentrations on 13 October 1998	5-35
5-24	Estimated Average Lead Concentrations for Baseline Year	5-36
5-25	Estimated Law 4/1994 Lead Limit Non-attainment Areas	5-37

List of Tables

Table No.	Title	Page No.
2–1	Law 4/1994 Limits for PM and Pb	2-3
3-1	CAIP Air Quality Monitoring Sites	3-3
3-2	Distribution of CAIP Sites by Land-use Classification	3-4
3-3	QC Procedures Summary	3-11
3-4	AirMetrics™ Sampler Flow Check Summary	3-12
3-5	Filter Blank Gravimetric Data Summary	3-12
3-6	Summary of Filter Blank Lead Data	3-13
3-7	Duplicate Measurements Summary	3-14
3-8	Monitoring Data Recovery Summary	3-16
3-9	Collocated Sampler Results Summary	3-17
4-1	Monthly and Annual Statistical Summary of PM2.5 Measurements at CAIP Sites	4-2
4-2	Monthly and Annual Statistical Summary of PM10 Measurements at CAIP Sites	4-3
4-3	PM10 Monitoring Data Statistics	4-8
4-4	Monthly and Annual Statistics on PM2.5 Lead Measurements at CAIP Monitoring Sites	4-12
4-5	Monthly and Annual Statistics on PM10 Lead Measurements at CAIP Monitoring Sites	4-13
4-6	Lead Monitoring Data Statistics	4-21
5-1	Spatial and Temporal Range Parameters for Small- and Large- scale Fluctuations	5-7
5-2	Variance Parameters for the Small-scale Fluctuation C_{01} and the Large-scale Fluctuation C_{02}	5-7
5-3	Lead Exposure Estimation	5-39

Executive Summary

The Cairo Air Improvement Project (CAIP) has established a 36-station network to monitor particulate matter and lead levels in the Greater Cairo area. The network began formal operation on October 1, 1998 and completed collection of monitoring data over a baseline period of one (1) year. The objective the first year of CAIP's air quality monitoring (AQM) program was to establish baseline levels and characteristics of particulate matter (PM) and lead in Cairo air. Baseline levels, derived from monitoring results and data analysis, are important to provide a basis for evaluating future trends in air quality that will result from air pollution abatement measures such as those implemented by CAIP and the Egyptian Environmental Affairs Agency (EEAA).

This report provides a complete compilation of the monitoring data collected during the baseline year and presents results of a unique analysis that uses the fixed site measurements to predict the spatial and temporal trends in particulate matter and lead levels. Brief summaries of the monitoring results, the analysis of the monitoring data, and the conclusions drawn, are provided below.

Particulate Matter (PM)

PM2.5 and PM10[1] concentrations were persistently high throughout the baseline year with maximum levels occurring during the period of October–December. Typically, high PM levels are not localized; instead they extend over a large area. The magnitude of the affected area rules out point source emissions as the sole cause of high PM levels. Rather, it is believed that a background PM level created by meteorological conditions plays an important role in determining PM levels in Cairo. The highest daily and annual average PM10 levels[2] (822 and 300 $\mu g/m^3$, respectively) were recorded in the Shoubra El-Kheima, Tebbin, and El-Massara areas. The high PM levels in these areas result from industrial emissions in addition to the background PM level.

[1] Particulate matter size fractions. For details, see description Chap. 2, Sec. 2.2.

[2] Measured in micrograms per cubic meter, abbreviated as $\mu g/m^3$.

The lowest annual average PM2.5 and PM10 levels (approximately 120μg/m³) were recorded at the outlying cities of 6th of October and 10th of Ramadan and at the Belbeis background site. The annual average PM10 level recorded in Heliopolis (144 μg/m³) was the lowest for a contiguous area in Cairo. However, even at the sites with the lowest PM levels, PM10 concentrations below the current 24-hour limit of 70 μg/m³ defined in the Egyptian Environmental Law No. 4/1994 (thereinafter referred to as Law 4/1994) were recorded only 32 times out of a total of 1769 measurements.

Lead (Pb)

The annual average lead levels at 19 of the CAIP monitoring sites were below the Law 4/1994 limit of 1 μg/m³. The Law 4/1994 limit was exceeded at 15 sites. The highest lead levels were recorded in Shoubra El-Kheima, where several lead smelters are located. At 2 stations in this area, the annual average lead concentration was approximately 25 times the Law 4/1994 limit. During the baseline year, 24-hour lead levels greater than 50 μg/m³ were recorded 11 times in Shoubra El-Kheima. The highest 24-hour lead concentration recorded during the baseline year (184 μg/m³) was at a site located in Shoubra El-Kheima.

The method used to analyze the baseline year data permitted estimation of the areas in Cairo where lead levels exceed the Law 4/1994 limit. The zones of non-attainment encompass the areas of Shoubra El-Kheima and Tebbin where lead smelters are located. From an analysis that combines geographical information systems (GIS), estimated non-attainment areas, and CAPMAS[1] data, it is estimated that nearly 4 million Cairo residents may be exposed to lead levels in excess of the Law 4/1994 limit. The estimate is based on a rudimentary analysis; however, the results indicate the severity of the lead exposure problem and the urgent need to implement abatement measures.

Summary of Conclusions

- The distribution of PM is characterized by large-scale spatial and temporal structures, which are probably created, in part, by meteorological conditions. Due to the arid climate, there is a persistent background PM level in Cairo that will probably always prevent reducing PM10 levels below the 24-hour limit of 70 mg/m³ defined in Law 4/1994.
- The distribution of lead is characterized by relatively small-scale spatial and temporal structures. The scale indicates that lead enters the atmosphere primarily from anthropogenic point sources and that the major impact of the

[1] Central Agency for Public Mobilization and Statistics

lead emissions is in the locality of the source. Using the Bayesian Maximum Entropy (BME) method, it was possible to estimate areas where the lead levels exceed the Law 4/1994 limit. The major areas of non-attainment are centered in Shoubra El-Kheima in the North and in Tebbin in the South. The sizes of non-attainment zones are approximately 150 km² in Shoubra El-Kheima and 80 km² in Tebbin. It is estimated that nearly 4 million people reside in these non-attainment areas.

- The intensive quality control (QC) effort applied to the CAIP monitoring program ensured that high quality monitoring data was collected. It also provided an assessment of the accuracy and precision of the monitoring data.
- The BME methodology used to analyze the baseline year data has proven to be a powerful tool to predict spatial and temporal variations in pollutant concentrations. BME expands the data collected at fixed sites into maps showing the spatial distribution of pollutants.
- Results of the baseline year study indicate that optimization of the monitoring network can be performed to increase operating efficiency and reduce costs. The optimization can be achieved without compromising the usefulness of the monitoring data for policy and regulatory decisions and for trends analysis.

The baseline year report is contained in four (4) separately bound volumes. Volume I presents the results and analysis of the particulate matter and lead monitoring conducted during the baseline year. Volume II provides tables listing the results of particulate matter, lead, and meteorological measurements performed during the baseline year. Volume III presents the results of quality control activities incorporated into CAIP's air quality monitoring program. Volume IV provides a complete description of each site including site photographs and a map showing site's exact location and surrounding sources of emissions.

Chapter One
Introduction

The dramatic increase in population and industrialization in Greater Cairo[1] over the past 10 years has been accompanied by a significant deterioration in air quality. Some indications of the extent and magnitude of the air pollution problem have been obtained in previous air monitoring programs [1–7][2]. Pollutants that have been identified in the previous studies as major health risks include particulate matter, sulfur dioxide, carbon monoxide, and lead. Unfortunately, previous work involved only short-term monitoring events. This provides "snapshots" of air quality problems, but does not provide data to characterize the temporal and spatial trends in air quality. Furthermore, results of these previous studies do not provide EEAA with sufficient data to make important policy and regulatory decisions necessary to achieve an improvement of air quality in Cairo.

During the past two years, two programs have been initiated to routinely collect air quality monitoring data on a continual basis, the Environmental Information and Monitoring Program (EIMP) and the Cairo Air Improvement Project (CAIP). EIMP has established a nation-wide monitoring network consisting of 40 air quality monitoring stations. Fourteen (14) of the EIMP sites are located in Greater Cairo. CAIP has established a network of 34 stations in the Greater Cairo area to monitor ambient air levels of particulate matter (PM) and lead (Pb). The CAIP monitoring effort is intended to provide data to assess the efficacy of CAIP and other initiatives to improve the air quality in Cairo. These initiatives include: implementation of a vehicle emission testing and tune-up program, introduction of CNG-fueled buses for public transportation, and abatement of lead by secondary lead smelter design improvements and lead smelter relocation.

Formal operation of the CAIP air quality monitoring network began on 1 October 1998. One full year of monitoring data was collected as of 30 September 1999. The period from 1 October 1998 through 30 September 1999 is considered a

[1] Greater Cairo comprises the governorates of Cairo, Giza, and Qalioubiya
[2] List of references is available at the end of Volume 1 of this report.

baseline year. The baseline year monitoring data will serve as a "benchmark" against which future monitoring data can be compared to assess air quality trends.

This report provides the CAIP air quality monitoring results obtained during the baseline year. A unique analysis of the monitoring results is presented that characterizes spatial and temporal trends during the baseline year. It is intended that procedures employed in analyzing the CAIP baseline year data and results obtained from the analysis will form the foundation for future annual assessments of air quality trends.

The baseline year report contains four separately bound volumes. Volume I presents the results and analysis of the PM and Pb monitoring conducted during the baseline year. Volume II contains tables listing the results of PM, lead, and meteorological measurements performed during the baseline year. Volume III presents the results of quality control activities incorporated into CAIP's AQM program. Volume IV provides a complete description of each site including site photographs and a map showing site's exact location and surrounding sources of emissions.

Chapter Two
Background and Objectives

This chapter provides a brief overview of the AQM program objectives, the monitoring system design, and the regulatory background.

2-1 CAIP Air Quality Monitoring Program Objectives

The primary objectives of CAIP's Air Quality Monitoring (AQM) Program are:

- Implementation of a monitoring system to routinely measure airborne levels of PM and lead in Greater Cairo.
- Establishment of the baseline characteristics of PM and lead in Cairo air.
- Institutionalizing the monitoring system in order to provide EEAA with high quality PM and lead monitoring data to support policy-making decisions, regulatory action, and future air quality trends analysis.

2-2 Monitoring System Design and Implementation Background

The design of the CAIP monitoring system and selection of equipment to collect the baseline year monitoring data were based on the following considerations:

- Rapid deployment and start-up of the monitoring operations to meet CAIP and EEAA milestones for establishing PM and lead baselines.
- Implementation of monitoring at numerous locations to provide detailed data on the spatial distribution of PM and lead levels and to identify "hot spots" in the Greater Cairo area.
- Providing measurements of fine particulate matter, namely PM2.5 and PM10, which are the size fractions that have the most pronounced adverse effect on human health.

- Fulfillment of the monitoring objectives as economically as possible.

The AirMetrics™ samplers selected to collect the baseline year PM and lead data were readily deployed and establishment of 36 sites was practical because of the relatively low cost of the samplers. After a three-month period for operators' training and equipment "shake-down", formal collection of the baseline year data commenced on 1 October 1998. The 36 sites provided baseline year data with the spatial distribution data necessary to identify areas within Cairo where high levels of PM and lead "hot spots" persist.

PM in the ambient air exists as a distribution of particles of different sizes, ranging from tens of micrometers (μm) to sub-micrometers in diameter. Larger particles do not pose a severe a health risk since gravitational forces cause sedimentation near the point of origin. Furthermore, human exposure through inhalation is minimized since the larger PM is removed by the nasal system. However, fine particles, smaller than 10 μm in aerodynamic diameter, remain suspended in the air and can be transported over relatively long distances. PM in the 0–10 μm diameter size range also constitutes a severe health threat since the fine particles are more readily taken into the body through inhalation. Recent research indicates that PM less than 2.5 μm in aerodynamic diameter poses the most significant health hazard since this material penetrates to the deepest regions of the lungs and may be retained in the lungs for prolonged periods of time. The toxic effects of the PM results from release of species contained in the particles into the body.

Depending on the origin, ambient PM may include pollutants such as sulfates, nitrates, fluorides, trace metals (Pb, Cd, Zn, etc.), polycyclic aromatic hydrocarbons, and a variety of other toxic inorganic and organic species. Because of the relationship between particle size and its impact on the human health, more recent methods have focused on the measurement of fine particles. The latest methods for measuring ambient levels of fine particles (PM2.5 and PM10) are employed in CAIP's AQM Program so that data most relevant to human health effects are obtained.

In order to assess the success of CAIP and other air pollution abatement initiatives, it is first necessary to establish a baseline, i.e. to thoroughly characterize the PM and lead levels before the interventions are implemented. In order to account for seasonal, meteorological, and source emission variations, it is necessary to collect at least one (1) year of monitoring data to establish an accurate pollutant baseline. If baseline data are collected for shorter periods, it is impossible to discern the cause of observed variations in ambient pollutant levels.

Comparison between the baseline data and monitoring data collected during subsequent years provides the means to quantitatively evaluate the efficacy of CAIP's initiatives as well as other mitigation measures implemented by EEAA.

It should be understood that the first phases of CAIP's programs are not likely to produce a widespread, measurable effect on air quality. Only after their expansion into full-scale programs by the Government of Egypt (GOE) will the monitoring effort likely be able to quantify the improvement in air quality from CAIP's initiatives. Since full-scale implementation of these initiatives will require several years, it is necessary to sustain the air quality monitoring effort for at least a comparable time period.

2-3 Egyptian Regulatory Background

In 1994, the GOE promulgated a Law for the Environment. The provisions of this Law became effective in March 1998. Law No. 4 for the Year 1994 specifies maximum limits for pollutants in ambient (outdoor) air, workplace atmospheres, and source emissions. The limits established by Law 4/1994 for PM10 and lead are shown in Table 2-1.

Table 2–1: Law 4/1994 Limits for PM and Pb

Pollutant	Environment	Maximum Limit	Averaging Period
PM10	Ambient Air	70 μg/m³	24 hours
	Source Emissions	None	—
Lead	Ambient Air	1 μg/m³	1 year
	Source Emissions	20 μg/m³	—

Law 4/1994 does not specify limits for PM2.5 mass concentration or the limits for lead in the PM2.5 or PM10 size fractions of ambient particulate matter. Furthermore, the Law specifies limits for only the averaging periods shown in Table 2-1. The measurement of lead in the PM10 size fraction is a surrogate for total lead. Thus, compliance to Law 4/1994 is determined from the lead concentration in the PM10 size fraction.

Chapter Three
Monitoring Procedures

In this chapter, the location and land-use classification of the CAIP monitoring sites are identified and the equipment and procedures employed to perform the PM and lead monitoring are described. The QC activities implemented to ensure the accuracy and precision of the monitoring data are described and summaries of the results of these QC activities provided. Several pictures have been included to illustrate typical monitoring equipment installations and the characteristics of areas around sites of different land-use classification.

3.1 Site Location, Classification, and Sampling Equipment

The AQM network established by CAIP comprises 36 sites located throughout Greater Cairo as shown in Figure 3-1. The monitoring stations are distributed within an area bordered by Qaha and Belbeis in the north, Tebbin in the south, the 10th of Ramadan City in the east, and the 6th of October City in the west. The identification, location, and classification of the monitoring sites and the sampling equipment located at each monitoring site are summarized in Table 3-1.

The locations of thirty-four (34) sites were selected to provide PM and lead measurements in the ambient air environment, i.e., in areas where people reside, work, and perform other activities associated with their daily lives. These ambient monitoring sites are further classified according to the predominant land-use surrounding the site into: residential, traffic, industrial, background, and mixed. Sites designated as "mixed" are those surrounded by a combination of residential/industrial or residential/commercial land-use areas, or by residential land-use areas with significant impact from mobile sources, i.e., traffic.

The remaining 2 of the 36 sites are designated as "source sites". They are located within approximately 250 m of buildings that house secondary lead smelting furnaces and are nominally downwind of the lead smelters. The source sites provide a measure of fugitive emissions from lead processing operations. The distribution of sites by land-use classification is shown in Table 3-2.

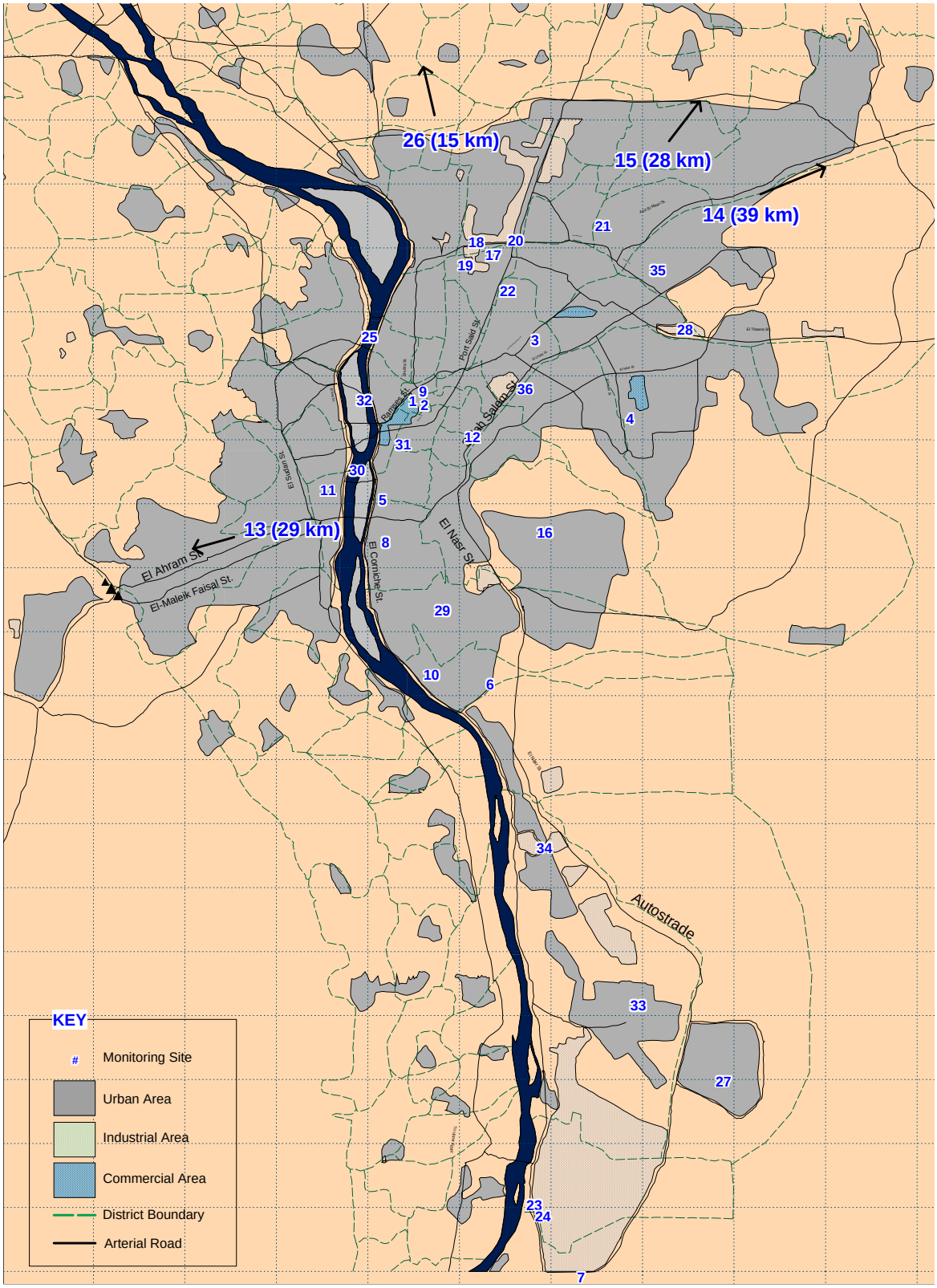

Figure 3-1: CAIP Monitoring Site Locations

Photographs in Figures 3-2 through 3-5 show areas around typical residential, traffic, industrial, and background sites.

Table 3-1: CAIP Air Quality Monitoring Sites

Site No.	Site Code	Site Location				Site Classification	Monitoring Equipment [b]		
		Governorate	District	UTM N	UTM E		PM2.5	PM10	Met
1 [a]	EQS	Cairo	El-Qolaly Sq.	3326603	0330594	Traffic	X	X	
2	GEM	Cairo	El-Gomhuriya St.	3326512	0330945	Traffic	X	X	
3	MET	Cairo	El-Wayli	3328951	0335190	Mixed	X	X	
4	NRC	Cairo	Nasr City	3325866	0338816	Residential	X	X	
5 [a]	FAK	Cairo	Fum Al-Khaleej	3322702	0329358	Traffic		X	
6	CAC	Cairo	Maadi (Degla)	3315496	0333471	Residential	X	X	
7 [a]	TBS	Giza	Tebbin South	3292317	0336948	Industrial	X	X	
8	UHC	Cairo	Old Cairo	3321031	0329469	Residential	X	X	
9	ERA	Cairo	Ramses Square	3326920	0330905	Traffic		X	
10 [a]	CAI	Cairo	Old Maadi	3315847	0331076	Residential	X	X	X
11	CEH	Giza	Giza	3323063	0327125	Residential	X	X	
12	AAU	Cairo	El-Darb El-Ahmar	3325152	0332644	Mixed		X	
13	OCT	Giza	6th October	3313591	0298716	Residential	X	X	
14	RAM	Sharkiya	10th Ramadan	3351235	0378586	Residential	X	X	
15	BLB	Sharkiya	Belbeis	3356629	0358434	Background	X	X	X
16	ATI	Cairo	Mokattam	3321420	0335413	Residential		X	
17	LSA	Qalioubiya	Shoubra El-Kheima	3332439	0333190	Source	X	X	
18	APC	Qalioubiya	Shoubra El-Kheima	3332591	0332797	Industrial	X	X	
19	TTI	Cairo	El-Sahel	3332027	0332511	Industrial	XC	XC	
20	MIC	Qalioubiya	Shoubra El-Kheima	3332842	0334295	Industrial	X	X	
21	DRC	Cairo	Matariya	3333406	0337635	Mixed	X	X	
22	AMP	Cairo	El-Wayli	3330857	0333996	Mixed		X	
23	TES	Cairo	Tebbin	3295144	0335006	Industrial	X	X	
24	LSB	Cairo	Tebbin	3294703	0335342	Source	XC	XC	X
25	HTI	Cairo	Imbaba	3329039	0328829	Residential		X	
26	KFC	Qalioubiya	Qaha	3350606	0326517	Background	X	X	X
27	MAY	Cairo	15th May City	3299968	0342241	Residential		X	
28	HDM	Cairo	Almaza	3329357	0340774	Residential		X	
29	LRC	Cairo	Basateen	3318364	0331495	Mixed		X	
30	CYC	Giza	Giza	3323867	0328339	Residential		X	
31	AUC	Cairo	Tahrir Square	3324855	0329990	Mixed	X	X	
32	BIS	Giza	Zamalek	3326590	0328661	Residential	X	X	
33	HFS	Cairo	Helwan	3302944	0338983	Residential	X	X	
34	SBH	Cairo	El-Massara	3309097	0335395	Mixed	X	X	
35	OLS	Cairo	Heliopolis	3331676	0339733	Residential	X	X	
36	EGS	Cairo	Abbasiya	3327037	0334658	Industrial	X	X	

a) CAIP samplers collocated at EIMP monitoring site

b) X: sampler or meteorological system is operated at the site
XC: Two (2) each, PM2.5 and PM10, collocated samplers operated at site
X (Met): WD, WS, WD Sigma, Temperature, and Barometric Pressure measurements

Table 3-2: Distribution of CAIP Sites by Land-use Classification

Classification	No. of Sites
Traffic	4
Industrial	6
Residential	15
Mixed	7
Source	2
Background	2
Total	**36**

The industrial Sites #18 and #19, in Shoubra El-Kheima and El-Sahel respectively, are placed at locations where a significant impact of secondary lead smelter emissions is expected. Site #18 is approximately 500 m south of a lead smelter stack. Site #19 is approximately 250 m south of the stacks of 2 lead smelters. Another secondary lead smelter is located approximately 1–1.5 km northeast of Site #19 but is not expected to have a major impact on the lead measurements at this site. The location of industrial Site #20 in Shoubra El-Kheima was selected to measure the fugitive emissions from a steel production plant. The site is approximately 300 m south of a building that houses the steel-making furnaces. Site #23 in Tebbin is located approximately 600 m in the nominally upwind direction (north) from a secondary lead smelter. Together with Site #24, these 2 sites provide PM and lead measurements upwind and downwind of the secondary lead smelter. The predominant wind direction in Cairo most of the year is from the northerly direction. Thus, the 2 background sites in Qaha (Site #15) and Belbeis (Site #26) are placed in rural locations in northwesterly and northerly directions, respectively, from the Cairo urban area. The Belbeis site is in a desert environment and the Qaha site is located in a rural area in the lower Nile delta.

The sampling equipment of the CAIP sites of El-Qolaly Square (Site #1) and Maadi (Site #10) is located at EIMP sites. EIMP performs PM10 measurements at the El-Qolaly site using a beta gauge instrument and at the Maadi site using a high volume sampler. The collocated siting and concurrent sampling arrangements provide the opportunity to directly compare EIMP's and CAIP's PM10 measurements. Both CAIP and EIMP conduct PM10 measurements in the same general areas at El-Gomhuriya Street, 10th of Ramadan City, and 6th of October City. However, only a qualitative comparison of CAIP and EIMP data from these sites can be made due to the distance between the sampling locations and differences in the sampler inlet heights.

Figure 3-2: 10th of Ramadan Residential Site

Figure 3-3: Gomhuriya Street Traffic Site

Figure 3-4: Tebbin South Industrial Site

Figure 3-5: Qaha Background Site

3.2 Sampling Procedures

AirMetrics™ samplers are used to collect PM from the air for gravimetric and lead analysis. A sampler pump draws in a sample of air at the rate of 5 liters per minute (lpm). The sampler inlets through which the incoming air passes are designed to separate the particulate matter according to size (aerodynamic diameter of the particles) and provide samples of the PM in either the 0-2.5 μm (PM2.5) or the 0-10 μm (PM10) size range. After passing through the size-fractionating inlet, the PM in the air sample stream is deposited on a tared 47-mm diameter quartz fiber filter.

Both PM2.5 and PM10 measurements are performed at 26 sites. Only PM10 and Pb10 measurements are performed at 10 ambient sites. Two each of the PM2.5 and PM10 samplers are placed at two sites (Sites #19 and #24). Data collected with these collocated samplers are used to estimate the precision of the PM and lead measurements (see Vol. I, Section 3.4.7 & Vol. III, Appendix H). A typical PM2.5 and PM10 sampler installation is shown in Figure 3-6. The collocated sampler installation at Site #19 (El-Sahel) is shown in Figure 3-7. For security, the samplers at each site are placed in a locked enclosure.

Samples are collected concurrently at all monitoring sites on an every-sixth-day schedule. A total of 60 sampling events[1] were conducted during the baseline year. The sampling event scheduled for 17 January 1999 was not conducted due to observance of the "Eid El-Fitr" celebration. During each sampling event, the samplers are programmed to continuously collect a PM sample over a 24-hour period (0000 to 2400 hours).

3.3 Gravimetric and Lead Analysis

The mass of PM deposited on the quartz filters is determined by weighing the filters before and after sample collection using a microbalance. Weight data obtained with the microbalance is recorded to 0.000001 grams. Prior to both the initial and final weighing, the filters are conditioned in a desiccation cabinet for at least 24 hours to obtain a constant weight. The filter conditioning and weighing operations are performed in a room in which the air temperature and humidity are controlled within the range of 17–23ºC and 45–55% relative humidity (RH).

[1] In this report, the term "sampling event" refers to the act of concurrently collecting 24-hour integrated samples at all of the 36 CAIP monitoring sites. Except for the one sampling event cancelled during Eid

Figure 3-6: Typical Sampler Installation

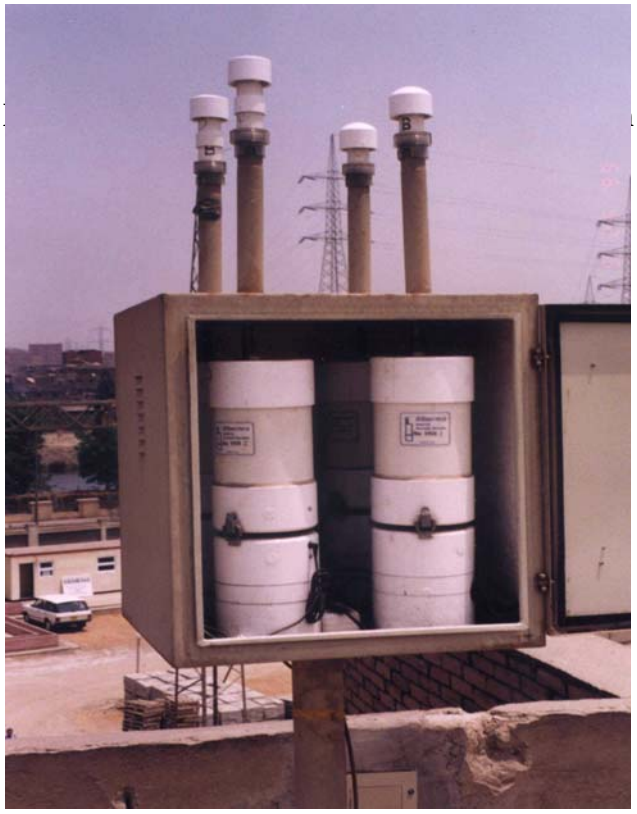

El-Fitr, sampling events were conducted every 6th day of the baseline year. A total of 60 sampling events were conducted during the baseline year (1 October 1998 through 30 September 1999).

Figure 3-8: Gravimetric Analysis of Filters

Figure 3-9: Lead Analysis by Flame Atomic Absorption Spectrometry

After the final weighing, lead is extracted from the filters' PM catch by digesting the filters in hot nitric acid solution. The lead content in the nitric acid extract solution is determined by **f**lame **a**tomic **a**bsorption **s**pectrometer (FAAS) using the lead absorption line at 217 μm. The **m**inimum **d**etection **l**imit (MDL) for lead on the filters by the FAAS method is 1.25 μg. The analytical detection limit corresponds to an MDL of 0.17 μg/m^3 for measurement of lead in ambient air. Photographs in Figures 3-8 and 3-9 show the work areas and the equipment used for the gravimetric and lead analysis respectively.

3.4 Quality Control Procedures

A summary of the quality control (QC) procedures incorporated into the CAIP PM and lead monitoring program is provided in Table 3-3. The purpose of these activities is to produce high quality PM and lead measurement data as defined in terms of accuracy, precision, and completeness. Volume III of the report provides detailed results of the various QC activities conducted during the baseline year. A summary of the results of these activities is provided below.

3.4.1 AirMetrics™ Sampler Flow Rate Checks

Results of pre- and post-sampling flow rate checks of the AirMetrics samplers performed during each baseline-year sampling event are provided in Vol. III, Appendix A. A summary of the flow check data is presented in Table 3-4 below. The flow checks are performed with a mini-BUCK™ automated bubble meter calibrator. The calibration of the mini-BUCK™ units is traceable to the U.S. National Institute of Standards and Technology (NIST). The design flow rate of the AirMetrics™ samplers is 5.0 lpm. Flow check results are considered acceptable if the sampler flow rate is within the range of 4.5–5.5 lpm, i.e.; the deviation from the design flow rate is ≤10%.

During the baseline year, 7732 flow checks were performed and unacceptable post-sampling flows were found on only three (3) occasions. Samples collected on these occasions were accordingly invalidated. Recovery or completeness of the flow check data is 98%.

3.4.2 Filter Blank Samples

Filter blanks are filters subjected to routine handling operations, but not used for sample collection. Blanks are collected to determine if systematic errors are introduced into the lead or mass measurements by filter damage or contamination during the handling operations.

Table 3-3: QC Procedures Summary

Operation	QC Activity	Frequency	Purpose
Field Sampling PM samplers	Sampler flow check	Before and after each sampling event	Ensure sampler operation at the proper flow rate (5 lpm)
	Trip blank filters	Two (2) with the set of samples used during a sampling event	Estimate weighing accuracy and check for filter contamination during transit between the laboratory and CAIP offices and during storage in CAIP work area.
	Field blank filters	Two (2) with the set of samples used during a sampling event	Estimate weighing accuracy and check for filter contamination during installation at field sites
Gravimetric and Lead Analysis of Filter Samples by Flame Atomic Absorption Spectrometry (FAAS)	Laboratory blank filters	Two (2) with the set of samples used during a sampling event	Estimate weighing accuracy and check for filter contamination during handling in the analytical laboratory
	FAAS system calibration for lead analysis	At start and end of analysis of all sets of samples and when interim calibration and blank check values are not within specified limits	Ensure the accuracy of the FAAS analysis
	Calibration and blank checks	After analysis of each 10 samples	Check for zero and calibration drift of the FAAS
	Duplicate sample analysis	Once during analysis of each set of 10 samples	Estimate precision of the FAAS analysis
	Matrix spikes		Determine if any sample matrix components adversely affect the lead measurements
Data Processing	Inspection for unacceptable field or laboratory QC checks	All data	Identify invalid data based on field and laboratory QC checks
	PM2.5/PM10 and Pb2.5/Pb10 ratio check	All pairs of PM2.5 and PM10 data and Pb2.5 and Pb10 data	Judge data validity data based on PM and Pb ratios, e.g. ratios >1
	Data Reasonableness check	All data not invalidated by other QC checks	Judge validity data based on reasonableness of the result compared to historical data

Table 3-4: AirMetrics™ Sampler Flow Check Summary

Month	Flow Check Difference %[a]			Count	Checks Accepted	Checks Rejected
	Average	Maximum	Minimum			
Oct-98	-0.52	6.0	-5.3	787	787	0
Nov-98	-0.44	7.2	-7.0	652	652	0
Dec-98	-0.12	7.9	-4.6	652	652	0
Jan-99	1.19	6.0	-5.0	524	524	0
Feb-99	1.30	9.8	-3.6	658	658	0
Mar-99	1.11	9.8	-4.2	658	658	0
Apr-99	0.76	7.0	-13.3	645	644	1
May-99	0.91	5.0	-4.2	658	658	0
Jun-99	0.85	5.0	-4.8	653	653	0
Jul-99	0.50	9.4	-5.4	646	646	0
Aug-99	0.12	4.0	-21.3	633	632	1
Sep-99	0.07	25.7	-7.9	566	565	1
Annual	**0.45**	**25.7**	**-21.3**	**7732**	**7729**	**3**

(a) Percent difference between sampler flow reading and sampler design flow rate (5 lpm)

Three types of blanks (laboratory, trip, and field) are collected to evaluate the potential error associated with different components of the filter handling operations. The gravimetric and lead analysis results for each type of filter blank samples are provided in Vol. III, Appendices B and C. Gravimetric data for the trip, field, and laboratory blanks are summarized in Table 3-5 below.

Table 3-5: Filter Blank Gravimetric Data Summary

Blank Type	Initial/Final Weighing Difference (mg)			Standard Deviation. of Differences, mg	No. of Blanks Collected
	Average	Maximum	Minimum		
Trip [a]	-0.009	0.022	-0.035	0.015	97
Field	-0.011	0.022	-0.030	0.014	112
Lab [a]	-0.005	0.023	-0.023	0.016	119

(a) One outlying value was excluded in calculating these summary statistics.

The average differences indicate a slight negative bias in the weight data. The bias may be due to a slight loss of fibers of the filter media during the various handling

operations. For PM2.5, the weighing error is 4.3%, at a 95% confidence interval, estimated from the gravimetric data for the filter blanks and average PM2.5 sample catch (0.694 mg). The error range is 0.9–16.7%, at a 95% confidence interval, estimated for the maximum and minimum PM2.5 filter catches (3.218 & 0.180 mg, respectively). For PM10, the weighing error is 2.1%, at a 95% confidence interval, estimated from the gravimetric data for the blanks and average PM10 sample catch (1.414 mg). The error range is 0.5–5.6%, at a 95% confidence interval, estimated for the maximum and minimum PM10 filter catches (6.180 and 0.539 mg, respectively). Except for low PM2.5 filter loading, the blank data indicates that the error in determining the mass of PM collected on the filters is <5%.

Lead analysis data for the trip, field, and laboratory blanks is summarized in Table 3-6. This data shows that the handling operations do not introduce a systematic error into the lead measurements. Lead appears in the blanks randomly and was detected in relatively few blanks (<6% of the total number of blank samples). The average lead levels detected in the blanks are low (approximately 2.4– 3.1 times the MDL) and correspond to an ambient air concentration of approximately 0.5 μg/m³. The maximum blank lead value (7.0 μg/filter) is 5.6 times the MDL and corresponds to an ambient lead concentration of approximately 1 μg/m³.

Table 3-6: Summary of Filter Blank Lead Data

Blank Type	Pb Content of Filter, μg/filter [a]		Total Blanks Collected	Blanks with Lead>ND
	Average [b]	Maximum		
Trip	3.0	4.3	98	5
Field	3.3	7.0	112	9
Lab	3.9	6.8	120	5

a) Lead minimum detection limit (MDL) is 1.3 μg/filter
b) Average in filter blanks that Pb exceeded the MDL.

3.4.3 FAAS Calibration Checks

Before beginning analysis of samples, the FAAS response is calibrated using a reagent blank solution and standard lead solutions at five different concentration levels. A series of **c**ontinuing **c**alibration **c**hecks (CCC) is performed during the analysis of each set of samples to verify that the FAAS calibration conditions do not shift beyond acceptable limits. The CCC are performed using a reagent blank solution, CCB[1], to check for zero drift, and a 2.48 μg Pb standard, CCS[1], to check

[1] CCB: Continuing Calibration Blank; CCS: Continuing Calibration Standard

for drift in the lead concentration/instrument response relationship established during the initial FAAS calibration. During analysis of sets of samples, continuing calibration checks of the FAAS system are performed before and after analysis of each set of 10 or fewer samples. The calibration of the FAAS is considered acceptable if the response for the blank sample is within ± 0.10 μg of Pb and the response for the 2.48 μg Pb standard is in the range of 2.25–2.75, i.e., the deviation from the standard value is ≤ 10%. If the continuing calibration results (either CCB or CCS) are not within the acceptable range, the FAAS is re-calibrated and analysis is repeated for the samples that were analyzed prior to the failed calibration check.

The CCC results recorded during analysis of the baseline year samples are listed in Vol. III, Appendix D. These results show that the FAAS system was within acceptable calibration limits during all sample analysis sessions.

3.4.4 Duplicate Mass and Lead Determinations

During tare and final weighing of filter sets, nominally one of each group of 10 filters is re-weighed as a QC check. The results of these duplicate gravimetric measurements are presented in Vol. III, Appendix E, Tables III-E-1 and III-E-2. Likewise, lead measurements are duplicated on one of each group of 10 samples. The duplicate lead measurements are performed by analysis of the same sample solution at two different times during the analysis sessions. The results of the duplicate lead measurements are presented in Vol. III, Appendix E, Table III-E-3.

A statistical summary of the duplicated mass and lead measurements is given in Table 3-7 below.

Table 3-7: Duplicate Measurements Summary

Statistic	Tare Weights, mg (a)	Final Weights, mg (b)	Pb Analysis, % (c)
Average Difference	-0.002	-0.002	-0.1
Std. Dev. of Differences	0.007	0.007	10.6
Max. Difference Value	0.021	0.028	28.1
Min. Difference Value	-0.035	-0.021	-54.4
Count (# Measurements)	730	689	261

(a) Three outlying values were excluded from the statistical calculations
(b) Two outlying values were excluded from the statistical calculations
(c) Two outlying values were excluded from the statistical calculations

The small average differences in both the duplicate weighing and lead analysis data indicate the absence of bias in the measurements. The variance in the duplicate weighing data, as indicated by the standard deviation, is acceptable and indicates that, at a 95% confidence interval, the differences between duplicate mass determinations can be expected to fall within a range of approximately ± 14 mg. The maximum and minimum weight difference range is approximately the same as the range obtained for the filter blank measurements. The statistics for the duplicate lead determinations are consistent with normal variations in the FAAS analytical method.

3.4.5 Matrix Spiked Samples

In FAAS analysis, some constituents in the sample matrix can interfere with accurate determination of the lead content. The matrix spiking procedure is used to identify such interference problems. After the initial lead determination, selected samples are spiked with a known quantity of lead (2.48 μg). The sample is then reanalyzed. The difference between the initial and second lead determinations divided by the spike quantity (and expressed as a percentage) is called "Spike Recovery". Large deviations of the spike recovery may indicate that a constituent in the sample is causing an unacceptable error in the lead analysis of the filter samples. An acceptable range for the spike recovery is 80–120%.

The matrix spiking results obtained during analysis of the CAIP baseline year lead samples are provided in Vol. III, Appendix F. Ninety-three (93) matrix spike samples were analyzed during the year. The average spike recovery value was 96.9% and the maximum and minimum spike recovery values were 117.5% and 79.8%, respectively. This indicates that the spike recoveries were within an acceptable range and that the samples do not contain constituents that adversely affect the accuracy of the lead analysis.

3.4.6 Data Recovery

Monitoring data recovery or completeness for sampling events, months of the baseline year, and for the baseline year are provided in Vol. III, Appendix G. The data recovery/completeness values reported are expressed as a percentage of the total number of measurements that yielded a valid result.

A summary of data recovery statistics for the baseline year is shown in Table 3-8. The annual average recoveries for PM and lead data are within an acceptable range. However, data recoveries for a few sampling events were below acceptable levels. In particular, low PM2.5 and PM10 data recoveries of 35.7% and 36.8%, respectively, were obtained from the 27 August 1999 sampling event. In this case,

data loss appears to result from a systematic error in the sample weights, possibly due to improper conditioning of the samples prior to gravimetric analysis.

Table 3-8: Monitoring Data Recovery Summary

Statistic	Data Recovery (as %)			
	PM2.5	PM10	Pb2.5	Pb10
Annual Average Recovery, %	88.7	87.6	76.4	80.7
Maximum Event Recovery, %	100.0	100.0	96.4	97.4
Minimum Event Recovery, %	35.7	42.18	46.4	60.5
Sampling Events < 70% Recovery	4	3	18	5
Sampling Events < 60% Recovery	1	1	2	0
Total Sampling Events	60	60	60	60

3.4.7 Collocated Sampler Data

During each sampling event, collocated pairs each of PM2.5 and PM10 samplers are operated concurrently at Site #19 (El-Sahel/TTI) and Site #24 (Tebbin/LSB). Under ideal conditions, the two PM2.5 samplers operated at each site should give the same result; likewise for the two PM10 samplers. Differences observed in the paired results provide a means of estimating the precision of the PM and lead measurements. It should be noted however that differences in paired measurements may also result from variations in the PM and lead content of the air samples withdrawn by the pair of samplers. In order to minimize the measurement variation from micro-scale differences in the airborne PM and lead concentrations, the sampler pair inlets are placed close together (approximately 50 cm apart). Still, this confounding source of variation cannot be completely eliminated and should not be disregarded in the interpretation of the collocated sampler data.

The results of all collocated measurements performed at the two monitoring sites are given in Vol. III, Appendix H. A summary of the statistical analysis of the paired measurement is presented in Table 3-9.

The standard deviation shown in Table 3-9 is an estimate of the method precision at a 67% (1 sigma, denoted as σ) confidence interval based on the paired, collocated measurements. An estimate of a 95% (2 σ) confidence interval for the method precision is also presented in Table 3-9. These precision estimates include variances associated with all operations (field sampling and laboratory analysis) involved in making the respective measurements, in addition to any variance due to concentration differences in the air sampled by the pairs of samplers.

Table 3-9: Collocated Sampler Results Summary

Site No.	Statistic	PM2.5	PM10	Pb2.5	Pb10
19/19C	Average of percent differences	3.2	1.0	2.2	-2.3
	Standard deviation of percent differences	±16.0	±10.5	±16.4	±13.4
	Upper limit, 95% confidence interval	34.5	21.6	34.3	24.0
	Lower limit, 95% confidence interval	-28.0	-19.5	-29.9	-28.5
24/24C	Average of percent differences	3.8	0.9	3.3	6.7
	Standard deviation of percent differences	±11.3	±13.7	±7.4	±15.8
	Upper limit, 95% confidence interval	26.0	27.7	17.8	37.7
	Lower limit, 95% confidence interval	-18.3	-26.0	-11.2	-24.3
19/19C 24/24C Pooled	Average of percent differences	3.5	1.0	2.6	0.7
	Standard deviation of percent differences	±14.0	±11.8	±13.6	±13.9
	Upper limit, 95% confidence interval	30.9	24.1	29.3	27.9
	Lower limit, 95% confidence interval	-24.0	-22.2	-24.1	-26.5

3.4.8 Data Validation

All the PM and lead monitoring data are subjected to a validation process before the data are reported. In the first step in the validation process, the data on the field sampling forms and results of all the field and laboratory QC activities discussed in the preceding sections are examined to identify conditions which yield data not within acceptable limits. Samples for which field-sampling errors occurred and/or sampling or laboratory QC checks were not within acceptable limits were invalidated.

The next validation step involves the examination of the PM mass concentration and Pb mass concentration ratios of each pair of PM2.5 and PM10 measurements and each pair of Pb2.5 and Pb10 measurements. The ratios are considered acceptable if the PM2.5/PM10 ratio is in the range of 0.15–1.0 and the Pb2.5/Pb10 ratio is in the range of 0.40–1.0. The upper value for the acceptance range, 1.0, is the theoretical limit for the ratio. The lower acceptance values for the PM and Pb ratios are derived from statistical analysis of the baseline year ratio data and correspond to the lower limit of the 99% (3 σ) confidence interval. When the ratio is not within expected limits, the assumption is that one or both of the measurement values may be erroneous. On the other hand, the fact that the ratio is within acceptance limits is not indisputable proof that the 2 measurements are valid. The PM and Pb ratio validity check cannot be applied to all samples since only PM10 and Pb measurements are performed at some sites. In addition,

the inherent variability in values approaching the lead MDL (0.17 μg/m³) restricts applying the ratio check to these data.

The final step in the validation process is a review of the data for outlying values. For the PM2.5 and PM10 data, values below 10 μg/m³ and 25 μg/m³, respectively, are declared outlying values. These criteria are based on statistical analysis of the baseline year data and represent the lower 95% confidence limit of the variations in the PM measurements. Measurement values that appear unusually high are treated individually. An outlier test is applied that uses the statistical variation in the historical measurements made at the same site from which the suspected outlying data originates.

3.4.9 AirMetrics/BGI Sampling Data Comparison

Results of concurrent PM10 measurements performed with collocated AirMetrics and BGI Model PQ-200 samplers are given in Vol. III, Appendix I. The BGI instrument has been assigned Federal Reference Designation Number RFPS-1298-125 in recognition that the unit meets the United States Environmental Protection Agency (USEPA) requirements for PM10 samplers. The sampler comparison includes 27 paired measurements performed over the period 16 June 1999–30 January 2000.

A regression analysis plot showing the relationship of the AirMetrics and BGI measurements is presented in Figure 3-10. The regression analysis parameters show that the AirMetrics samplers provide PM10 results that agree very well with the BGI Federal Reference Method (FRM) sampler. Since the USEPA requires that all FRM's yield comparable results, it can be inferred that the AirMetrics samplers will provide PM10 data comparable to other FRMs, e.g., the high volume PM10 samplers used at the EIMP sites. CAIP and EIMP are conducting concurrent, collocated measurements at two monitoring sites (El-Qolaly Square and Maadi) to demonstrate comparability of the PM10 collected by the two programs.

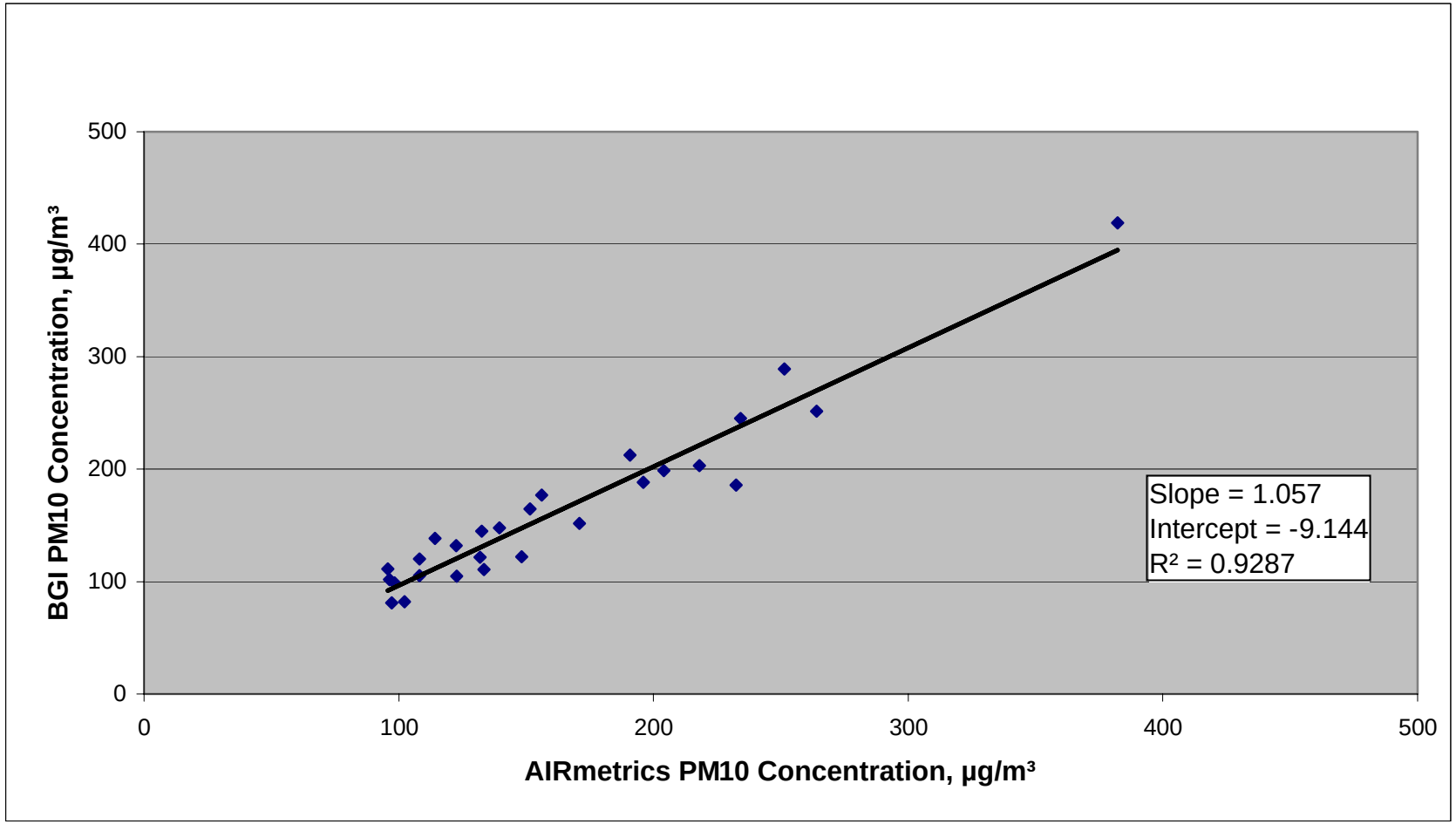

Figure 3-10: Comparison of Measurements with AirMetrics and BGI PM10 Samplers

Chapter Four
Summary of Data

This chapter provides an overview of the data collected during the baseline year and its significance. A more detailed listing is provided in Volume II of this report.

4.1 Ambient Particulate Matter Data

This section contains a summary of PM2.5 and PM10 monitoring data with the most significant statistics as well as a graphical representation. Full details of the results of all ambient air PM2.5 and PM10 measurements performed during the baseline year are shown in Vol. II, Appendices A and B. Summaries of PM2.5 and PM10 monitoring data are presented in Tables 4-1 and 4-2 below, respectively. The tables show the following statistical values:

- The arithmetic average values of the PM2.5 and PM10 measurements performed at each site during each month of the baseline year;
- The arithmetic average, maximum, and minimum values of PM2.5 and PM10 measurements performed at all sites during each month of the baseline year;
- The arithmetic average, maximum, and minimum values of PM2.5 and PM10 measurements performed at each site during the baseline year;
- The arithmetic average, maximum, and minimum values of PM2.5 and PM10 measurements performed at all sites during the baseline year;
- The number (count) of valid PM2.5 and PM10 measurements obtained from each sampling event and each site during the baseline year and the total number of valid measurements obtained during the baseline year.

Generally high levels of PM2.5 and PM10 were recorded in the entire Greater Cairo area during the baseline year. The variation in PM levels throughout the baseline year is shown in Figures 4-1 and 4-2. The arithmetic average of PM2.5 and PM10 concentrations for each sampling event of the baseline year is shown in Figure 4-1. The average value for each sampling event is calculated from valid measurements obtained at all of the ambient monitoring sites during the sampling event. The correlation in the PM2.5 and PM10 concentration variations can be seen. Typically, the PM2.5 mass concentration is 0.5 times that of PM10.

Table 4-1: Monthly and Annual Statistical Summary of PM2.5 Measurements at CAIP Sites

Site No.	Site Code	Site Location	Average Monthly: PM2.5 Concentration, μg/m³												Annual Site Statistics			
			Oct	Nov	Dec	Jan	Feb	Mar	Apr	May	Jun	Jul	Aug	Sep	Avg	Max	Min	Count
01	EQS	El-Qolaly Sq.	120.2	126.2	145.2	144.3	125.4	112.8	80.9	94.8	86.4	83.2	100.5	79.5	107.8	172.2	60.2	50
02	GEM	El-Gomhuriya St.	176.1	157.6	173.0	139.9	123.7	116.4	84.4	105.3	91.6	88.7	95.4	82.8	121.0	296.9	42.6	56
03	MET	El-Wayli	136.4	150.3	120.5	96.8	72.2	88.0	60.5	70.7	61.4	65.9	75.9	63.8	88.0	236.6	37.3	55
04	NRC	Nasr City	124.2	78.9	140.2	79.4	61.1	46.7	48.1	55.4	64.6	62.1	46.4	66.4	75.2	208.0	29.3	49
05	FAK	Fum Al-Khaleej [a]	-	-	-	-	-	-	-	-	-	-	-	-	-	-	-	0
06	CAC	Maadi/Degla	109.0	70.8	177.0	98.1	59.4	66.8	66.5	68.6	49.0	67.2	68.3	41.4	77.7	281.9	29.0	54
07	TBS	Tebbin South	158.5	108.4	106.5	101.0	118.9	91.6	105.2	113.0	100.5	110.0	107.0	100.5	112.0	200.6	36.7	56
08	UHC	Old Cairo	133.4	163.0	181.4	137.1	90.6	88.8	62.4	78.9	68.1	74.4	75.3	70.0	102.3	332.5	45.3	52
09	ERA	Ramses Square [a]	-	-	-	-	-	-	-	-	-	-	-	-	-	-	-	0
10	CAI	Old Maadi	111.2	99.4	168.7	104.2	73.0	74.6	67.7	69.0	63.9	58.3	65.1	64.1	83.2	240.9	37.6	53
11	CEH	Giza	126.1	113.0	135.4	119.4	86.6	80.4	69.9	72.4	60.6	66.4	58.8	63.3	88.2	272.2	28.6	51
12	AAU	El-Darb El-Ahmar [a]	-	-	-	-	-	-	-	-	-	-	-	-	-	-	-	0
13	OCT	6th October City	86.4	118.6	45.9	65.9	71.5	73.2	56.0	55.3	48.8	47.9	33.9	51.3	61.8	146.3	25.1	49
14	RAM	10th Ramadan	84.5	89.9	63.3	65.5	60.1	53.8	52.1	51.6	53.0	46.2	50.7	55.6	60.3	110.0	25.1	54
15	BLB	Belbeis	124.9	86.8	98.9	68.5	60.6	47.2	77.4	60.3	50.1	55.7	62.7	48.5	70.0	219.1	27.8	52
16	ATI	Mokattam [a]	-	-	-	-	-	-	-	-	-	-	-	-	-	-	-	0
18	APC	Shoubra El-Kheima	167.4	139.5	199.3	130.9	142.7	129.8	110.4	148.1	136.2	102.4	104.2	108.8	134.8	259.7	26.5	52
19	TTI	El-Sahel	215.9	172.6	191.4	115.8	214.5	135.8	128.9	127.9	129.0	123.4	147.7	111.0	154.8	269.6	25.0	54
20	MIC	Shoubra El-Kheima	265.2	230.9	196.8	166.7	251.9	196.1	140.6	202.0	119.4	95.3	106.6	119.0	178.6	447.0	35.4	56
21	DRC	Matariya	159.3	92.4	133.9	107.6	75.4	71.3	61.4	71.8	60.9	76.7	59.6	69.8	90.1	261.2	40.2	52
22	AMP	El-Wayli [a]	-	-	-	-	-	-	-	-	-	-	-	-	-	-	-	0
23	TES	Tebbin	111.8	96.9	129.4	112.0	90.0	92.8	78.5	70.6	60.0	69.5	76.8	66.8	90.0	209.0	38.8	51
25	HTI	Imbaba [a]	-	-	-	-	-	-	-	-	-	-	-	-	-	-	-	0
26	KFC	Qaha	117.4	71.2	105.6	104.7	92.4	78.2	63.9	62.4	74.5	64.2	62.7	73.9	80.7	203.7	40.4	52
27	MAY	15th May City [a]	-	-	-	-	-	-	-	-	-	-	-	-	-	-	-	0
28	HDM	Almaza [a]	-	-	-	-	-	-	-	-	-	-	-	-	-	-	-	0
29	LRC	Basateen [a]	-	-	-	-	-	-	-	-	-	-	-	-	-	-	-	0
30	CYC	Giza [a]	-	-	-	-	-	-	-	-	-	-	-	-	-	-	-	0
31	AUC	Tahrir Square	146.9	144.4	164.9	114.9	96.7	88.3	55.9	84.8	78.9	77.7	74.6	72.6	101.9	292.5	31.0	53
32	BIS	Zamalek	131.1	181.8	128.1	90.3	99.4	84.5	50.5	80.8	67.5	73.4	73.4	63.6	92.0	250.8	38.4	56
33	HFS	Helwan	103.7	98.2	142.2	121.1	78.3	69.6	57.0	67.7	66.6	74.0	55.3	61.9	82.2	220.4	27.8	53
34	SBH	El-Massara	127.1	111.9	160.7	121.6	77.9	80.0	70.7	81.1	59.7	72.2	70.0	72.0	93.4	271.9	31.5	55
35	OLS	Heliopolis	122.7	85.7	127.6	77.4	66.9	63.7	70.0	55.6	61.8	61.2	63.5	55.1	76.7	210.6	31.7	49
36	EGS	Abbasiya	139.8	79.6	141.3	91.1	63.8	80.3	52.7	70.1	62.6	71.8	63.0	61.7	80.4	215.5	34.3	51
Monthly Site Statistics		Average	138.1	120.3	140.5	107.4	99.3	86.8	76.2	84.4	72.9	74.6	76.9	71.0	Annual Statistics – All Sites			
		Maximum	366.4	447.0	332.5	267.3	379.2	323.2	291.5	293.2	208.3	176.2	268.2	195.1				
		Minimum	27.8	28.6	28.9	37.2	29.6	32.5	29.6	36.3	37.4	29.3	25.0	29.0				
		Count	135	92	104	90	111	111	94	113	107	112	90	105	**96.4**	**447.0**	**25.0**	**1264**

(a) PM2.5 measurement is not performed at this site.

Table 4-2: Monthly and Annual Statistical Summary of PM10 Measurements at CAIP Sites

Site No.	Site Code	Site Location	Average Monthly: PM10 Concentration, µg/m³												Annual Site Statistics			
			Oct	Nov	Dec	Jan	Feb	Mar	Apr	May	Jun	Jul	Aug	Sep	Avg	Max	Min	Count
01	EQS	El-Qolaly Sq.	280.4	394.7	279.2	264.3	268.3	276.8	190.8	236.6	206.5	206.2	227.6	166.4	239.2	394.7	108.8	47
02	GEM	El-Gomhuriya St.	277.3	309.7	376.5	279.7	226.7	263.0	180.9	199.3	214.7	212.9	211.5	194.2	246.9	649.6	110.5	57
03	MET	El-Wayli	246.6	260.3	225.2	246.1	122.8	168.8	125.2	160.0	142.6	139.0	145.8	143.5	175.8	515.1	65.8	54
04	NRC	Nasr City	214.0	187.1	294.0	148.8	108.3	126.8	97.7	117.5	116.7	103.1	119.1	134.5	153.7	414.3	56.1	50
05	FAK	Fum Al-Khaleej	185.4	220.2	253.1	247.3	169.3	200.2	149.6	148.3	141.1	182.5	115.5	112.2	184.3	431.0	77.8	49
06	CAC	Maadi/Degla	222.4	181.5	483.3	222.5	126.7	167.5	109.6	145.7	122.1	134.9	110.2	122.2	169.9	639.6	42.8	54
07	TBS	Tebbin South	354.7	298.5	225.6	228.7	234.3	287.4	279.5	265.0	216.3	259.6	256.4	252.7	265.4	597.0	119.6	52
08	UHC	Old Cairo	243.4	413.5	375.0	289.5	175.2	215.7	156.3	192.8	147.0	174.6	165.0	143.7	224.2	858.3	101.3	55
09	ERA	Ramses Square	270.9	282.5	400.8	290.6	199.1	234.2	169.3	176.7	160.8	164.8	126.7	165.2	223.7	703.3	85.6	56
10	CAI	Old Maadi	197.6	221.9	306.8	196.2	140.4	161.5	156.0	165.2	139.3	150.1	157.1	148.8	176.3	509.1	94.9	54
11	CEH	Giza	194.9	195.6	247.8	242.3	155.8	168.4	146.1	148.7	124.6	135.5	106.5	158.2	167.0	474.2	31.9	52
12	AAU	El-Darb El-Ahmar	245.9	245.6	332.0	219.3	231.0	194.1	179.1	178.0	143.5	128.5	135.8	148.4	202.1	684.7	86.4	54
13	OCT	6th October City	157.7	158.6	111.9	122.5	132.4	138.9	125.2	115.1	102.3	97.3	83.8	124.7	123.9	244.4	40.8	49
14	RAM	10th Ramadan	155.9	177.5	145.5	112.6	106.6	100.8	84.8	104.5	93.5	95.9	77.3	95.9	112.7	206.8	29.2	54
15	BLB	Belbeis	185.3	177.5	150.4	96.7	89.5	99.3	107.8	118.5	98.5	112.1	93.0	78.2	117.8	307.1	38.7	51
16	ATI	Mokattam	208.1	239.0	281.5	194.8	120.7	139.5	137.1	140.8	121.4	136.9	123.2	102.9	163.9	428.9	75.1	51
18	APC	Shoubra El-Kheima	289.3	268.4	356.1	259.4	238.3	268.4	222.9	256.8	234.6	200.3	199.7	166.8	249.3	658.5	68.9	52
19	TTI	El-Sahel	399.7	339.2	413.0	282.1	364.4	278.9	264.2	291.9	235.3	232.2	249.8	233.5	300.4	674.2	83.1	56
20	MIC	Shoubra El-Kheima	411.3	398.0	401.0	280.6	380.5	321.5	231.1	341.9	219.3	175.2	176.6	204.4	301.5	648.6	128.4	56
21	DRC	Matariya	327.9	225.7	291.9	205.0	148.9	162.7	116.2	164.9	153.7	177.6	147.1	154.6	194.2	822.3	72.2	51
22	AMP	El-Wayli	291.6	287.4	359.1	204.3	165.7	177.9	143.1	191.6	163.4	153.5	133.1	167.0	202.4	626.1	92.2	51
23	TES	Tebbin	227.9	235.2	233.4	206.7	166.9	198.7	201.5	188.1	113.9	128.9	153.0	218.8	188.9	409.8	82.1	51
25	HTI	Imbaba	231.8	242.8	230.0	216.8	177.3	171.0	118.6	168.7	118.0	123.1	191.0	148.1	181.3	423.2	90.7	51
26	KFC	Qaha	172.5	143.4	213.3	155.1	150.7	147.7	116.5	129.4	126.0	123.6	119.9	134.7	143.1	437.8	67.9	50
27	MAY	15th May City	170.9	246.4	222.6	213.5	127.7	177.4	253.3	129.8	118.4	110.2	124.4	128.1	164.7	531.5	77.8	49
28	HDM	Almaza	198.6	192.1	249.5	139.3	111.5	131.2	120.1	122.1	101.0	125.9	103.5	113.2	144.7	433.0	76.8	49
29	LRC	Basateen	273.7	277.3	398.4	279.5	200.4	246.8	183.2	225.5	175.4	202.3	216.1	178.6	238.4	828.6	114.1	59
30	CYC	Giza	220.4	230.2	277.6	187.4	156.4	166.0	138.1	158.5	120.5	150.6	130.1	136.2	170.4	507.9	87.0	52
31	AUC	Tahrir Square	235.1	319.4	297.1	199.2	165.2	172.0	135.5	150.9	155.9	162.0	126.5	136.7	190.9	637.9	98.8	53
32	BIS	Zamalek	226.9	299.0	229.3	155.9	167.6	162.5	115.4	155.6	121.9	157.0	139.2	140.1	172.5	521.1	91.3	53
33	HFS	Helwan	192.2	278.6	323.8	251.6	151.7	164.2	142.4	154.8	137.7	155.1	135.9	156.4	182.2	578.9	70.0	54
34	SBH	El-Massara	301.3	284.5	401.5	285.7	196.2	208.2	227.5	201.2	170.4	219.2	177.5	217.5	243.8	707.1	53.9	55
35	OLS	Heliopolis	199.9	129.6	292.9	155.1	102.2	128.6	117.3	127.2	111.9	121.6	116.1	112.2	144.4	408.9	58.5	52
36	EGS	Abbasiya	260.8	186.6	285.7	190.0	116.5	173.7	107.3	140.8	126.4	123.5	141.0	135.6	163.7	518.1	71.5	50
Monthly Site Statistics		Average	244.2	251.3	292.6	214.9	175.0	188.2	158.8	173.9	147.7	155.6	150.1	151.9	Annual Statistics – All Sites			
		Maximum	822.3	767.5	858.3	442.7	568.3	427.4	531.5	518.1	321.2	324.2	421.3	331.0				
		Minimum	65.7	40.8	57.6	77.5	56.3	48.7	29.2	77.8	69.9	68.9	31.9	68.9				
		Count	189	133	154	129	152	150	140	163	146	155	128	144	**193.1**	**858.3**	**29.2**	**1783**

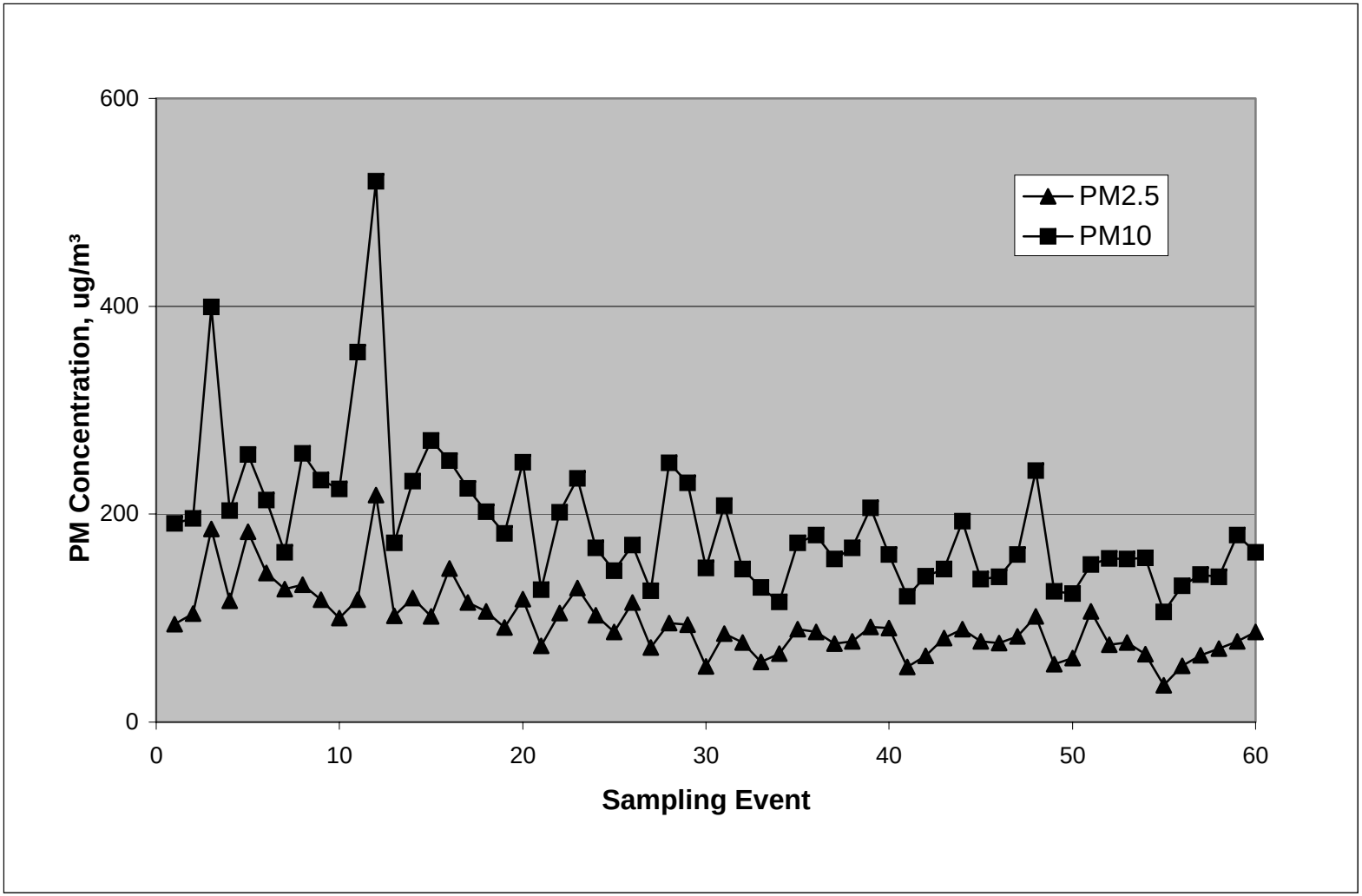

Figure 4-1: Average PM2.5 and PM10 Concentrations for Sampling Events during Baseline Year October 1998 through September 1999

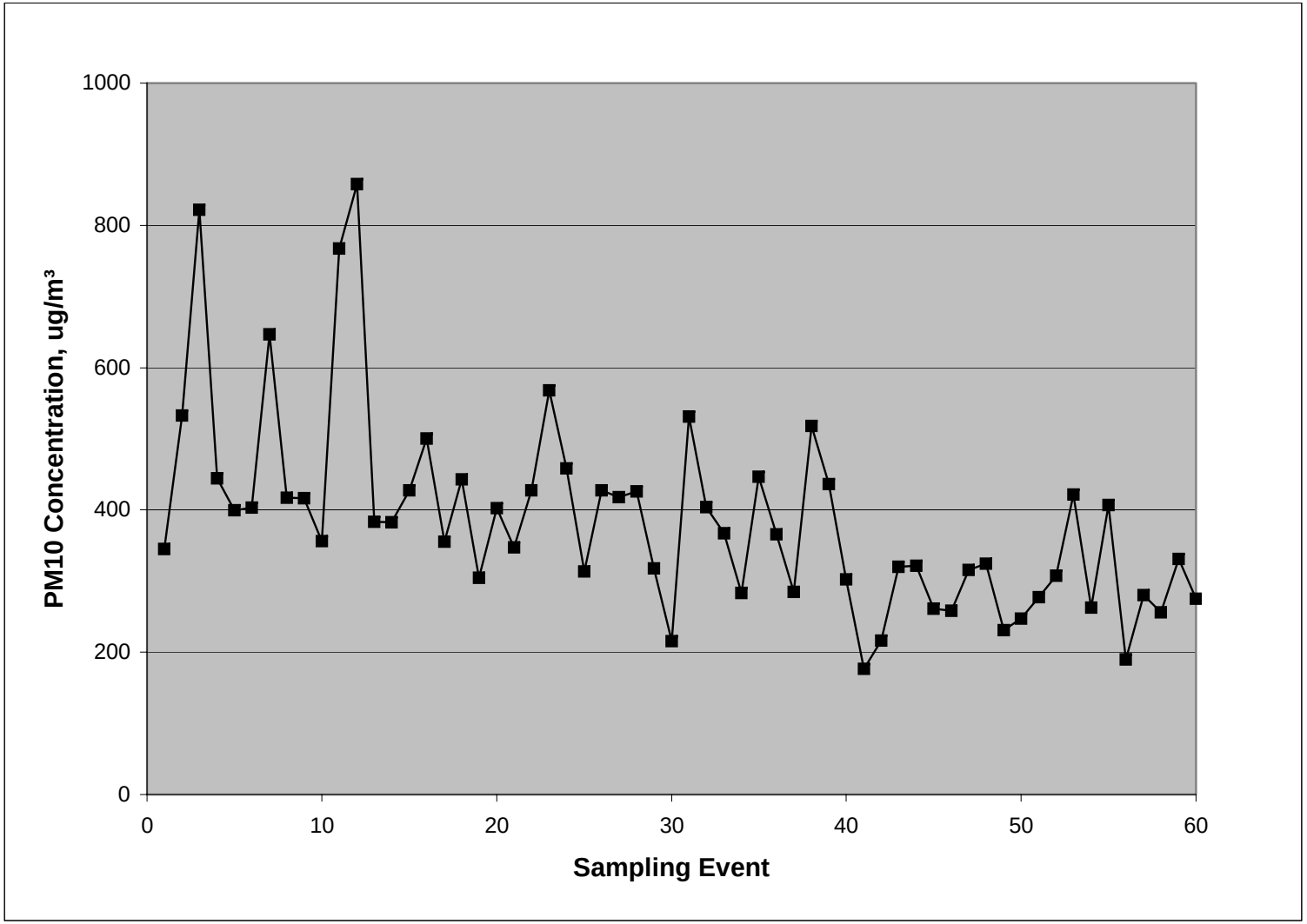

Figure 4-2: Maximum PM10 Concentrations for Sampling Events during Baseline Year October 1998 through September 1999

The maximum PM10 concentration recorded during each sampling event is shown in Figure 4-2. The highest PM levels of the baseline year were recorded during the period of October–December 1998. The highest PM2.5 concentration, 447.0 μg/m³, was recorded on 6 November 1998 at Site #20 in Shoubra El-Kheima. The steel mill near the site is the likely source of the high PM level. The highest PM10 concentration, 858.3 μg/m³, was recorded on 6 December 1998 at Site #29 in Basateen. PM2.5 measurements are not performed at the Basateen site. The highest average PM2.5 and PM10 concentrations recorded for a sampling event (218.4 and 520.1 μg/m³, respectively) occurred on 6 December 1998.

Following the October–December 1998 period of high PM levels, concentrations decreased to a minimum during the months of June and July 1999. The temporal variation shown in Figure 4-1 suggests that there may be a seasonal trend in PM levels. The baseline year data also indicates that there is a day-of-the-week trend in PM levels. A lower average PM level was recorded on Fridays and Saturdays, then the average PM level would increase over the period from Sunday through Thursday. A more detailed discussion of seasonal and "day-of-the-week" trends in PM level is provided in Section 5.2.1.

The arithmetic averages of PM10 concentrations recorded at the 34 ambient monitoring sites during the baseline year are shown in Figure 4-3. The sites in Figure 4-3 are ranked (from top to bottom) in order of decreasing PM10 concentration. As a reference, the Law 4/1994 PM10 standard of 70 μg/m³, averaged over 24 hours, is indicated by the blue bars. The GOE has not adopted an annual average limit for PM10. The highest annual average PM levels, approximately 300 μg/m³, were recorded at monitoring Sites #19 and #20 in the heavily industrialized area of Shoubra El-Kheima. Annual average PM10 levels greater than 200 μg/m³ were recorded at the sites in the Tebbin, El-Massara and central Cairo areas. The lowest particulate levels, in the range of 113–124 μg/m³, were recorded at the Belbeis background site and at sites in the more remote cities of 6th of October and 10th of Ramadan. The annual average PM10 level recorded at the Heliopolis site, 144 μg/m³, was the lowest for a contiguous area of Cairo.

Statistics on the number of sampling events during which the maximum PM10 concentration was recorded at various sites are shown Table 4-3. The frequency shown in Table 4-3 is the number of maximum PM10 values recorded at the site divided by the total number of sampling events, 60, and is expressed as a percentage. The three sites with the highest frequency of maximum PM10 levels are in Shoubra El-Kheima (30 %), Tebbin South (18 %), and El-Sahel (15 %). The location of the Shoubra Site #20 is nominally downwind of a steel mill. The Tebbin South site is surrounded by several industries (steel mill, brick factories, and lead smelters). The El-Sahel site location is nominally downwind of lead smelters and numerous other industrial sources in Shoubra El-Kheima.

Figure 4-3:Baseline Year Average PM10 Concentrations at Ambient Monitoring Sites October 1998 through September 1999

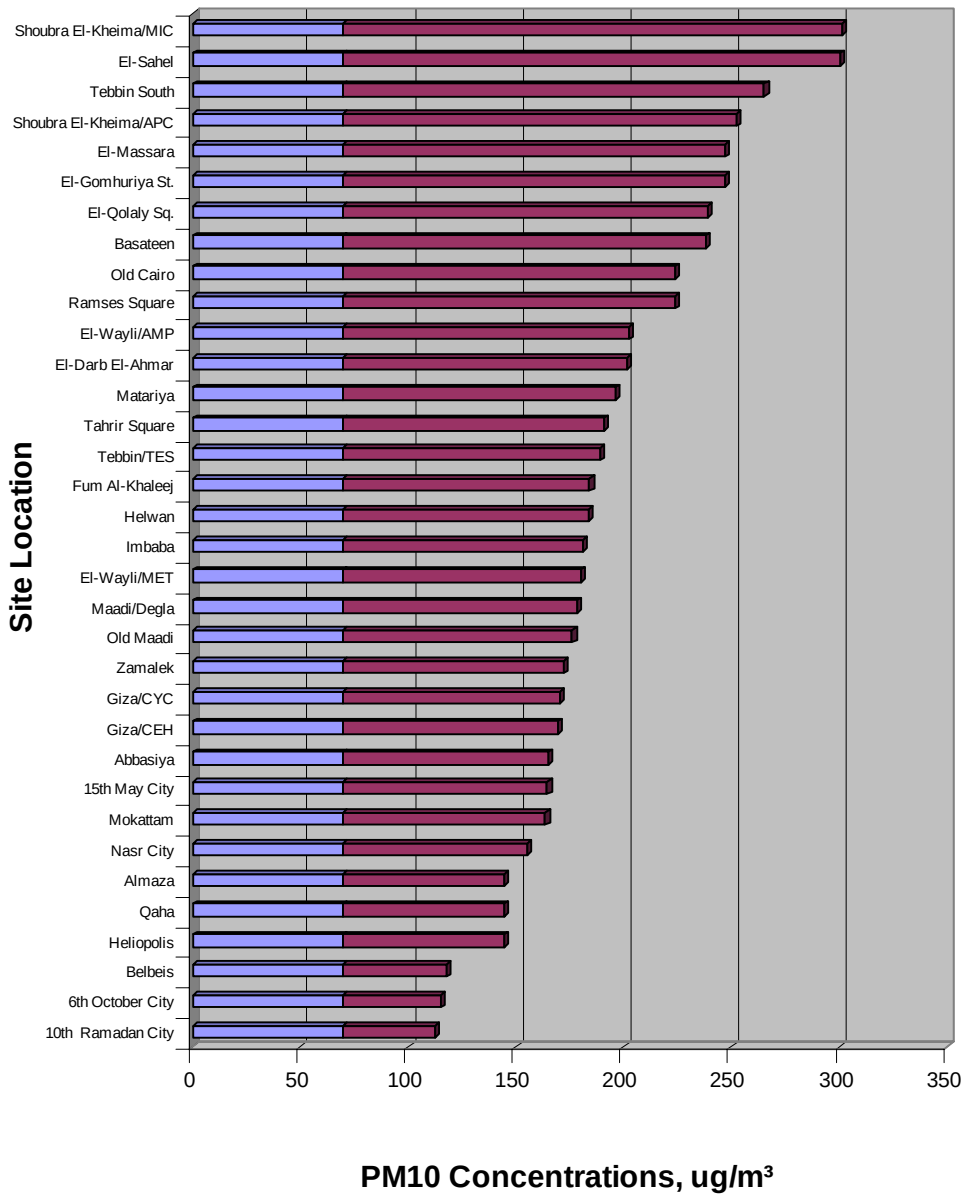

Blue + Red - PM10 Concentration
Blue - Law No. 4 PM10 Limit

Table 4-3: PM10 Monitoring Data Statistics

Site No.	Site Code	Site Location	#of Maximum Values [a]	Frequency, %	Law 4/1994 Attainment Days
20	MIC	Shoubra El-Kheima	18	30.0	0
07	TBS	Tebbin South	11	18.3	0
19	TTI	El-Sahel	9	15.0	0
08	UHC	Old Cairo	4	6.7	0
34	SBH	El-Massara	4	6.7	1
09	ERA	Ramses Square	3	5.0	0
01	EQS	El-Qolaly Square	2	3.3	0
29	LRC	Basateen	2	3.3	0
03	MET	El-Wayli	1	1.7	2
06	CAC	Maadi/Degla	1	1.7	4
21	DRC	Matariya	1	1.7	0
23	TES	Tebbin	1	1.7	0
25	HTI	Imbaba	1	1.7	0
27	MAY	15th May City	1	1.7	0
33	HFS	Helwan	1	1.7	1
02	GEM	El-Gomhuriya St.	0	0.0	0
04	NRC	Nasr City	0	0.0	1
05	FAK	Fum Al-Khaleej	0	0.0	0
10	CAI	Old Maadi	0	0.0	0
11	CEH	Giza	0	0.0	1
12	AAU	El-Darb El-Ahmar	0	0.0	0
13	OCT	6th October City	0	0.0	4
14	RAM	10th Ramadan	0	0.0	6
15	BLB	Belbeis	0	0.0	8
16	ATI	Mokattam	0	0.0	0
18	APC	Shoubra El-Kheima	0	0.0	0
22	AMP	El-Wayli	0	0.0	0
26	KFC	Qaha	0	0.0	1
28	HDM	Almaza	0	0.0	0
30	CYC	Giza	0	0.0	0
31	AUC	Tahrir Square	0	0.0	0
32	BIS	Zamalek	0	0.0	0
35	OLS	Heliopolis	0	0.0	3
36	EGS	Abbasiya	0	0.0	0
		Totals	60	100.0	32

a) Number of sampling events in which the highest PM10 concentration occurred at the site.

The last column of Table 4-3 shows, for each site, the number of days of the baseline year on which the PM10 level was below Law 4/1994 limit. At 30 sites, the PM10 levels exceeded the Law 4/1994 limit of 70μg/m³ (averaged over a 24-hour period) on all days on which valid PM samples were obtained. PM10 levels below the Law 4/1994, 24-hour limit were recorded at only 11 monitoring sites and for a total of only 32 days during the baseline year. Compliance with the Law 4/1994 limit was achieved on eight (8) days at the Belbeis site, six (6) days at the 10th of Ramadan City site, four (4) days each at the Maadi/Degla and 6th of October City sites, three (3) days at the Heliopolis site, two (2) days at the El-Wayli/MET site, and one (1) day each at the El-Massara, Helwan, Giza, Nasr City, and Qaha sites.

The PM10 levels for the various site classifications are shown in Figure 4-4. The PM10 concentration data shown in this diagram denote the average of all baseline year measurements performed at sites of similar land-use classification. The average PM10 concentration ranges from a maximum of 257 μg/m³ for the industrial sites to a minimum of 138 μg/m³ for the background sites. The order of the site classification, ranked in order of decreasing average PM10 concentration is: (1) industrial, (2) traffic, (3) mixed, (4) residential, (5) background.

The average PM2.5/PM10 ratios for all sites during the baseline year are shown in Figure 4-5. Annual statistics for this ratio are shown in an inset in Figure 4-5.

Although the PM2.5/PM10 ratio data shows numerous fluctuations, most of the ratio values are within one standard deviation (±0.13) of the annual average ratio (0.50). The average PM2.5/PM10 ratios for the sampling events on 25 October 1998 (0.68), 22 February 1999 (0.64), 6 March 1999 (0.65), and 3 August 1999 (0.67) slightly exceed the upper limit of the standard deviation range, which is 0.63. The average PM2.5/PM10 ratio for the sampling event on 27 August 1999 (0.31) exceeds the lower limit of the standard deviation range, which is 0.37. However, the average ratio for 27 August 1999 is based on measurements at only five (5) sites. The average ratio for the sampling event on 30 November 1998 (0.36) is very close to the lower limit of the standard deviation range. The higher the PM2.5/PM10 ratio, the greater the proportion (by weight) of PM in the 0–2.5 μm aerodynamic diameter size range. The contribution of all PM to the PM2.5 size fraction is typically generated by mobile, combustion, and industrial sources, and by photochemical and other atmospheric reactions that produce secondary aerosols, such as sulfates and nitrates. The lower the PM2.5/PM10 ratio, the greater the proportion (by weight) of PM in the 2.5–10 μm aerodynamic diameter size range. The sources of coarser PM are geological material suspended by the wind, air turbulence along roadways, construction activities, etc., in addition

to industries that use geological materials as feedstock, such as the cement industry.

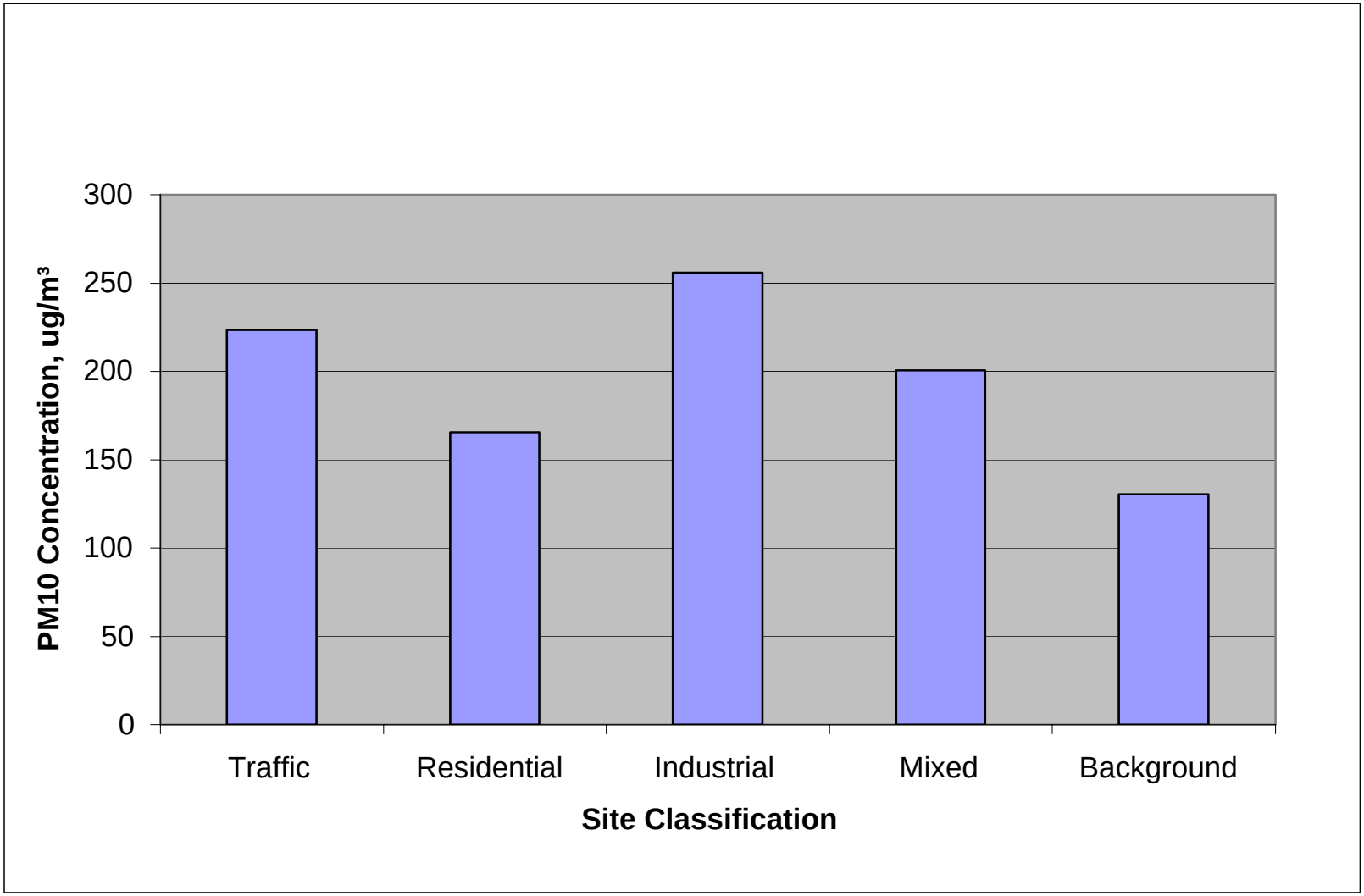

Figure 4-4: Annual Average PM10 Concentrations for Site Classifications October 1998 through September 1999

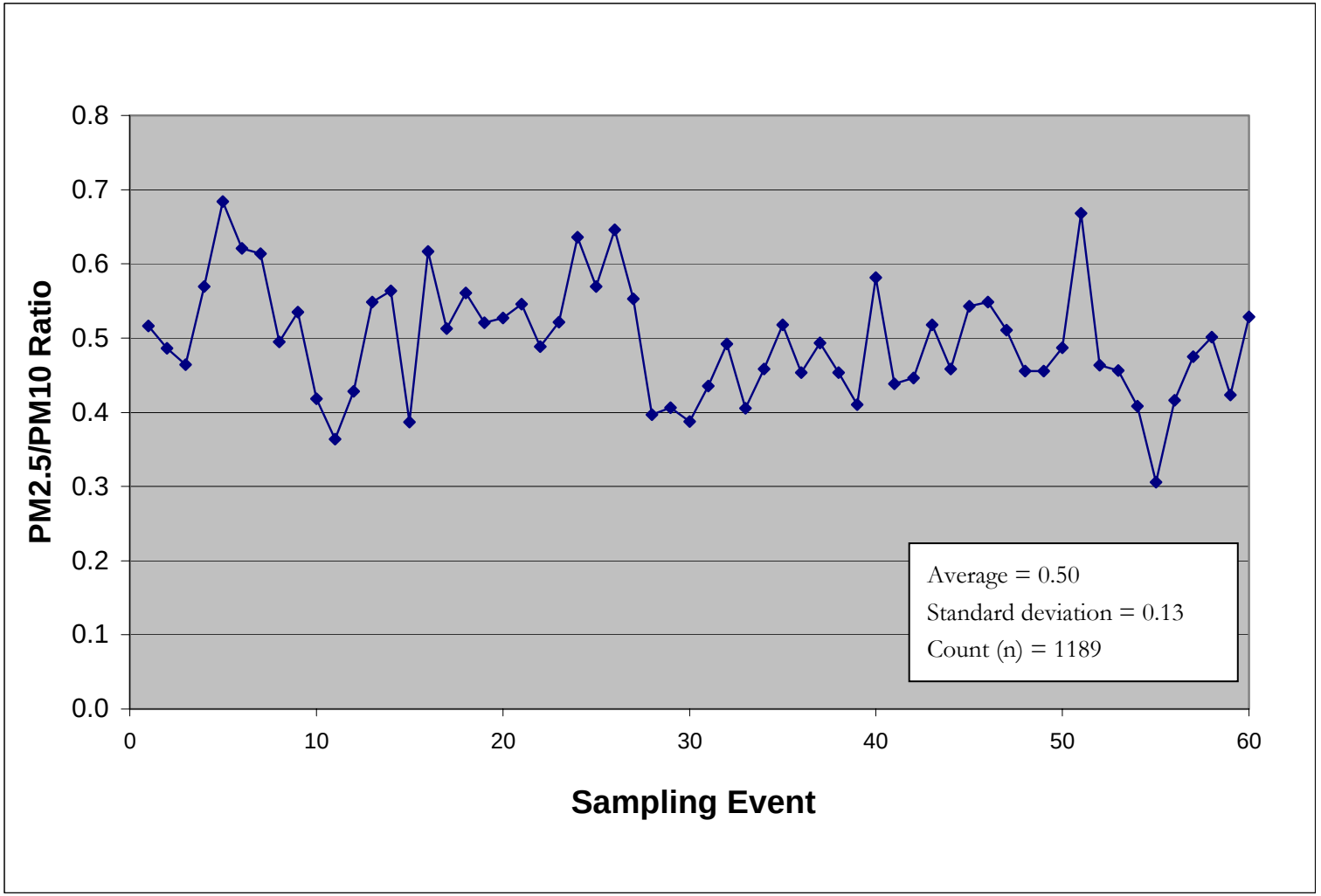

Figure 4-5: Average PM2.5/PM10 Ratios for Sampling Events during Baseline Year October 1998 through September 1999

Table 4-4: Monthly and Annual Statistics on PM2.5 Lead Measurements at CAIP Monitoring Sites

Site No.	Site Code	Site Location	PM2.5 Lead Concentration[a], μg/m³												Annual Site Statistics		
			Oct	Nov	Dec	Jan	Feb	Mar	Apr	May	Jun	Jul	Aug	Sep	Avg	Max	Count
01	EQS	El-Qolaly Sq.	3.55	2.45	0.94	1.34	2.43	0.64	0.55	1.77	1.16	1.96	0.82	0.90	1.56	7.97	43
02	GEM	El-Gomhuriya St.	3.08	2.20	2.17	0.35	3.06	1.34	0.42	1.88	1.59	0.61	2.43	1.83	1.60	6.81	53
03	MET	El-Wayli	1.06	0.76	1.99	0.34	ND	0.22	0.25	0.65	0.72	ND	1.38	1.20	0.66	4.59	48
04	NRC	Nasr City	0.48	0.80	1.18	0.22	ND	ND	0.25	ND	0.29	ND	ND	ND	0.41	3.92	41
05	FAK	Fum Al-Khaleej [b]	-	-	-	-	-	-	-	-	-	-	-	-	-	-	0
06	CAC	Maadi/Degla	0.61	0.75	2.00	0.43	ND	ND	ND	0.37	0.22	0.43	0.84	0.43	0.54	6.46	47
07	TBS	Tebbin South	4.33	1.99	0.54	1.17	0.87	ND	2.70	1.90	2.71	1.82	1.12	2.49	1.88	13.48	41
08	UHC	Old Cairo	1.40	1.16	1.22	0.66	0.71	0.60	0.28	0.84	0.66	0.51	ND	0.47	0.75	3.33	41
09	ERA	Ramses Square [b]	-	-	-	-	-	-	-	-	-	-	-	-	-	-	0
10	CAI	Old Maadi	1.12	0.61	2.09	0.30	0.19	0.47	0.29	0.68	0.33	0.54	0.55	1.22	0.62	3.66	44
11	CEH	Giza	0.77	0.97	0.97	ND	0.84	0.81	0.23	0.79	0.51	0.44	ND	ND	0.65	2.26	35
12	AAU	El-Darb El-Ahmar [b]	-	-	-	-	-	-	-	-	-	-	-	-	-	-	0
13	OCT	6th October City	ND	ND	ND	ND	0.25	0.36	ND	0.35	0.23	0.50	ND	0.48	0.28	0.95	44
14	RAM	10th Ramadan	0.20	0.26	0.32	0.24	0.24	ND	ND	ND	0.18	ND	0.79	ND	0.25	0.79	47
15	BLB	Belbeis	0.32	ND	0.85	ND	ND	ND	ND	0.31	0.42	ND	ND	0.81	0.33	1.85	45
16	ATI	Mokattam [b]	-	-	-	-	-	-	-	-	-	-	-	-	-	-	0
18	APC	Shoubra El-Kheima	21.39	7.16	9.74	8.91	12.83	13.07	23.54	49.05	37.23	21.50	30.88	20.73	20.30	98.07	51
19	TTI	El-Sahel	26.45	8.03	8.26	ND	25.25	7.08	24.64	20.58	14.05	9.84	47.94	10.12	18.59	158.40	51
20	MIC	Shoubra El-Kheima	6.42	4.66	5.44	6.14	4.50	4.12	3.11	3.52	3.71	1.57	1.29	1.34	3.97	14.66	48
21	DRC	Matariya	1.29	0.60	1.19	1.70	ND	ND	ND	ND	ND	0.72	ND	ND	0.59	5.32	44
22	AMP	El-Wayli [b]	-	-	-	-	-	-	-	-	-	-	-	-	-	-	0
23	TES	Tebbin	1.81	3.21	7.15	3.66	0.41	3.95	2.16	0.34	0.70	0.64	ND	0.68	2.24	27.79	44
25	HTI	Imbaba [b]	-	-	-	-	-	-	-	-	-	-	-	-	-	-	0
26	KFC	Qaha	ND	ND	0.66	ND	ND	ND	ND	0.35	0.30	ND	ND	ND	0.28	2.60	44
27	MAY	15th May City [b]	-	-	-	-	-	-	-	-	-	-	-	-	-	-	0
28	HDM	Almaza [b]	-	-	-	-	-	-	-	-	-	-	-	-	-	-	0
29	LRC	Basateen [b]	-	-	-	-	-	-	-	-	-	-	-	-	-	-	0
30	CYC	Giza [b]	-	-	-	-	-	-	-	-	-	-	-	-	-	-	0
31	AUC	Tahrir Square	1.44	2.23	1.41	0.30	1.57	0.72	ND	1.40	1.07	0.37	0.73	0.86	1.08	4.17	42
32	BIS	Zamalek	0.45	1.44	0.99	0.64	1.60	1.26	0.24	0.94	0.20	ND	1.65	ND	0.84	2.99	42
33	HFS	Helwan	0.59	0.87	2.24	0.84	ND	ND	ND	0.25	0.32	ND	ND	ND	0.60	5.01	46
34	SBH	El-Massara	0.53	0.67	3.05	0.91	0.20	0.33	0.19	ND	0.31	ND	ND	0.80	0.63	6.63	44
35	OLS	Heliopolis	ND	ND	1.36	0.18	ND	ND	ND	0.35	0.32	0.51	ND	0.51	0.36	3.60	49
36	EGS	Abbasiya	1.86	0.54	2.19	ND	ND	ND	ND	0.36	0.52	0.56	ND	0.55	0.62	5.75	42
Monthly Site Statistics		Average	3.98	1.82	2.46	1.44	2.57	1.73	2.83	3.82	3.43	2.08	4.16	1.66	Annual Statistics, All Sites		
		Maximum	56.29	21.75	36.60	31.25	32.67	42.99	98.07	80.51	59.06	74.28	158.40	21.85			
		Count	112	92	91	71	103	90	104	92	81	81	87	72	2.71	158.40	1076

(a) ND: Not Detected; lead minimum detection limit (MDL) is 0.17 μg/m³.
(b) PM2.5 measurement is not performed at this site

Table 4-5: Monthly and Annual Statistics on PM10 Lead Measurements at CAIP Monitoring Sites

Site No.	Site Code	Site Location	PM10 Lead Concentration[(a)], μg/m³												Annual Site Statistics		
			Oct	Nov	Dec	Jan	Feb	Mar	Apr	May	Jun	Jul	Aug	Sep	Avg	Max	Count
01	EQS	El-Qolaly Sq.	5.09	2.89	1.10	2.14	3.61	0.78	0.82	2.35	1.54	2.51	0.95	1.36	2.14	11.61	42
02	GEM	El-Gomhuriya St.	4.32	2.85	2.65	0.37	4.18	1.95	0.53	2.24	1.99	0.89	1.04	1.75	2.13	10.06	53
03	MET	El-Wayli	1.82	1.02	2.57	0.43	ND	0.25	0.26	0.70	1.00	ND	1.20	2.58	0.89	7.06	49
04	NRC	Nasr City	0.68	1.07	1.70	0.25	0.22	0.20	0.27	ND	0.39	ND	0.42	0.85	0.55	5.31	42
05	FAK	Fum Al-Khaleej	1.49	1.26	1.99	0.77	1.36	1.04	0.47	1.13	0.82	0.56	0.67	0.86	1.03	4.34	55
06	CAC	Maadi/Degla	0.87	1.04	3.23	0.54	ND	ND	ND	0.44	0.24	0.38	0.64	0.66	0.69	7.46	45
07	TBS	Tebbin South	4.85	2.35	0.77	1.53	0.99	ND	2.89	2.24	3.03	3.45	0.58	2.57	2.22	15.11	39
08	UHC	Old Cairo	1.89	1.84	2.60	0.94	0.99	1.05	0.35	1.17	0.92	0.60	0.44	0.79	1.14	4.84	43
09	ERA	Ramses Square	7.11	3.42	2.33	1.30	4.30	2.02	1.33	2.35	1.65	0.84	1.50	1.59	2.62	20.74	58
10	CAI	Old Maadi	1.41	0.82	2.32	0.45	0.24	0.73	0.36	0.91	0.61	0.67	0.57	1.47	0.88	4.89	45
11	CEH	Giza	0.96	1.47	1.30	ND	1.02	1.21	0.41	1.07	0.81	0.42	0.50	ND	0.87	2.83	36
12	AAU	El-Darb El-Ahmar	2.39	1.93	3.25	0.42	1.94	0.40	0.54	2.07	1.17	0.70	1.49	0.92	1.50	8.28	57
13	OCT	6th October City	0.18	0.43	ND	ND	0.33	0.53	0.18	0.42	0.24	0.45	0.38	0.56	0.34	1.25	44
14	RAM	10th Ramadan	0.38	0.32	0.40	0.28	0.25	0.20	0.19	ND	0.24	ND	0.51	ND	0.31	0.99	46
15	BLB	Belbeis	0.37	ND	1.25	ND	ND	0.22	ND	0.41	0.52	ND	ND	0.88	0.41	2.94	41
16	ATI	Mokattam	0.80	2.08	3.19	0.25	0.82	0.24	2.10	0.43	0.40	ND	1.04	0.77	1.04	9.79	60
18	APC	Shoubra El-Kheima	28.88	8.53	12.34	10.35	18.77	19.34	32.88	63.50	44.05	25.75	29.85	21.78	26.18	128.75	51
19	TTI	El-Sahel	39.90	9.84	11.50	ND	35.66	9.08	35.67	28.49	20.74	16.32	55.25	14.74	25.44	184.24	50
20	MIC	Shoubra El-Kheima	9.05	6.05	6.55	7.91	5.48	5.12	3.76	4.47	4.67	1.99	1.33	1.96	5.08	20.88	48
21	DRC	Matariya	1.66	1.01	1.37	2.05	ND	ND	ND	ND	0.19	0.78	0.40	0.49	0.76	6.76	42
22	AMP	El-Wayli	1.67	1.18	2.01	1.40	3.04	0.27	0.75	1.16	1.93	0.62	ND	2.04	1.40	10.98	53
23	TES	Tebbin	2.06	3.95	8.03	4.71	0.49	4.89	1.97	0.39	0.82	0.94	0.41	0.85	2.62	31.12	45
25	HTI	Imbaba	0.79	1.58	1.04	1.20	2.45	2.06	0.60	0.93	0.62	0.44	1.31	0.92	1.14	6.24	53
26	KFC	Qaha	0.18	ND	0.97	ND	ND	ND	0.17	0.36	0.32	ND	0.47	ND	0.34	4.19	42
27	MAY	15th May City	0.28	0.86	1.99	1.22	0.50	0.45	0.19	0.41	0.37	0.43	0.40	0.64	0.61	4.74	54
28	HDM	Almaza	1.14	0.77	1.62	0.37	ND	ND	ND	0.36	0.68	ND	0.53	0.65	0.57	4.87	59
29	LRC	Basateen	1.95	1.82	2.70	0.48	0.58	0.38	0.41	1.22	0.93	0.53	0.80	0.90	1.08	6.56	60
30	CYC	Giza	1.23	1.30	1.16	0.92	1.05	1.17	0.29	1.57	0.70	0.41	1.26	0.96	0.98	3.42	55
31	AUC	Tahrir Square	2.92	3.10	1.83	0.42	2.66	0.80	ND	1.60	1.34	0.40	0.82	1.10	1.64	6.87	41
32	BIS	Zamalek	0.67	1.88	1.31	0.87	2.03	1.68	0.30	1.32	0.30	0.44	1.87	ND	1.14	3.81	41
33	HFS	Helwan	0.68	1.05	2.83	0.99	0.21	ND	ND	0.43	0.40	ND	ND	ND	0.73	6.12	48
34	SBH	El-Massara	0.67	0.86	3.73	1.09	0.30	0.37	0.21	ND	0.45	ND	ND	1.03	0.78	8.39	45
35	OLS	Heliopolis	0.19	0.20	1.70	0.26	ND	ND	ND	0.37	0.41	0.49	ND	2.16	0.49	3.80	49
36	EGS	Abbasiya	3.22	0.69	2.34	ND	0.25	0.24	0.17	0.41	0.58	0.64	ND	1.07	0.82	7.39	41
Monthly Site Statistics		Average	4.40	2.09	2.80	1.45	2.87	1.82	2.88	3.43	3.14	2.08	3.75	1.83	Annual Statistics, All Sites		
		Maximum	79.88	23.56	46.53	36.52	41.30	63.72	133.61	106.53	74.33	85.76	184.24	32.87			
		Count	169	139	139	110	148	135	152	143	127	122	126	122	2.75	184.24	1632

(a) ND: Not Detected; lead minimum detection limit (MDL) is 0.17 μg/m³.

4.2 Ambient Lead Data

The results of all ambient air lead measurements performed during the baseline year are given in Vol. II, Appendices C and D. Summaries of Pb2.5 and Pb10 monitoring data are presented in Tables 4-4 and 4-5 above, respectively. The tables show the following statistical values:

- The arithmetic average values of the Pb2.5 and Pb10 measurements performed at each site during each month of the baseline year;
- The arithmetic average and maximum values of Pb2.5 and Pb10 measurements performed at all sites during each month of the baseline year;
- The arithmetic average and maximum values of Pb2.5 and Pb10 measurements performed at each site during the baseline year;
- The arithmetic average and maximum values of Pb2.5 and Pb10 measurements performed at all sites during the baseline year;
- The number (count) of valid Pb2.5 and Pb10 measurements obtained from each sampling event and each site during the baseline year and the total number of valid measurements obtained during the baseline year.

The arithmetic average of all valid lead measurements performed at each monitoring site during the baseline year is shown in Figure 4-6. In this diagram, sites are ranked (from top to bottom) in order of decreasing lead concentration. The green bars represent the Law 4/1994 lead limit of 1 $\mu g/m^3$ (annual arithmetic average). The highest annual average lead levels were recorded at Site #18 in Shoubra El-Kheima (26.2 $\mu g/m^3$) and at Site #19 in El-Sahel (25.4 $\mu g/m^3$).

Baseline year average lead concentrations in the range of approximately 2–5 $\mu g/m^3$ were recorded at Site #20 in Shoubra El-Kheima; Sites #1, #2, and #9 in the Central Cairo area; and Sites #7 and #23 in the Tebbin area. For the remaining 26 sites, baseline year average lead levels were <2 $\mu g/m^3$ at 7 sites and ≤ 1 $\mu g/m^3$ at 19 sites.

The maximum lead concentration recorded during each of the baseline year sampling events is shown in Figure 4-7. The highest lead concentration during the baseline year, 184.2 $\mu g/m^3$, was recorded on 15 August 1999 at Site #19 in the El-Sahel District. Lead concentrations exceeding 50 $\mu g/m^3$ were recorded at the Shoubra El-Kheima and El-Sahel Sites during 11 of the baseline year sampling events. The El-Sahel and Shoubra El-Kheima Sites #18 and #20, where the highest baseline year lead levels were recorded, are approximately 700 m and 300 m, respectively, downwind (south) of secondary lead smelters. Data in Figure 4-7 shows that ambient lead levels exhibit a high temporal variability and

that the concentration fluctuations cover a wide range. The temporal variation and concentration fluctuations probably result from a combination of meteorological conditions and production schedules of the lead smelters. CAIP sites are situated so that maximum impact of the lead smelter emission at the site occurs when the wind is from the NNW to the NNE direction, i.e. the sites are SSW to SSE of the lead smelters. When wind deviates from a NNW to NNE direction, lower lead concentrations are recorded. Occasionally, especially during the months of December and January, the wind blows from a southwesterly direction, in which case the CAIP sites are upwind of the lead smelters. Under these meteorological conditions, lead levels near background values may be recorded at sites where normally the highest lead levels are observed. Obviously, lead levels will also be low when the lead smelters are not in operation.

The presence of a seasonal trend in the ambient lead concentration is not evident from the baseline year data. However, a day-of-the-week trend in lead levels is clearly evident. The indicated trend is that lead levels are low on Friday, then increase over the period from Saturday through Thursday. A discussion of the seasonal and "day-of-the-week" trends in ambient lead levels appears in Sec. 5.3.1.

The Pb10 levels for the various site classifications are shown in Figure 4-8. The lead concentration data shown in Figure 4-8 is the arithmetic average of all baseline year Pb10 measurements performed at sites of similar classification. The average Pb10 concentration ranges from a maximum of approximately 12 $\mu g/m^3$ for the industrial sites to a minimum of 0.4 $\mu g/m^3$ for the background sites. The order of the site classification, ranked in decreasing average Pb10 concentration, is: (1) industrial, (2) traffic, (3) mixed, (4) residential, (5) background.

Figure 4-6: Baseline Year Average Pb10 Concentrations at Ambient Monitoring Sites

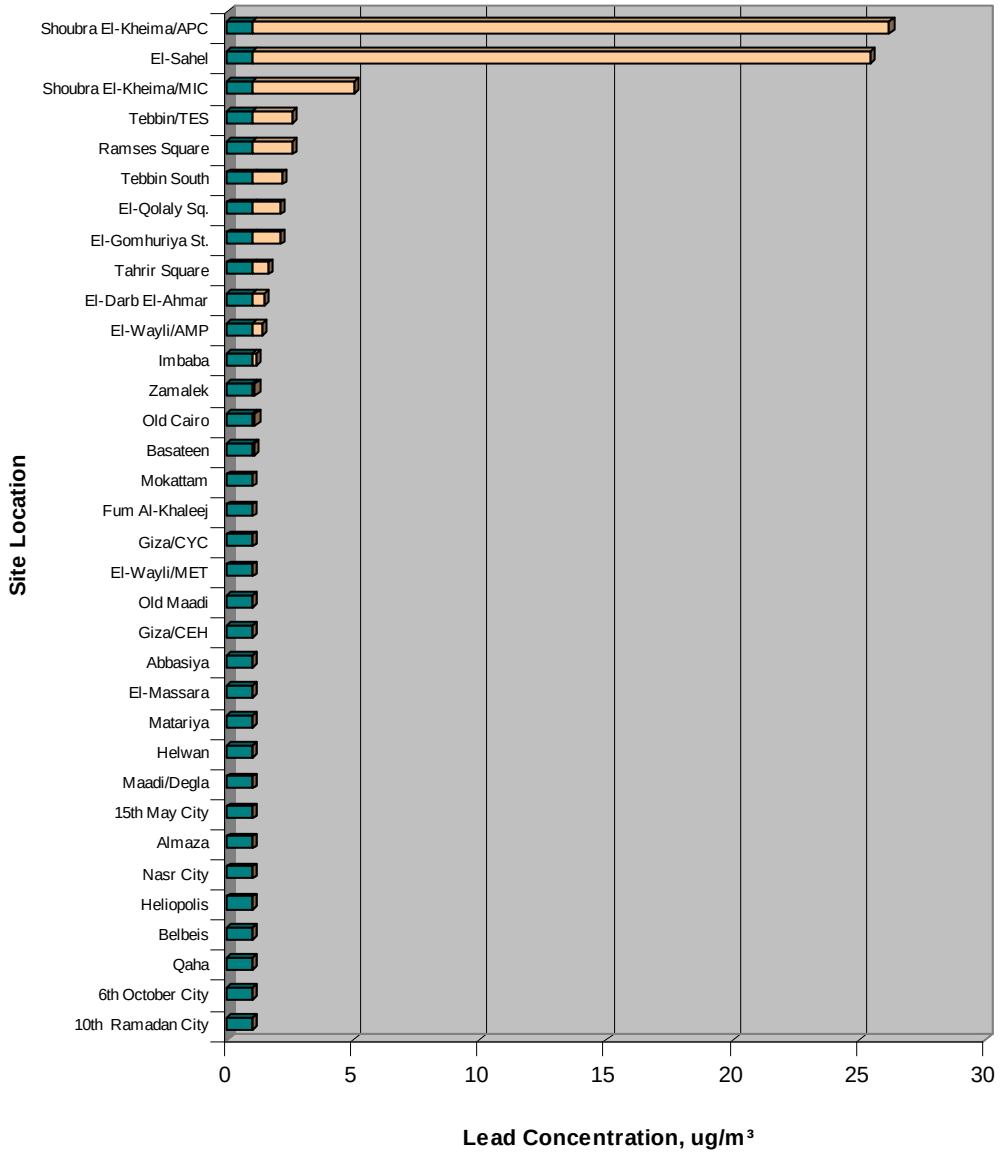

Green + Orange - Lead Concentration
Green - Law No. 4 Lead Limit

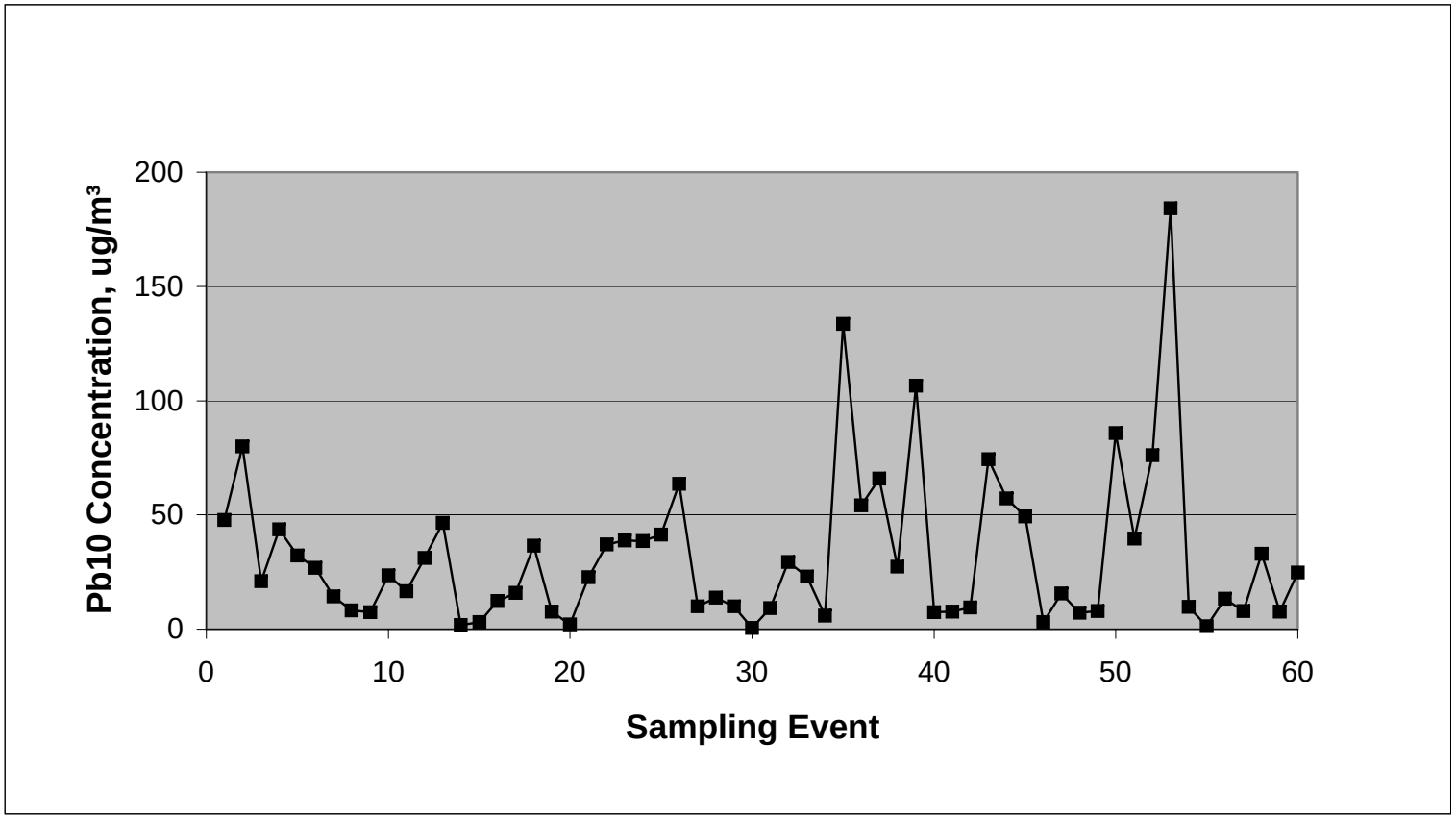

Figure 4-7: Maximum Lead Concentrations for Sampling Events during Baseline Year October 1998 through September 1999

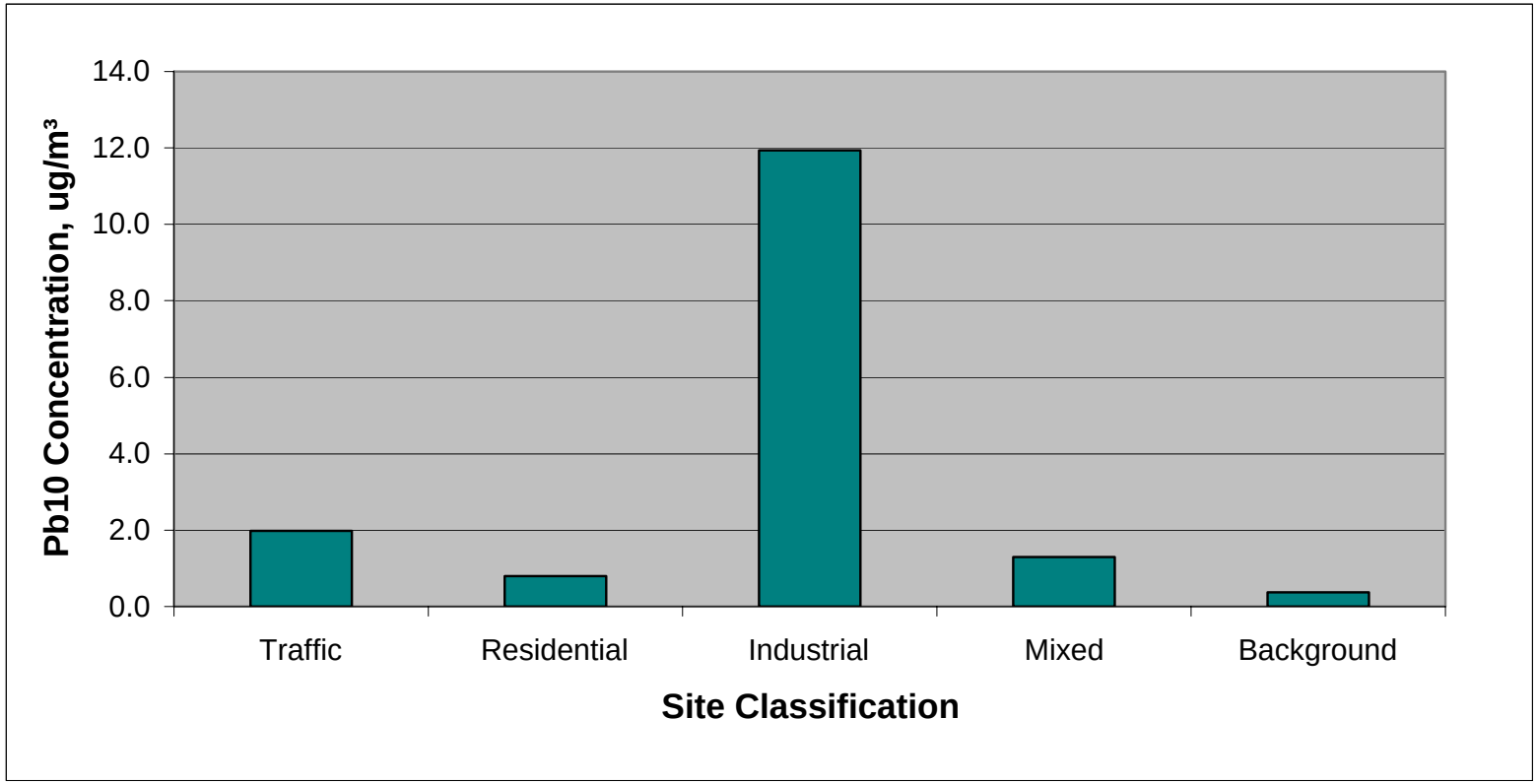

Figure 4-8: Annual Average Lead Concentration for Site Classifications October 1998 through September 1999

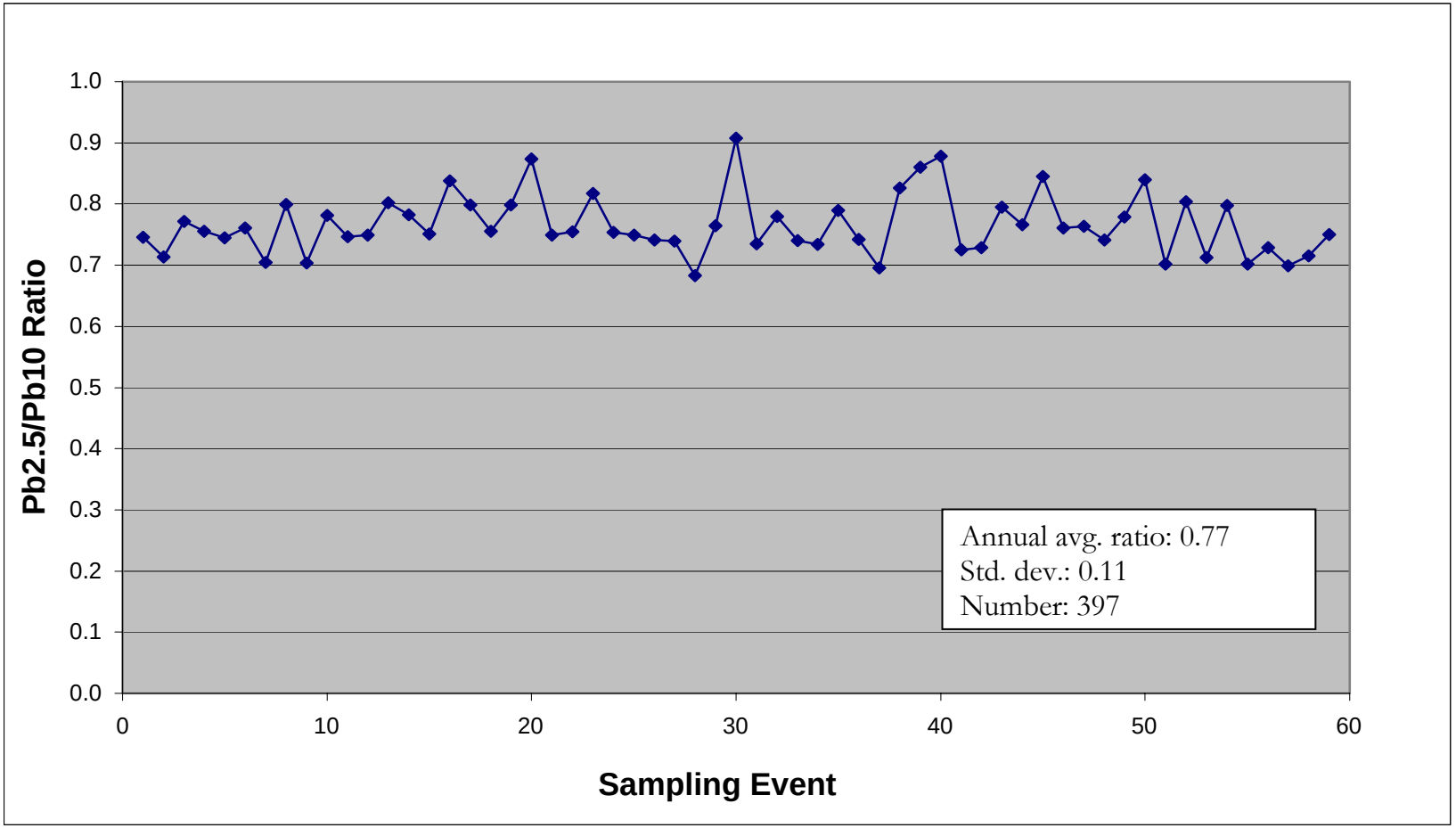

Figure 4-9: Average Pb2.5/Pb10 Ratios for Sampling Events during Baseline Year October 1998 through September 1999

Table 4-6 indicates statistical results of analyzing the lead data collected. The sites are sorted according to the annual average lead concentration. Statistics on the number of sampling events, during which lead concentrations greater than 1μg/m³ were recorded at various sites, are shown in Column #5. The frequency, shown as a percentage, Column #6, denotes the number of sampling events with lead concentration greater than 1 μg/m³ at the site divided by the total number of valid samples collected at the site during the baseline year. Column #7 shows the number of sampling events for which the maximum lead concentration was recorded at the various sites in the network. Column #8 shows the baseline year average lead concentration at all the ambient monitoring sites in order of decreasing concentration. Column #9 indicates whether the annual average lead concentration recorded at the site exceeds the Law 4/1994 ambient lead limit of 1 μg/m³ (annual average). The monitoring results show that the limit was exceeded at 15 sites, while the annual average lead levels are below the limit at 19 sites. The sites where the limits were exceeded are located in Shoubra El-Kheima, central Cairo, and Tebbin.

The arithmetic average of the Pb2.5/Pb10 ratio computed for each sampling event during the baseline year is shown in Figure 4-9. Each point on the graph represents a sampling event. The sampling event ratio values are the arithmetic average of all paired Pb2.5 lead and Pb10 lead measurements performed during the sampling event. The Pb2.5/Pb10 lead ratio data shows some sampling-event-to sampling-event variation, however, all except one ratio value are within one standard deviation (±0.11) of the annual average ratio (0.77). The average PM2.5/PM10 ratio for the sampling event on 5 April 1999 (0.91) exceeds the upper limit of the standard deviation range (0.88). However, the 5 April 1999 average ratio is based on only two measurements. None of the average Pb2.5/Pb10 ratios exceed the lower limit of the standard deviation range (0.66).

Since lead has been removed from gasoline sold in Cairo, the primary source of airborne lead is secondary lead smelters and, to a lesser extent, lead found in emissions from other non-ferrous metallurgical industries. Lead in emissions from secondary lead smelters is primarily in a particle size range of less the 1 μm. Therefore, it is expected that a high proportion of lead would be found in the PM2.5 size fraction and that a high value would be obtained for the ratio of lead in the PM2.5 and PM10 size fractions.

Table 4-6: Lead Monitoring Data Statistics

Site No. (a)	Site Code	Site Location	Valid Samples	No. Samples >1 μg Pb/m³	% Samples >1 μg Pb/m³	No. Max Values (b)	Annual Avg μgPb/m³	Law 4 Attained (c)
18	APC	Shoubra El-Kheima	51	42	82.4	22	26.2	No
19	TTI	El-Sahel	50	41	82.0	21	25.4	No
20	MIC	Shoubra El-Kheima	48	41	85.4	7	5.1	No
23	TES	Tebbin	45	14	31.1	5	2.6	No
09	ERA	Ramses Square	58	34	58.6	0	2.6	No
07	TBS	Tebbin South	39	19	48.7	1	2.2	No
01	EQS	El-Qolaly Square	42	25	59.5	0	2.1	No
02	GEM	El-Gomhuriya St.	53	24	45.3	0	2.1	No
31	AUC	Tahrir Square	41	22	53.7	0	1.6	No
12	AAU	El-Darb El-Ahmar	57	22	38.6	1	1.5	No
22	AMP	El Wayli	53	25	47.2	0	1.4	No
25	HTI	Imbaba	53	19	35.8	0	1.1	No
32	BIS	Zamalek	41	16	39.0	0	1.1	No
08	UHC	Old Cairo	43	21	48.8	0	1.1	No
29	LRC	Basateen	60	20	33.3	0	1.1	No
16	ATI	Mokattam	60	12	20.0	1	1.0	Yes
05	FAK	Fum Al-Khaleej	55	20	36.4	0	1.0	Yes
30	CYC	Giza	55	23	41.8	0	1.0	Yes
03	MET	El Wayli	49	12	24.5	1	0.9	Yes
10	CAI	Old Maadi	45	12	26.7	0	0.8	Yes
11	CEH	Giza	36	12	33.3	0	0.9	Yes
36	EGS	Abbasiya	41	9	22.0	0	0.8	Yes
34	SBH	El Massara	45	10	22.2	0	0.8	Yes
21	DRC	Matariya	42	8	19.0	0	0.8	Yes
33	HFS	Helwan	48	7	14.6	1	0.7	Yes
06	CAC	Maadi/Degla	45	5	11.1	0	0.7	Yes
27	MAY	15th May City	54	7	13.0	0	0.6	Yes
28	HDM	Almaza	59	6	10.2	0	0.6	Yes
04	NRC	Nasr City	42	4	9.5	0	0.6	Yes
35	OLS	Heliopolis	49	4	8.2	0	0.5	Yes
15	BLB	Belbeis	41	3	7.3	0	0.4	Yes
26	KFC	Qaha	42	1	2.4	0	0.3	Yes
13	OCT	6th October City	44	2	4.5	0	0.3	Yes
14	RAM	10th Ramadan	46	0	0.0	0	0.3	Yes
All Events, All Sites			1632	534		60	2.8	No: 15 Yes: 19

(a) Sites are ranked in decreasing order of the annual average lead concentration.
(b) Number of sampling events for which the maximum PM10 concentration occurred at the site.
(c) Law 4/1994 specifies an ambient air lead limit of 1 μg/m³ based on the annual arithmetic average.

4.3 Source Site Measurements

The results of PM and lead measurements at the two locations characterized as source sites (Sites #17 and #24) are shown in Vol. II, Appendix E. The monthly average PM10 concentrations at the two source sites, LSA and LSB, are shown below in Figures 4-10 and 4-11, respectively. The monthly average PM10 levels at Site #17 (LSA) range from 238–605 μg/m³ and are 1.5–2.7 times the average monthly PM10 levels for the ambient sites. The maximum PM10 concentration measured at Site #17 (LSA) is 909 μg/m³. The PM10 levels at Site #24 (LSB) range from 200–452 μg/m³ and are 1–3 times the average monthly PM10 levels for the ambient sites. The maximum PM10 concentration recorded at Site #24 is 734 μg/m³.

The monthly average Pb10 concentrations at the two source sites are shown in Figures 4-12 and 4-13. The monthly average lead levels recorded at Site #17 (LSA) range from 15–67 μg/m³. The maximum lead concentration measured at Site #17 (LSA) is 135 μg/m³. The monthly average lead levels recorded at Site #24 (LSB) range from 1–142 μg/m³. The maximum lead concentration measured at Site #24 (LSB) is 217 μg/m³.

The higher levels of PM and lead measured at the source sites result from fugitive emissions emitted from the secondary lead smelter operations. The variations in the lead concentrations measured at source Site #24 (LSB) reflect that the facility does not operate on a regular schedule due to lack of feedstock (used batteries).

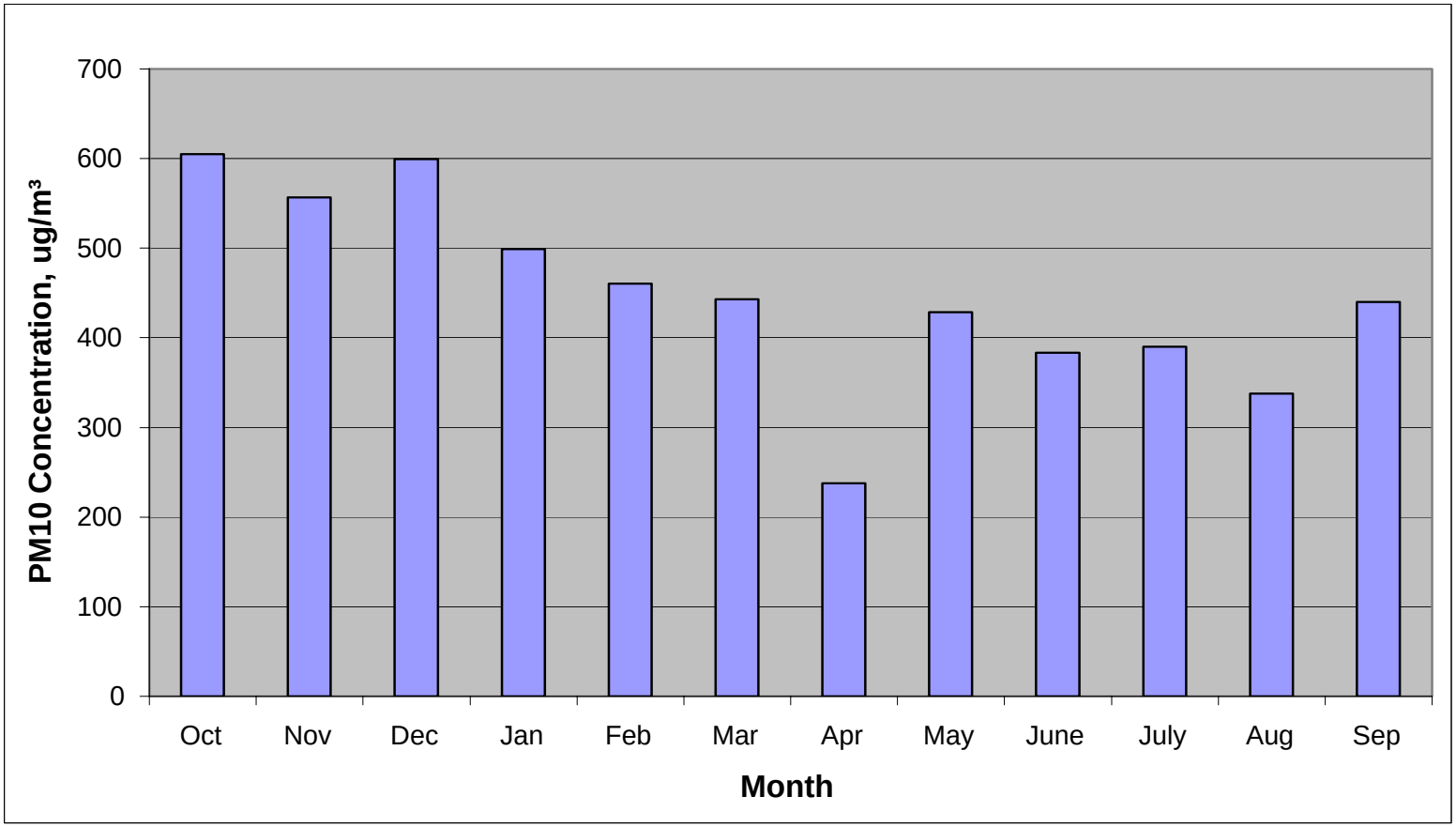

Figure 4-10: Average Monthly PM10 Concentration at Source Site LSA October 1998 through September 1999

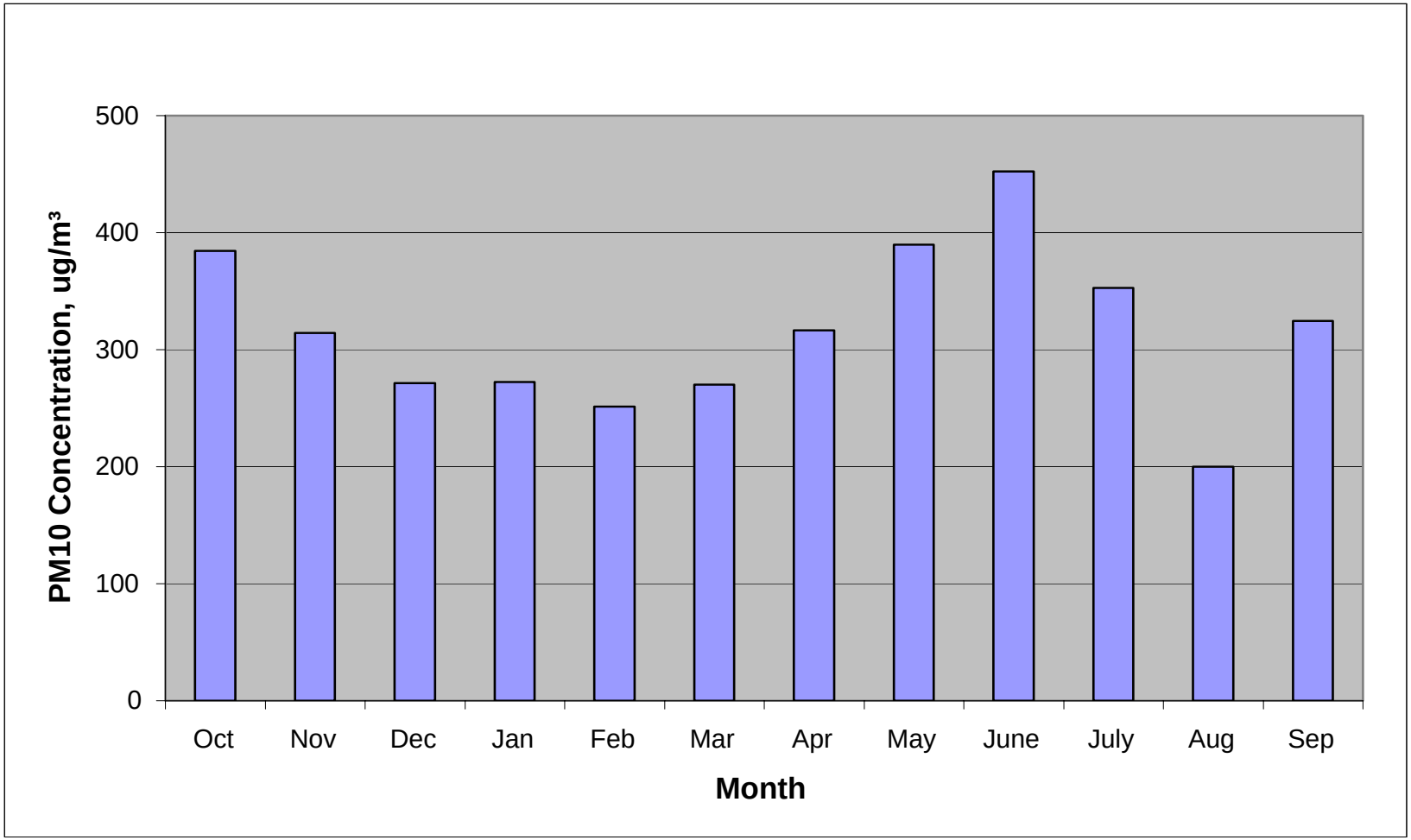

Figure 4-11: Average Monthly PM10 Concentrations at Source Site LSB October 1998 through September 1999

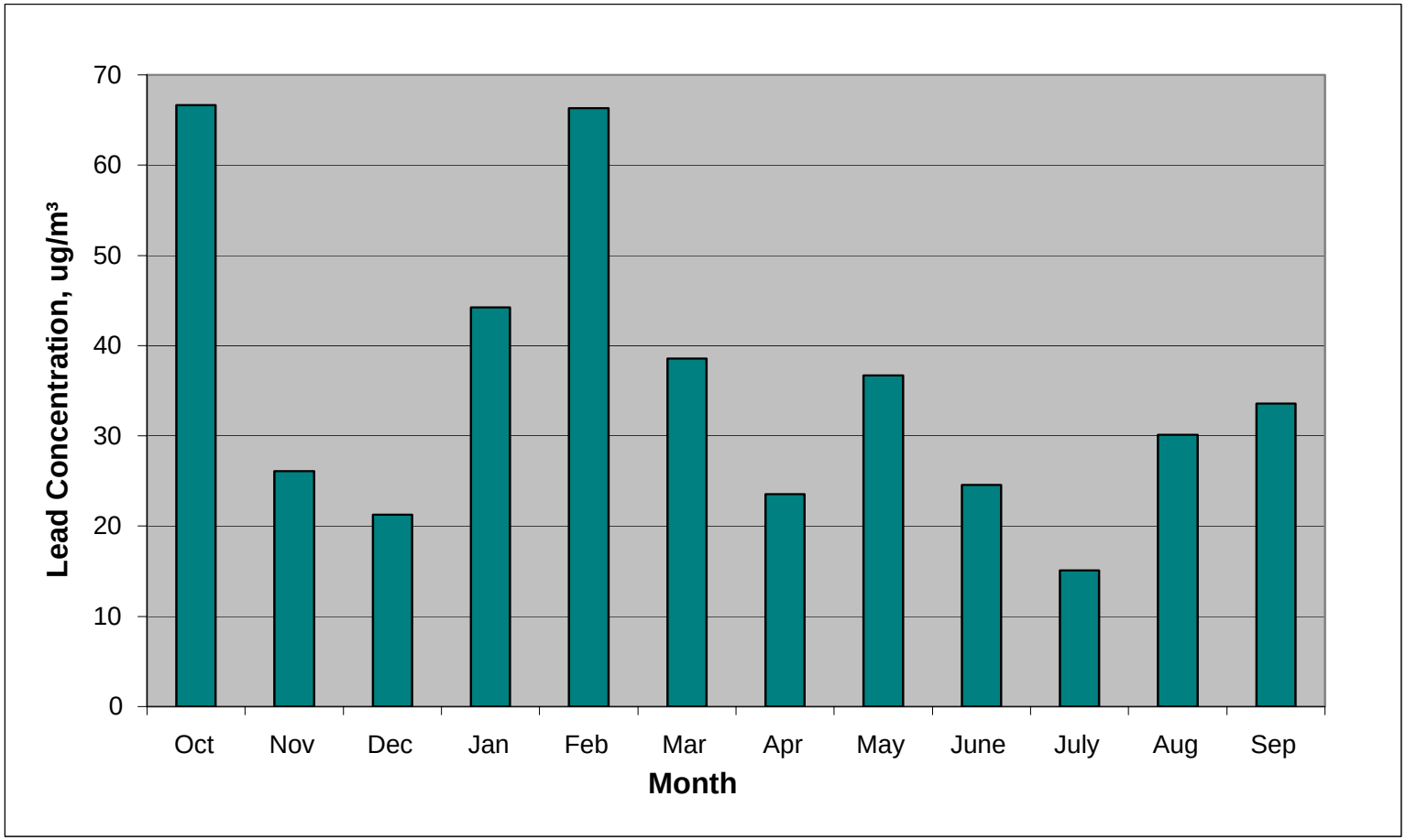

Figure 4-12: Average Monthly Lead Concentrations at Source Site LSA October 1998 through September 1999

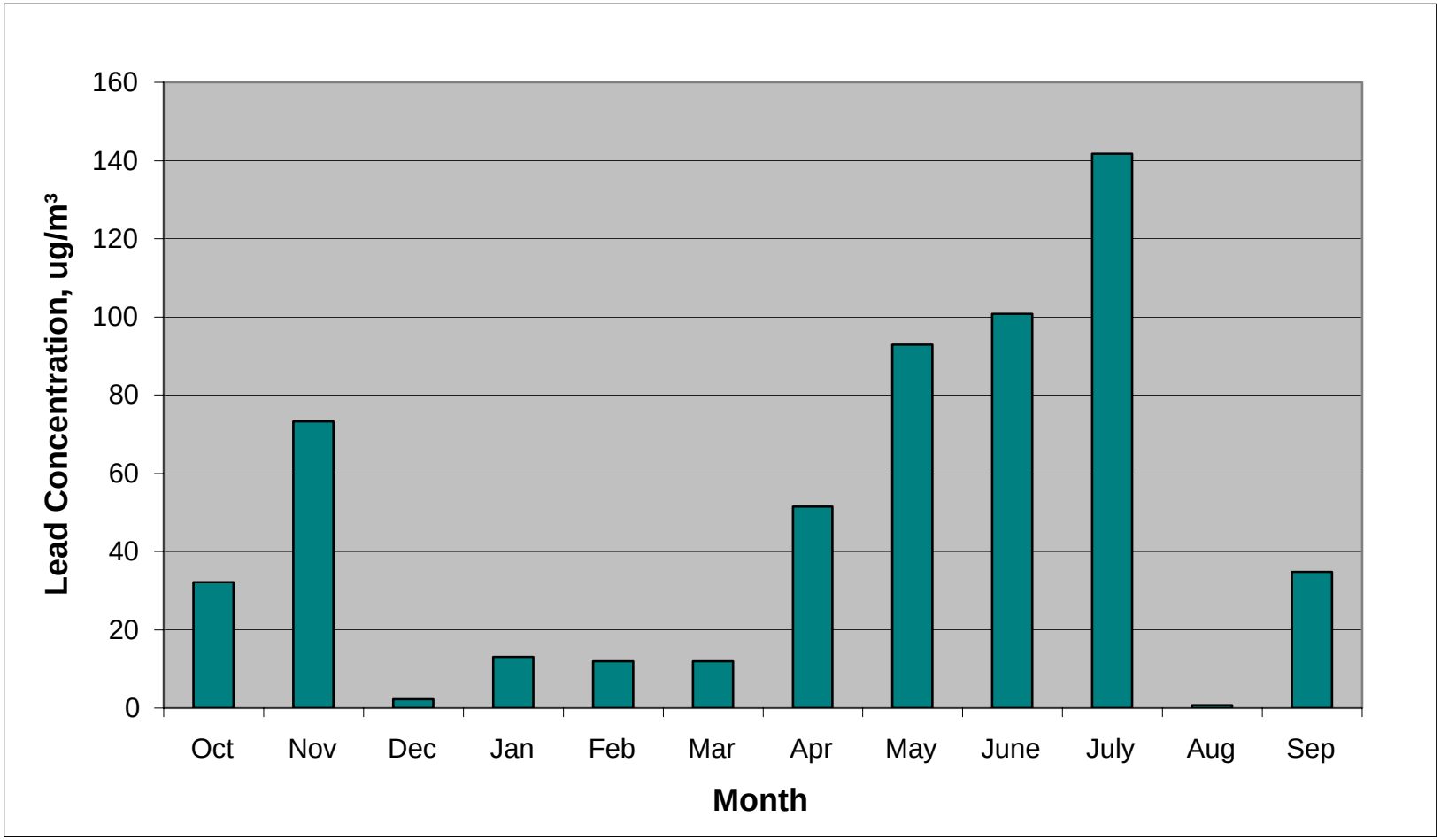

Figure 4-13: Average Monthly Lead Concentrations at Source Site LSB October 1998 through September 1999

4.4 Meteorological Measurements

Meteorological data collected during the baseline year is shown in Vol. II, Appendices F-J. Tables in these Appendices provide the average daily, monthly, and annual values of wind speed (WS), wind direction (WD), ambient temperature (AT), and barometric pressure (BP) recorded at sites in Maadi (Site #10), Belbeis (Site #15), Tebbin (Site #24), and Qaha (Site #26). Hourly average data for the meteorological parameters are available, but a hard-copy compilation of these data (1460 pages) is too bulky to be included in this report.

Wind data for the baseline year, displayed in windroses, is presented in Vol. II, Appendix J. Monthly average wind speed and wind direction data were used to prepare the windroses. A set of windroses prepared using annual average wind data from the four meteorological monitoring sites is shown in Figure 4-14. The windroses are constructed by segregating the wind speed and direction data by compass direction into 16 groups, each group containing data for a 22.5-degree arc. Wind direction during the averaging period (one year in Figure 4-14) is indicated by the different directions in which the 22.5-degree cones radiate toward the center of the windrose. The length of the cone indicates the frequency of the wind from the given direction. A scale with frequency, expressed as a percentage, is located at the bottom right side of each windrose. The wind speed range and wind speed range frequency are indicated by the areas of different shading and length of sections of the cones. The shading/wind speed scale is shown to the right of the windrose.

The windroses of annual wind conditions presented in Figure 4-14 show that winds in Cairo blow from a northwesterly to northeasterly direction most of the year. Winds from the SE direction occur most frequently during the months of December and January. The windrose for the Tebbin site shows a strong westerly wind component that is not evident at the other monitoring sites.

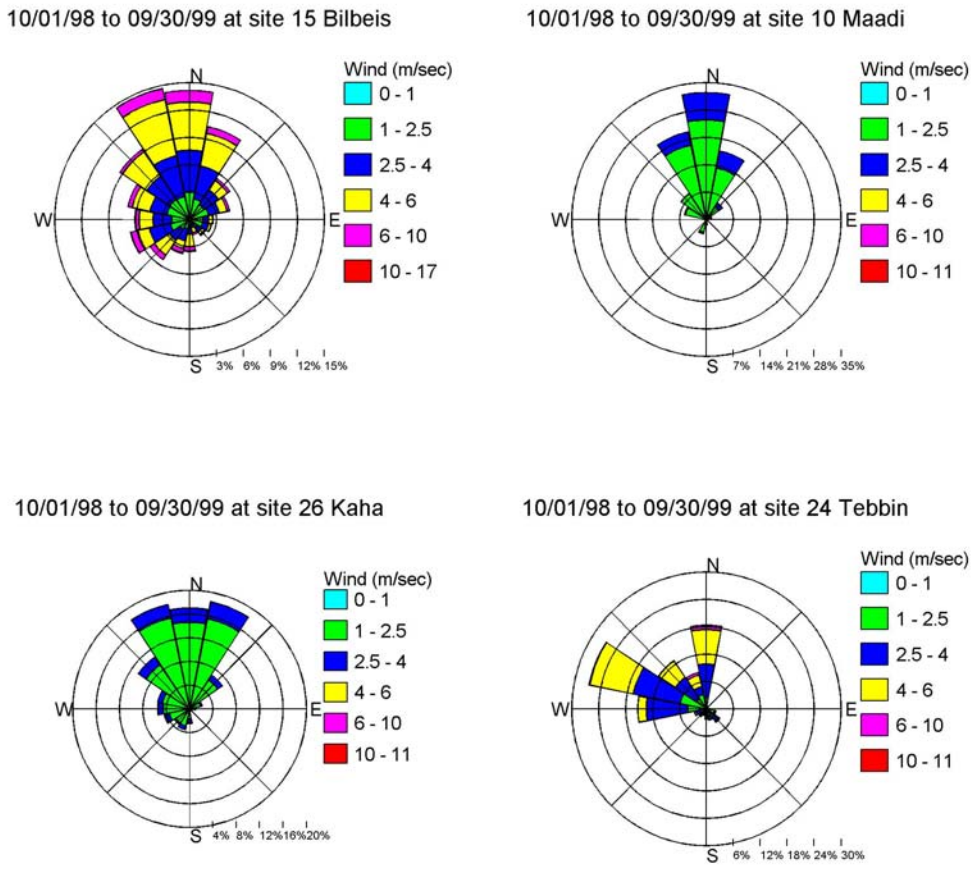

Figure 4-14: Windroses of Annual Average Wind Conditions

Chapter Five
Data Analysis and Characterization

Ambient air pollutants are characterized by a high variability in both space and time, and by complex physico-chemical processes governing their fate and transport in the atmosphere. Using a deterministic approach that solves the physical laws governing ambient air pollutants requires a very sophisticated model and results in a high numerical complexity that would be prohibitive for this study. Hence in this analysis we use a stochastic approach, which offers an efficient alternative to the complex physical-based models, and leads to accurate mapping of the ambient air pollutants. Other studies have demonstrated the usefulness of the stochastic approach when mapping ambient air pollutants such as ozone [8] or PM10 [9] and when studying the health effects associated with environmental exposure [10].

The stochastic estimation technique used in this analysis is the BME method. BME is a novel stochastic method of modern geostatistics, which provides a rigorous framework to account for hard data (exact measurements), as well as soft information (expert knowledge, inaccurate measurements, etc.), and physical laws governing ambient air pollution. BME is a more powerful and general method than the traditional methods of geostatistics. It reduces to the well-known kriging case under the proper set of limiting assumptions (e.g., when using only hard data) and leads to a more accurate estimation when additional information (e.g., soft data, non-Gaussian distribution) is included in the analysis [11–16]. Additionally, a unique feature of BME is the ability to incorporate physical laws such as those governing air pollutants [17–18]. This feature makes it possible to extend the analysis presented herein by incorporating meteorological parameters and opens the door to near-term forecasting of air quality.

In the analysis of the CAIP baseline year monitoring data, the BME method is used to produce maps showing the estimated distribution of daily PM and lead concentrations over Greater Cairo, as well as plots displaying the temporal variation of estimated concentrations at each monitoring site. The BME method also provides an assessment of the estimation accuracy of the maps and temporal plots by means of confidence intervals. Using the maps of daily estimated PM and lead ambient concentration, the general temporal and spatial characteristic of PM

and lead are analyzed for the baseline year. The general characteristics of PM and lead during the baseline year provide a benchmark assessment of the current level of pollution in Cairo, which will be useful for designing pollution mitigation measures and assessing their efficiency.

In this chapter, the BME data analysis methodology is explained, and then the analysis and mapping results for particulate matter and lead are presented.

5.1 Data Analysis Methodology

5.1.1 The Bayesian Maximum Entropy Framework

Two key issues that need to be addressed when mapping air pollutants are:

- the distribution of air pollutants exhibits a high variability in both space and time, and,
- the measurements of air pollutants at monitoring stations may have varying degree of reliability.

The BME method offers a rigorous framework to address these issues. In the first stage of the analysis, BME processes the space/time variability of the air pollutants by means of the covariance function. The covariance function is a statistical moment describing the general property of air pollutants and is incorporated in the BME analysis as 'general knowledge'. In the second stage (also called 'posterior stage'), BME processes specific information about the air pollutants, such as exact measurements (hard data); and readings of non-discrete values, expert opinions, etc. (soft data). This information that is incorporated during the posterior stage is referred to as 'specific knowledge' because it relates to information collected at a specific site location and specific times. Once the general and specific knowledge is processed, BME provides estimated values of the air pollutant concentrations at locations and times where measurements have not been performed. By estimating PM and lead at the nodes of a regular grid covering the Greater Cairo area, it is possible to obtain a map showing the spatial distribution of PM and lead at a given time. Similarly, by estimating PM and lead at different points in time for a specific monitoring site, a plot can be generated that shows the temporal profile of the estimated air pollutant concentration at that monitoring site.

One aspect of primary importance when generating the spatial maps and temporal plots of air pollutants is the accuracy of these maps and plots. The estimation of pollutant concentrations in areas between monitoring sites may introduce an interpolation error. This interpolation error increases as distance from the monitoring sites increases. BME is a stochastic estimation method and hence it

provides a very accurate measure of the accuracy estimation, by means of the confidence intervals. In the following sections, confidence intervals are reported along with the estimated concentration data.

5.1.2 Representation of the Raw Measurements by Means of Hard and Soft Data

The data collected at the CAIP monitoring stations are checked for data quality using a data validation procedure. A set of validation flags is used to characterize each measurement, and only valid measurement values are used for data analysis and interpretation. An independent assessment of the data quality of the valid measurements was performed as part of this mapping analysis by using collocated measurements (at Sites #19 and #24) and it was found that the measurements were of good quality. Since these measurements are considered exact measurements, they were modeled as 'hard data' in the BME methodology.

Measurements of airborne lead concentration frequently yielded results that were equal to or below a minimum detection limit (MDL) of 0.17 μg Pb/m³. A discrete value cannot be assigned to these samples; however, it is known that the concentration is in a range between 0 and a MDL of 0.17 μg/m³. Although the MDL data are not discrete values, they provide valuable information that can and should be used in the data analysis. Fortunately, the BME methodology permits incorporation of the MDL data as soft data of the interval type, where the lower and upper boundaries of the interval are set to 0 μg/m³ and the MDL 0.17 μg/m³, respectively. For example, in the case of data points flagged as MDL, the information used in the BME analysis is that the lead at that site had a concentration that could be anywhere between 0 and 0.17 μg/m³.

5.1.3 PM and Lead Data Distribution and Transformation

The histogram of PM and lead measurement values is shown in Figure 5-1. For display purposes the values shown on Figure 5-1 are truncated at 550 μg/m³ for PM10, and at 7.5 μg/m³ for lead, but note that the maximum recorded PM10 and lead (PM10 size fraction) concentrations during the baseline year were 858 μg/m³ and 184 μg/m³, respectively. It is evident from Figure 5-1 that the distributions of PM and lead are skewed toward extremely high values (particularly in the case of lead values), and hence the usual assumption of Gaussian-distributed variables is not valid. Consequently, it is necessary to use the log transform of the measurement values in the mapping analysis. Using the log of the PM and lead concentrations produces log-transformed variables which may better be approximated as Gaussian-distributed variables, and results in a more accurate estimation of ambient air pollutant distribution. Consequently, the BME mapping analysis described in this report is applied to the log-transform of PM and lead

values, and the estimated values are transformed back to the original scale before being presented in the maps and the figures included below.

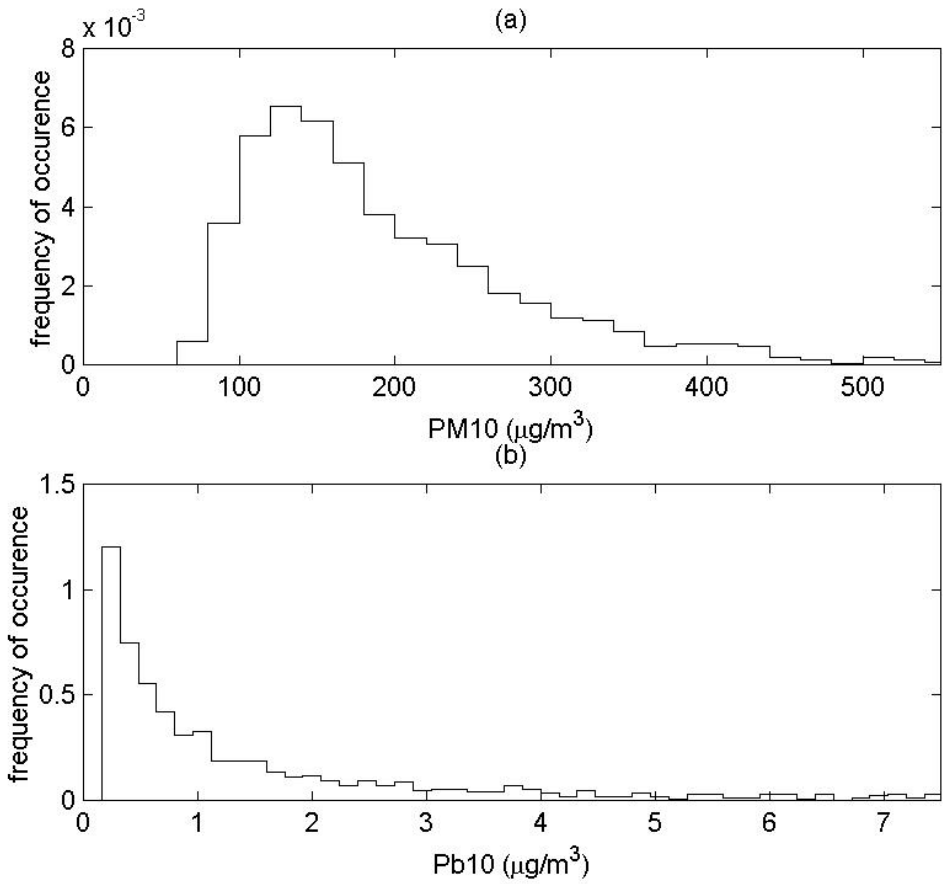

Figure 5-1: Distribution of Daily Concentrations for PM10 and Pb10

5.1.4 De-trending of Large-scale Spatial and Temporal Fluctuations

In the BME methodology, a Space/Time Random Fields (S/TRF) Z(**s**,t) is used to model the log-transform of air pollutant at a point with spatial coordinates **s**=(x,y) and at time t. Generally, Z(**s**,t) is decomposed into the sum of an expected value $\overline{Z}(\mathbf{s},t)$ and a residual S/TRF X(**s**,t), as follows:

$$Z(\mathbf{s},t) = \overline{Z}(\mathbf{s},t) + X(\mathbf{s},t),$$

where the $\overline{[.]}$ operator specifies the stochastic expected value. The residual X(**s**,t) is a S/TRF with an expected value of zero (i.e. $\overline{X}(\mathbf{s},t) = 0$) and is said to be homogeneous in space and stationary in time. The expected value $\overline{Z}(\mathbf{s},t)$ is a deterministic quantity representing the trend of the log transform of the air pollutant in space and in time, and may be referred to as the mean trend. This mean trend needs to be modeled using a deterministic (non-random) function and removed from the data in order to work with the homogenous/stationary residual X(**s**,t). After investigation of the data, the following mean trend model was found to be a reasonable choice to model the log-transform of PM and Lead:

$$\overline{Z}(\mathbf{s},t) = Y_s(\mathbf{s}) + a\cos(2\pi/365.25*(t-t_0)),$$

where the spatial component $Y_s(\mathbf{s})$ is a deterministic function that is only a function of the spatial coordinate **s**, and the temporal component is a cosine function with parameters a (amplitude) and t_0 (time when the maximum occurs).

The spatial component $Y_s(\mathbf{s})$ of the trend was obtained by taking the average of the log transform of PM and lead measured at each monitoring site, and then applying an exponential smoothing function to remove the local fluctuations. The parameters a and t_0 were determined by calculating the average $Y_t(t)$ of the log transform of PM and lead for each day t when measurements were taken, plotting $Y_t(t)$ as a function of time, and fitting the cosine function K+a cos(2p/365.25*(t-t_0)).
A least-square approach and expert judgement were used to yield the best values for a and t_0 for PM10, Pb10, and PM2.5.

Using the function $Y_s(\mathbf{s})$ and the parameters a and t_0 obtained for PM10, lead, and PM2.5, the mean trend of the air pollutant at any point in space and time can be determined and the trend can be removed from the data. All hard- and soft monitoring data was de-trended, so that the subsequent BME analysis steps could be performed using a homogeneous and stationary residual, X(s,t).

5.1.5 Modeling the Space/Time Variability by Means of the Covariance Function

The space/time variability of the air pollutants is described by the covariance function:

$$C_Z(r = \|\mathbf{s}-\mathbf{s}'\|, \tau = |t-t'|) = \overline{(Z(\mathbf{s},t)-\overline{Z}(\mathbf{s},t))(Z(\mathbf{s}',t')-\overline{Z}(\mathbf{s}',t'))}$$

The covariance function is a statistical moment of second order describing the variability of the data in space and time. Using the PM and lead monitoring data, it is possible to estimate values of the covariance function for different spatial lags, r, and different temporal lags, τ, and then fit a covariance model to the monitoring data values. The covariance model selected to fit the PM and lead monitoring data is the superposition of two exponential models with different spatial and temporal scales, determined using the following equation:

$$C_Z(r,\tau) = C_{01}\exp(r/ar_1)\exp(\tau/at_1) + C_{02}\exp(r/ar_2)\exp(\tau/at_2)$$

In each of the two exponential covariance components, C_0 is the variance (amount of variability); *ar* the spatial range of the fluctuations; and *at* the temporal range of the fluctuations. The first covariance component with parameters C_{01}, ar_1 and at_1 is used to model the small-scale structures of the air pollutant variability in space and time, while the second component with parameters C_{02}, ar_2 and at_2 is used to model the large-scale structures of the space/time variability.

The PM10, Pb10, and PM2.5 spatial covariance relationships, as a function of the spatial lag (r) are shown in the three graphs on the left-hand side of Figure 5-2. The three graphs on the right-hand side of Figure 5-2 show the PM10, Pb10, and PM2.5 temporal covariance relationships, as a function the time lag (τ). The circles, connected by the dashed line in the graphs of Figure 5-2, represent the covariance estimated for the PM and lead monitoring data, while the covariance model is shown as a solid line in the graphs. The parameters of the covariance models for the different air pollutants were obtained using a least-squares approach to obtain the best fit of the monitoring data values.

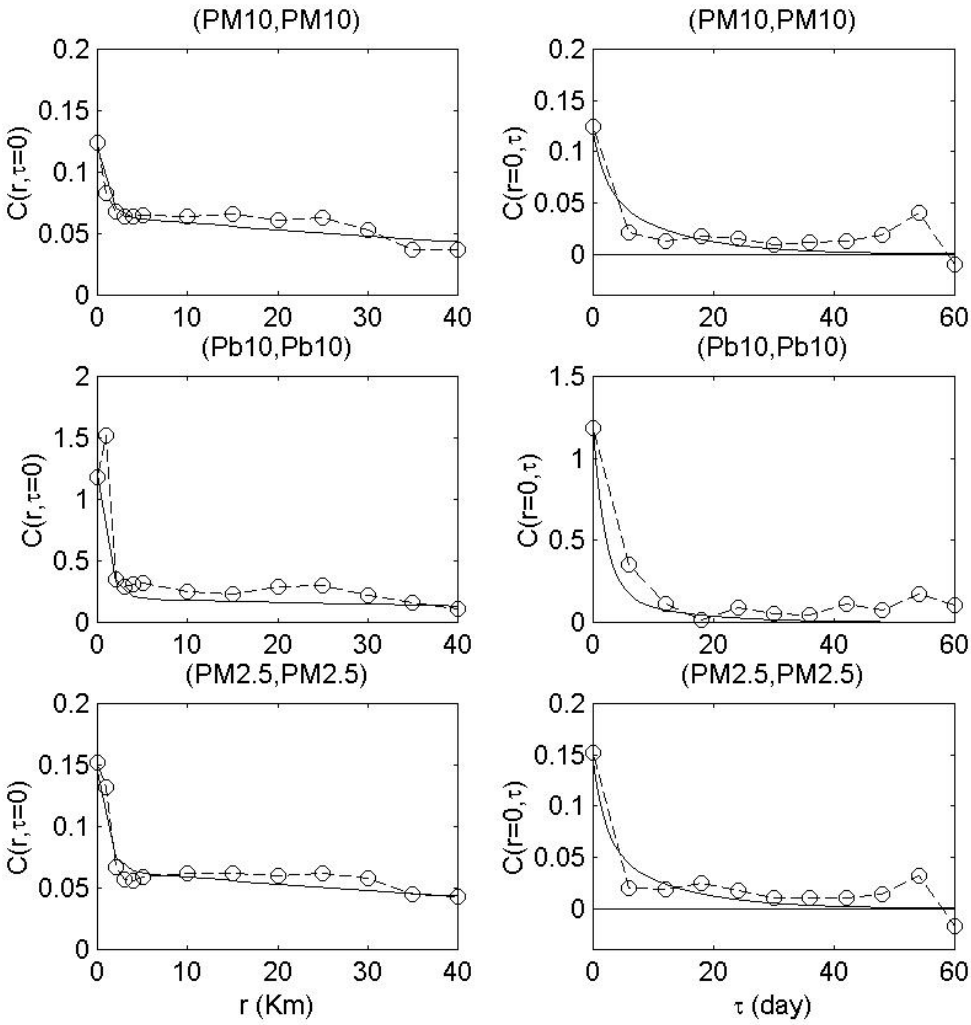

Figure 5-2: Spatial and Temporal Covariance for the PM and Pb as a Function of Distance (km) and Time Lag (t)

Table 5-1: Spatial and Temporal Range Parameters for Small- and Large-scale Fluctuations

Parameter	Small-scale Fluctuations	Large-scale Fluctuations
Spatial range (km)	ar_1=1 km	ar_2=100 km
Temporal range (days)	at_1=2 days	at_2=12 days

Table 5-2: Variance Parameters for the Small-scale Fluctuation C_{01} and the Large-scale Fluctuation C_{02}

Covariance Parameter [a]	Variance for small-scale fluctuations (C_{01})	Variance for large-scale fluctuations (C_{02})	Fraction of small-scale fluctuation variance $100\ C_{01}/(C_{01} + C_{02})$
log(PM10)	0.055	0.065	45%
log(Pb10)	1.0	0.2	83%
log(PM2.5)	0.08	0.065	55%

(a) PM and Pb in μg/m³.

The covariance parameters have an important physical significance and provide some interesting insights concerning the space/time variability of PM and lead concentrations. The spatial covariance graphs in Figure 5-2 show two components in the pollutant profiles. The long-range component of the profiles can extend as far as 100 km, while the short-range components extend to a distances as short as 1 km. The long-range component is probably due to macro-scale meteorological conditions, such as, wind speed and direction, temperature inversions, etc. The short-range components of the spatial distribution profiles are probably due to emission from anthropogenic point sources. Similarly, the temporal distribution profiles exhibit two components, which a probably caused by the same factors that produce the dual ranges in the spatial distribution profiles. The long-term component in the temporal fluctuations last as long as 12 days, while the short-term components have a duration as short as 2 days.

While the ranges of short-scale and large-scale space/time fluctuations are the same for both PM and lead, it is interesting to note that the relative importance of each scale varies from one air pollutant to the other. For PM10, the variance associated with small-scale fluctuation is only 45% of the total variance, which means that the space/time distribution of PM10 may be largely driven by large-scale weather patterns. Note that in the case of PM2.5 the fraction of variance associated with small-scale fluctuations increases to 55%, which can be explained by the fact that the smaller PM2.5 comes more predominantly from anthropogenic sources. In the case of lead, 83% of the fluctuations occur at the

small scale. The predominance of the small-scale fluctuations for lead is due to the fact that lead comes mostly from point sources (mainly secondary lead smelters). Thus, the spatial distribution of lead consists mostly of areas of relatively small size (often less than 1 km). Temporal fluctuations may occur rapidly, resulting in significant day-to-day variations in lead levels.

There are two interesting implications from these considerations for the space/ time estimation of PM and lead. The first is that because PM10 is characterized by large-scale spatial patterns that can be as large as 100 km, even the monitoring sites located as far as 30 km from the city may be influenced by air pollution in Cairo. Hence, caution should be exercised when using these monitoring stations to obtain the background level of PM (i.e. the level of "natural" PM concentration corresponding to a clean environment in the desert climate outside Cairo). The second interesting implication from these findings is that lead, because of the small-scale fluctuations, is more difficult to map than PM.

5.1.6 BME Estimation and Confidence Intervals

The mapping analyses of the air pollutants in the Greater Cairo area involves the estimation of air pollution concentration at the nodes of a grid, followed by generation of color maps based on the estimated values. The advantage of the BME estimation method used in this analysis is that it yields the probability distribution function of the air pollution concentration at each estimation point. This pdf is referred to as the BME 'posterior' pdf, because it is obtained at the posterior stage of the BME analysis, when all the available information has been rigorously incorporated in the analysis. The BME posterior pdf provides a much more informative and accurate description of the air pollutant concentration than that provided by classical geostatistical methods, which merely provide an estimated value. By giving a complete probabilistic description of air pollution, the BME posterior pdf provides the flexibility to obtain any estimator desired (such as mode, the mean, or quartile), as well as an accurate assessment of estimation precision. This flexibility is especially useful when assessing health risks, which is an issue of concern for this study in Greater Cairo.

To illustrate this issue, consider the typical BME posterior pdf shown in Figure 5-3 obtained at some estimation point for Xk, where Xk is the log of the air pollutant concentration. The BME posterior pdf shows the probabilistic distribution of air pollution at this estimation point. From the posterior pdf, we may easily obtain the mode, which represents the most "probable" level of air pollution existing at the estimation point. Another estimator of interest is the mean of the posterior pdf, since this estimator is known to minimize the mean square error. Additionally, any confidence interval can be extracted from the BME posterior pdf, as shown in Figure 5-3. At a given level of confidence, the width of

confidence interval (the difference between upper and lower limits of the interval) is a measure of the accuracy of the prediction. Figure 5-3 gives an illustration of BME estimation of air pollution and of the confidence interval, which will be used in the figures presented below.

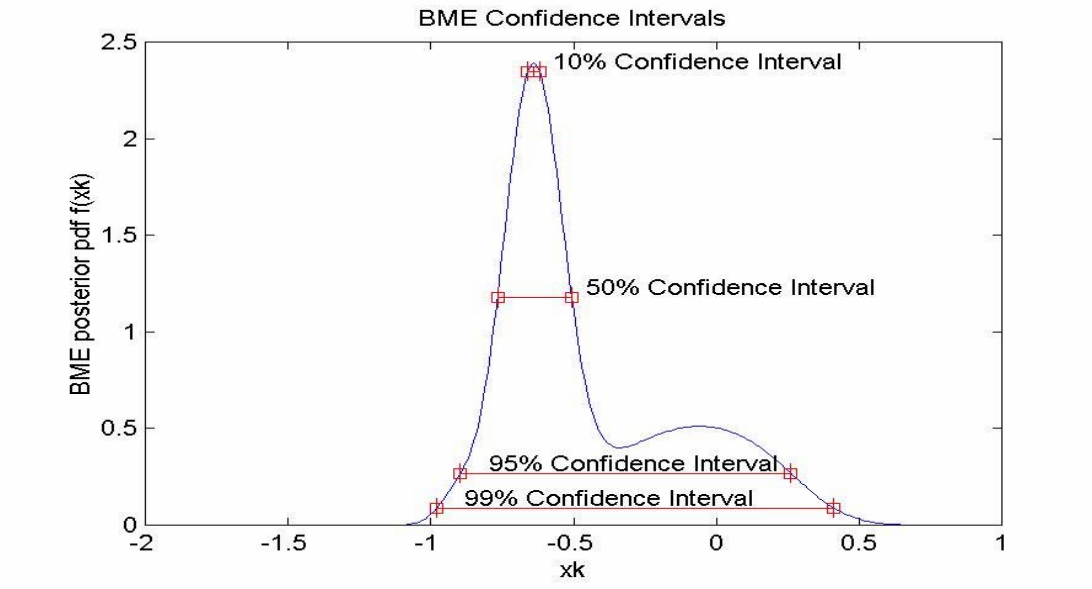

Figure 5-3: Typical BME Posterior pdf Showing the Probabilistic Distribution of an Estimated Variable (Xk) with Intervals Shown for Different Confidence Levels

5.2 Particulate Matter

5.2.1 Temporal Characteristics

<u>Typical Estimated PM Profiles at a Selected Monitoring Station</u>

It is useful to estimate how the air pollution changes with time between measurement events at any given monitoring station. As an example, the temporal profiles of PM10 and PM2.5 for Site #6 are shown in Figures 5-4(a) and 5-4(b), respectively. Site #6 is located in the Maadi/Degla area and was selected as an illustration because the temporal profile is typical of the other sites. The estimated profiles are shown in Figures 5-4(a) and 5-4(b) as dashed lines, which correspond to the BME mean estimators. This profile indicates how the air pollution evolves between measurement events. Additionally, the lower and upper bounds of the 68% confidence interval are shown in the figures as dotted lines, which are an indication of the level of confidence in the estimated air pollution profile: the smaller the confidence interval, the more precise (informative) the estimation.

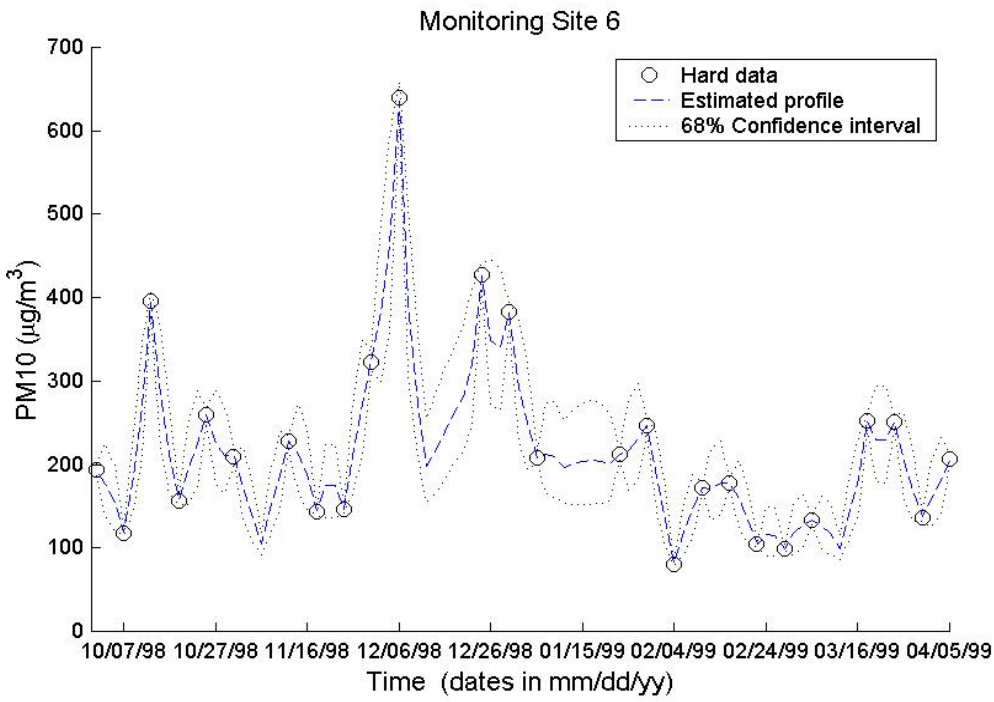

Figure 5-4(a): Estimated Daily PM10 Concentration Profile for CAIP Site #6 in Maadi/Degla

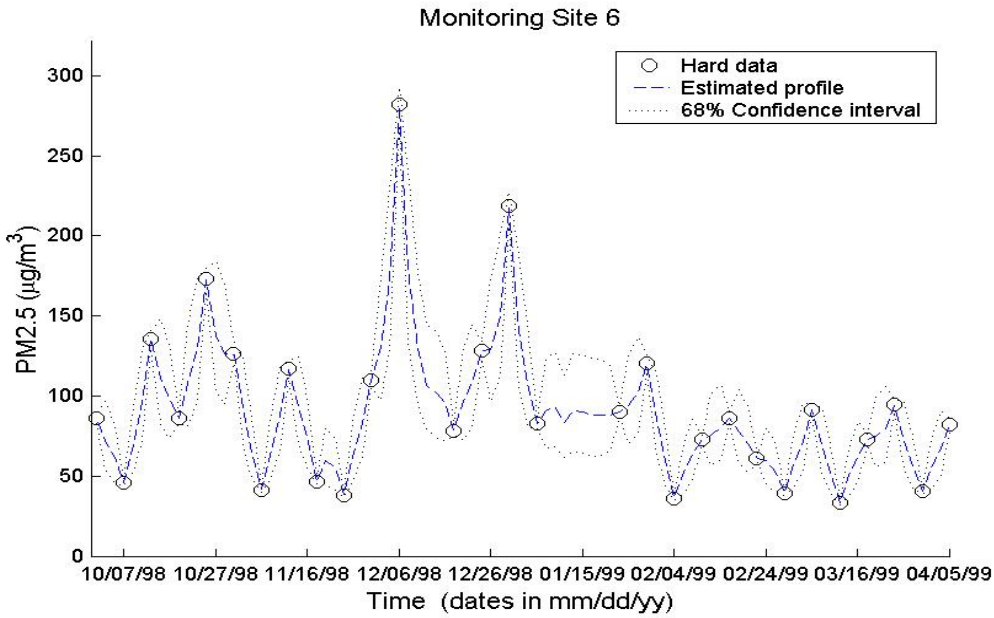

Figure 5-4(b): Estimated Daily PM2.5 Concentration Profile for CAIP Site #6 in Maadi/Degla

It is worthwhile commenting on the shape of the typical pollution profiles shown in Figure 5-4(a) and 5-4(b). In these plots, the estimated profile (dashed line) passes through the hard data points (represented by circles), since these are considered as "exact" measurements. Additionally, it is noted that the width (difference between upper and lower limits) of the confidence interval is small

(near zero) at the data points, while this width increases between measurement events. This observation simply illustrates the logical behavior that the air pollutant concentration is known more precisely at times closer to the measuring events. Conversely, the estimate of air pollutant concentration becomes less precise for extrapolations from the measuring event. Finally, it is interesting to note that the PM10 profile in Figure 5-4(a) has a peak concentration on 6 December 1998, and then the concentration is predicted to drop sharply to a minimum level six days later. Note that a measured value was not obtained during the 6-December 1998 sampling event.

The predictive capability displayed in this situation is a feature of the BME estimation method, which uses data points obtained at the same site but on different dates (temporal neighborhood), as well as data for the same date obtained from sites in the same general vicinity (spatial neighborhood) of Site #6. The reasonableness of the predicted PM10 profile is verified by a similar decrease in the measured PM2.5 concentration at Site #6 on 6 December 1998. The predictive capability illustrated in this example demonstrates that the BME method employed in this data analysis generates true space/time relationships, which leads to a more accurate mapping estimation.

Seasonal Trend in PM Levels

The mean temporal trend of PM pollution in Greater Cairo is shown in Figure 5-5(a) for PM10 and in Figure 5-5(b) for PM2.5. Several types of averaging may be used when calculating the mean value of PM pollution over the city for a particular measuring event. In Figures 5-5(a) and 5-5(b), the mean PM value for a specific measurement day is obtained by averaging the logarithm of PM concentration values recorded at all the monitoring sites (maximum 34 values), as well as values estimated at approximately 60 points evenly distributed throughout the city. The average obtained in this manner yields a mean value that is more stable than the arithmetic average of only the measurements performed at the monitoring stations, and hence provides a better indicator to study the temporal trend of PM pollution during the year. The logarithm of the average value obtained for each measurement day is shown as crosses connected by a solid line.

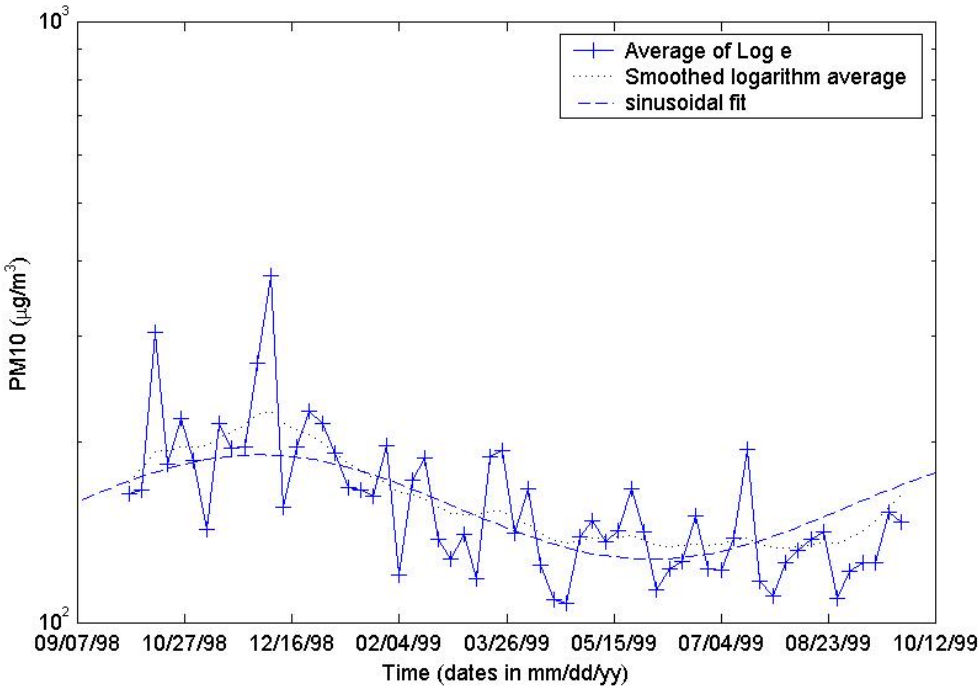

Figure 5-5(a): Plot of Average of the Logarithm of PM10 Measurements during the Baseline Year

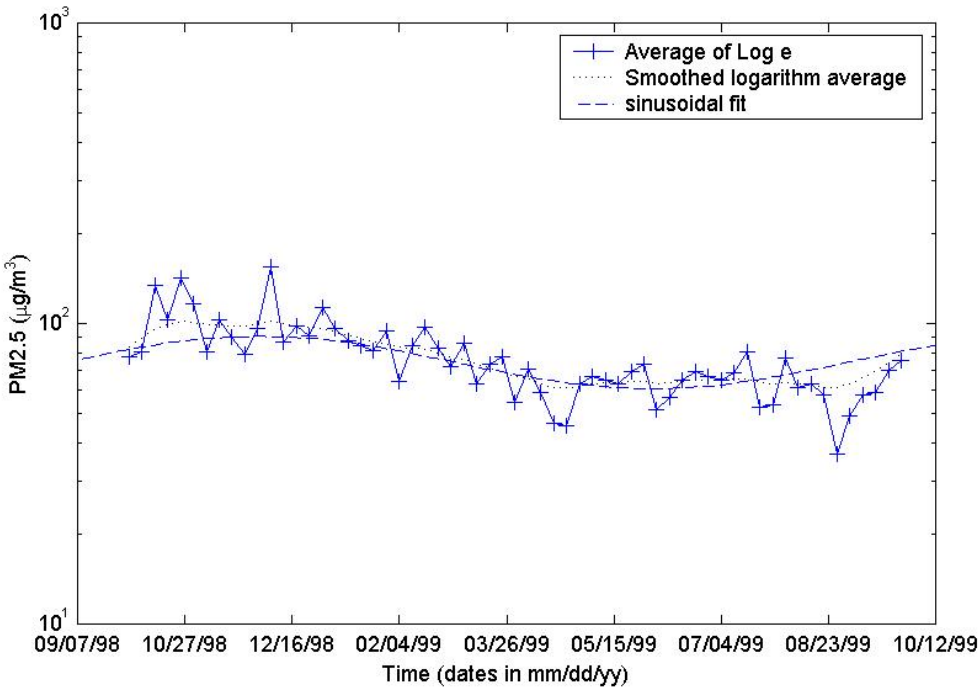

Figure 5-5(b): Plot of Average of the Logarithm of PM2.5 Measurements during the Baseline Year

The logarithmic profiles in Figures 5-5(a) and 5-5(b) appear to indicate a seasonal trend for both PM10 and PM2.5. Because of the variability in logarithmic profiles, it is helpful to use a smoothed curve, such as the curves shown in dotted lines in

Figures 5-5(a) and 5-5(b). The smoothed curve indicates that higher PM concentrations occur during the October–December period, while the season with lowest concentrations occurs during the May–July period. Additionally, the shape of the smoothed line confirms that the cosine function, discussed in Section 5.1.4, to model the space/time mean trend of PM provides a reasonable representation of the seasonal trend in PM concentrations. The parameters of the cosine function used for PM10 space/time mean trend function are a=0.2 (amplitude of the variation of the log of PM10 $\mu g/m^3$) and t_0 = 1 December 1999 (date when the maximum occurs). Figure 5-5(a) shows that a cosine function with the above parameters provides a good fit to the measured data. For PM2.5, the parameters are the same, and the corresponding cosine function is shown as a dashed line.

To assess the reliability of the sinusoidal trend model, refer to the plot of different percentiles of PM10 in Figure 5-6. The 95-percentile in Figure 5-6 represents the value that is exceeded at only 5% of the sites for that day. The other percentiles have similar significance. The percentile lines indicate that though there is a high variability in the PM10 data, the seasonal trend of PM is still pronounced even at higher percentile levels.

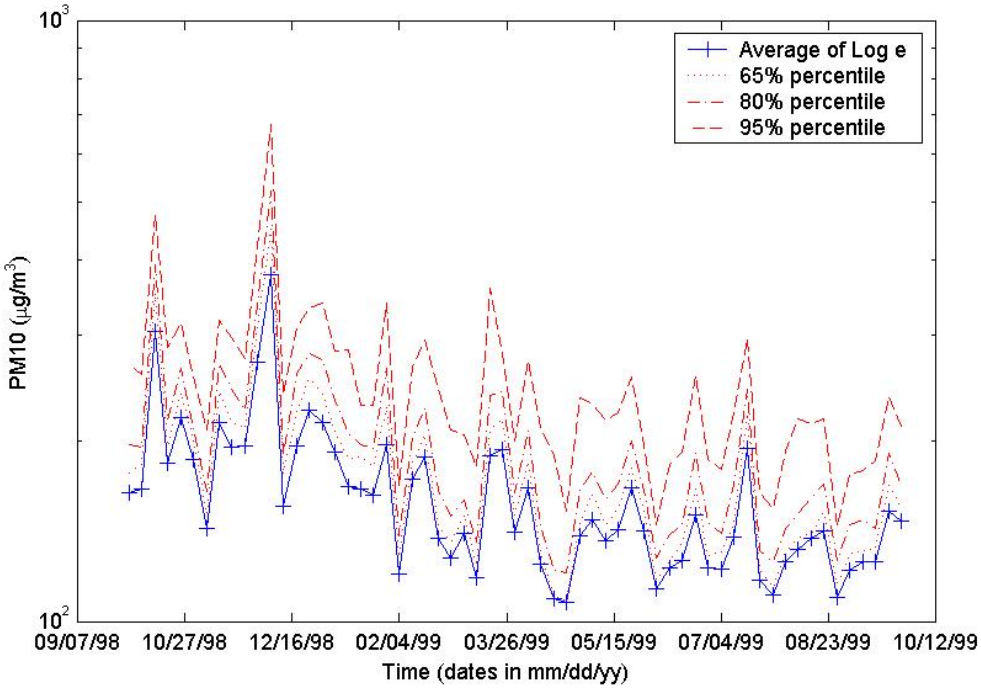

Figure 5-6: Plot of Different Percentiles in the Temporal Variations in PM10 Concentration

Day-of-the Week Trend in PM Levels

In addition to the seasonal trend of PM levels, there is also a day-of-the-week trend in the PM concentration. The day-to-day trend is evident in Figure 5-7,

which provides a plot of the median PM10 concentration as a function of the day of the week. The median PM10 values are normalized to a value of 1 for Friday. For a given day, the median PM10 concentration is the value that is exceeded by 50% of all measurement preformed on that day of the week. Figure 5-7 clearly shows that the lowest PM10 concentration occurs during the weekend days of Friday and Saturday, and that the concentration increases after the weekend, reaching a maximum in the middle of the week, on or around Tuesday. The increase in median PM10 concentration from the weekend to the mid-week period is approximately 14%. The weekday trend analysis for PM10 is based on measurement data obtained from the 60 sampling events conducted during the baseline year.

The weekly pattern in PM10 concentration is most probably due to socio-economic factors. Friday and Saturday are normally non-work days for many, and most of the industries do not operate or operate at reduced production on these days. Vehicular traffic is also normally lower on the non-work days. As anthropogenic activities increase on the workdays, the PM10 builds to a maximum on Tuesday. The day-of-the-week trend observed for PM10 is typical for a large urban area such as Cairo. The trend for other air pollutants also normally follows a similar pattern.

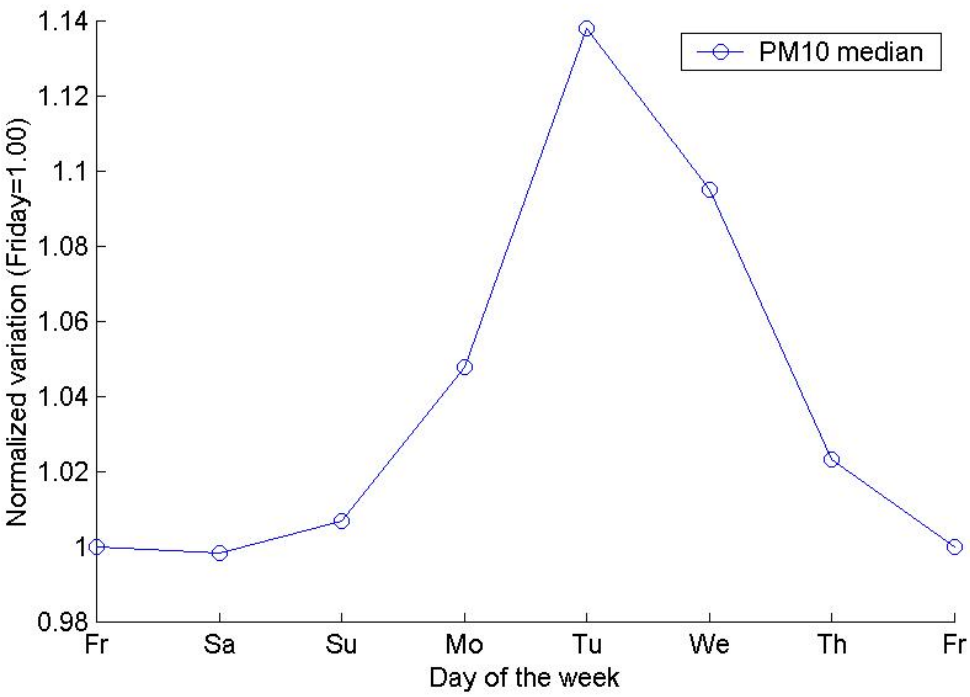

Figure 5-7: Median PM10 concentration as a function of the day of the week

5.2.2 Spatial Characteristics

Typical PM Concentration Profile Maps for Selected Days

Maps showing the spatial distribution of PM10 over the Greater Cairo area are obtained by estimating the PM10 concentration on the nodes of a dense regular grid, and plotting the result using a color scale. Such maps were produced for each measuring day of the baseline year, resulting in a total of 60 maps. Three of these maps, selected to illustrate the typical features of the PM10 distribution over Greater Cairo, are shown in Figures 5-8, 5-9, and 5-10. The maps were created for the following dates: 7 October 1998 (Figure 5-8), 13 October 1998 (Figure 5-9), and 28 July 1999 (Figure 5-10).

The map for Figure 5-8 illustrates a day when typical, medium-level PM10 concentrations prevailed. Figure 5-9 shows a map for a day when very high PM10 levels were recorded. The map in Figure 5-10 portrays a day when PM10 levels were relatively low. The color scale used to represent the PM10 concentration in each of the maps begins at 70 $\mu g/m^3$ (the Law 4/1994, 24-hour PM10 standard) and is truncated at 400 $\mu g/m^3$ in order to provide the same scale for each map. The maximum concentration level predicted for each day is shown at the top of the maps. On 7 October and 13 October, the maximum estimated PM10 concentration exceeded the upper limit of the color scale (400 $\mu g/m^3$). For reference, the delineation of the Nile River, CAPMAS districts, and some major streets are shown on the maps. Site numbers and names of some CAIP monitoring sites are also included in the maps.

The maps reveal some important characteristics of the spatial distribution of PM10 throughout Greater Cairo. The short-scale and large-scale structures are easily recognized, with several clusters as small as 1 km visible on the medium- and low-level pollution days of 7 October 1998 and 28 July 1999. In contrast, a large-scale structure of high PM10 levels, covering a distance in excess of 50 km, developed throughout the entire city on the high pollution day: 13 October. The PM10 distributions shown in Figures 5-8 through 5-10 are in agreement with the covariance analysis. The covariance analysis predicts that 45% of PM10 variance is associated with small-scale fluctuations of about 1 km, while the remainder of the variance is associated with large-scale structures of up to 100 km.

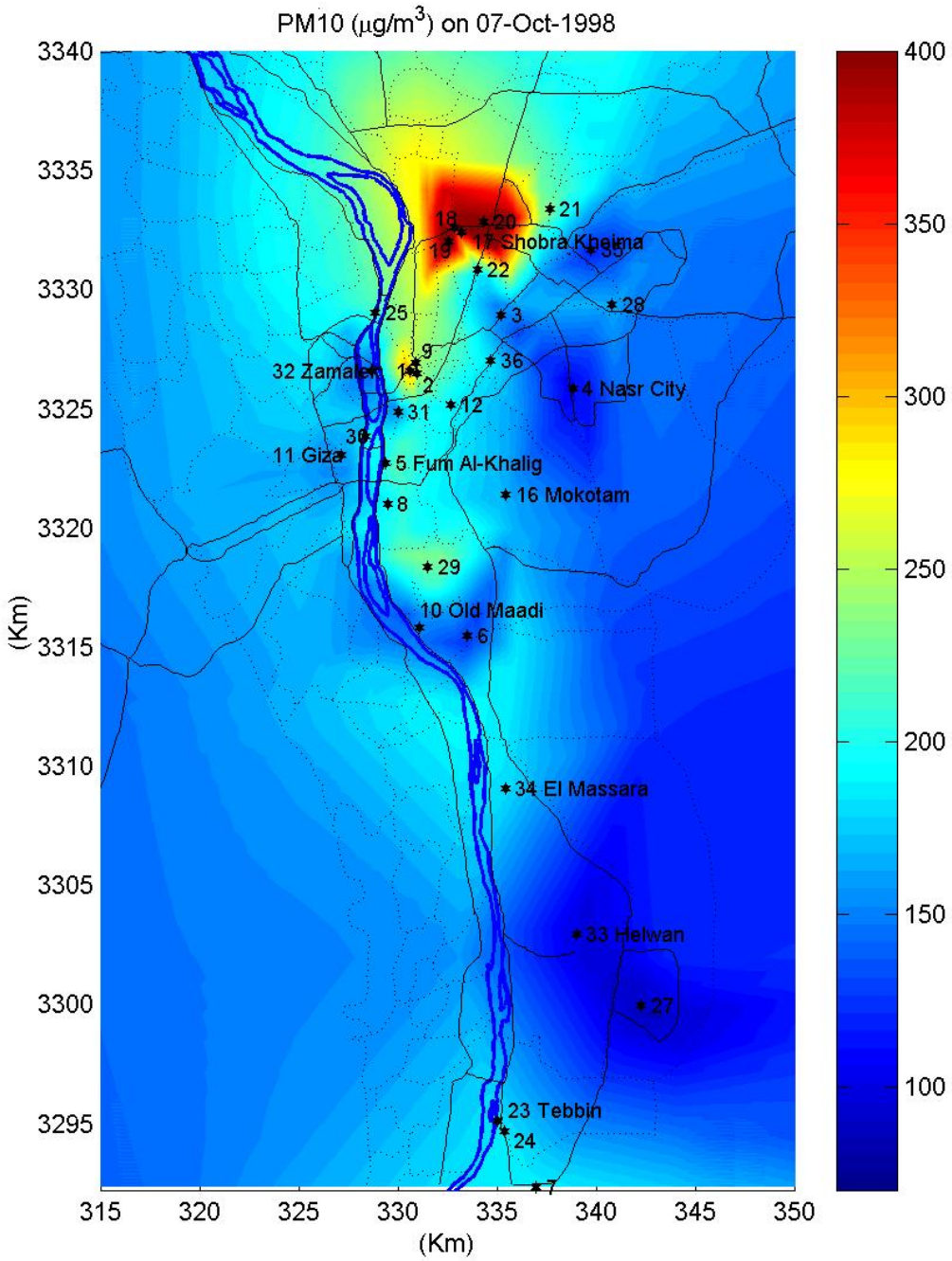

Figure 5-8: Estimated PM10 Concentrations on 7 October 1998 (Color Scale Indicates PM10 Concentration in μg/m³)

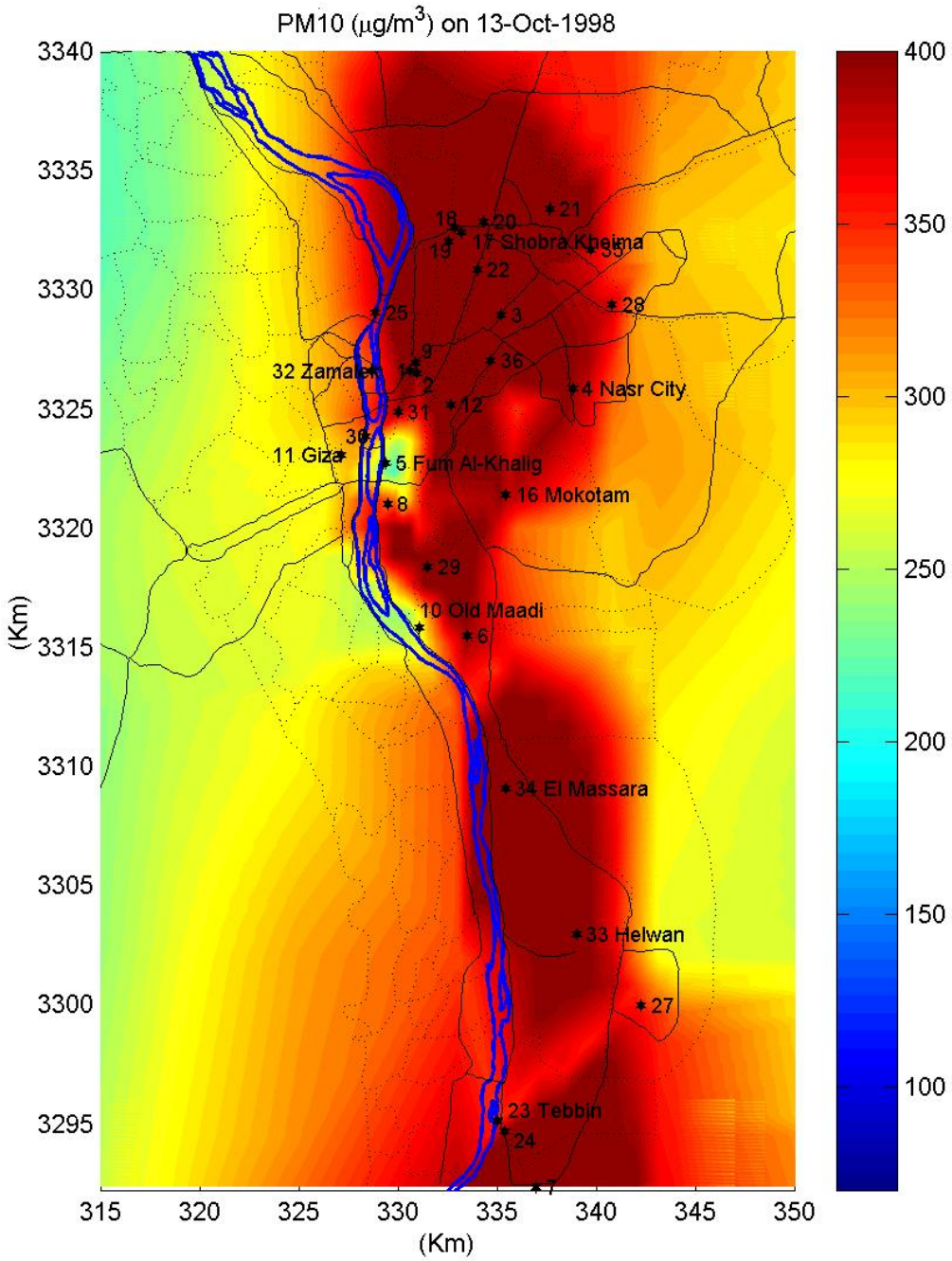

Figure 5-9: Estimated PM10 Concentrations for 13 October 1988 (Color Scale Indicates PM10 Concentration in μg/m³)

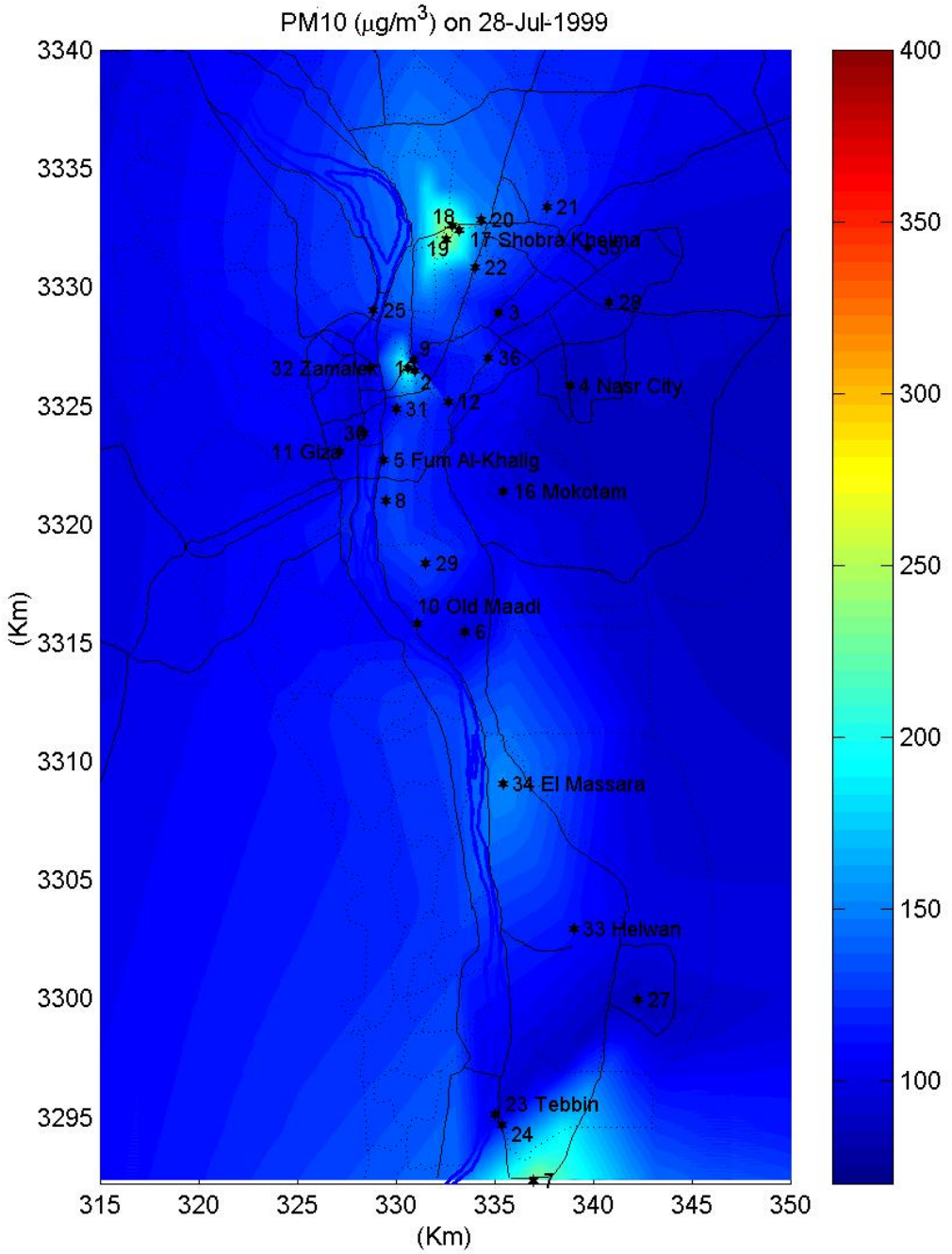

Figure 5-10: Estimated PM10 Concentrations 28 July 1999 (Color Scale Indicates PM10 Concentration in μg/m³)

Maps of PM2.5 concentration distribution are very similar to those for PM10. The similarity is expected since, as reported earlier in this document, a fairly constant PM2.5/PM10 mass ratio (0.50 ± 0.13) was obtained for baseline year PM measurements. The similarity in the estimated PM2.5 and PM10 spatial distributions may be observed by comparison of maps shown in Figures 5-9 and 5-11. Both of the maps of estimated PM2.5 and PM10 distribution in these figures are for the same date, 13 October 1998. The values used for the color scale on the PM2.5 map are approximately half of the values used for the PM10 maps.

As illustrated in Section 5.2.1, the width of the confidence interval represents a good measure of the mapping accuracy. Note also that the width of the 68% confidence interval is approximately equal to the standard deviation of the estimation error. An illustration of the 68% confidence interval for PM10 concentration estimates made for 7 October 1998 is shown in Figure 5-12. The uncertainty in the PM10 concentration estimates, in $\mu g/m^3$, is indicated by a range of colors. The bottom of the scale, which is blue, indicates a low uncertainty in the concentration estimation, while the upper limit of the scale (red/brown) indicates an uncertainty of 150 $\mu g/m^3$. Figure 5-12 shows that, as expected, the estimation error is smallest where the monitoring site density is the highest, and estimation error increases at locations that are more remote from any monitoring sites.

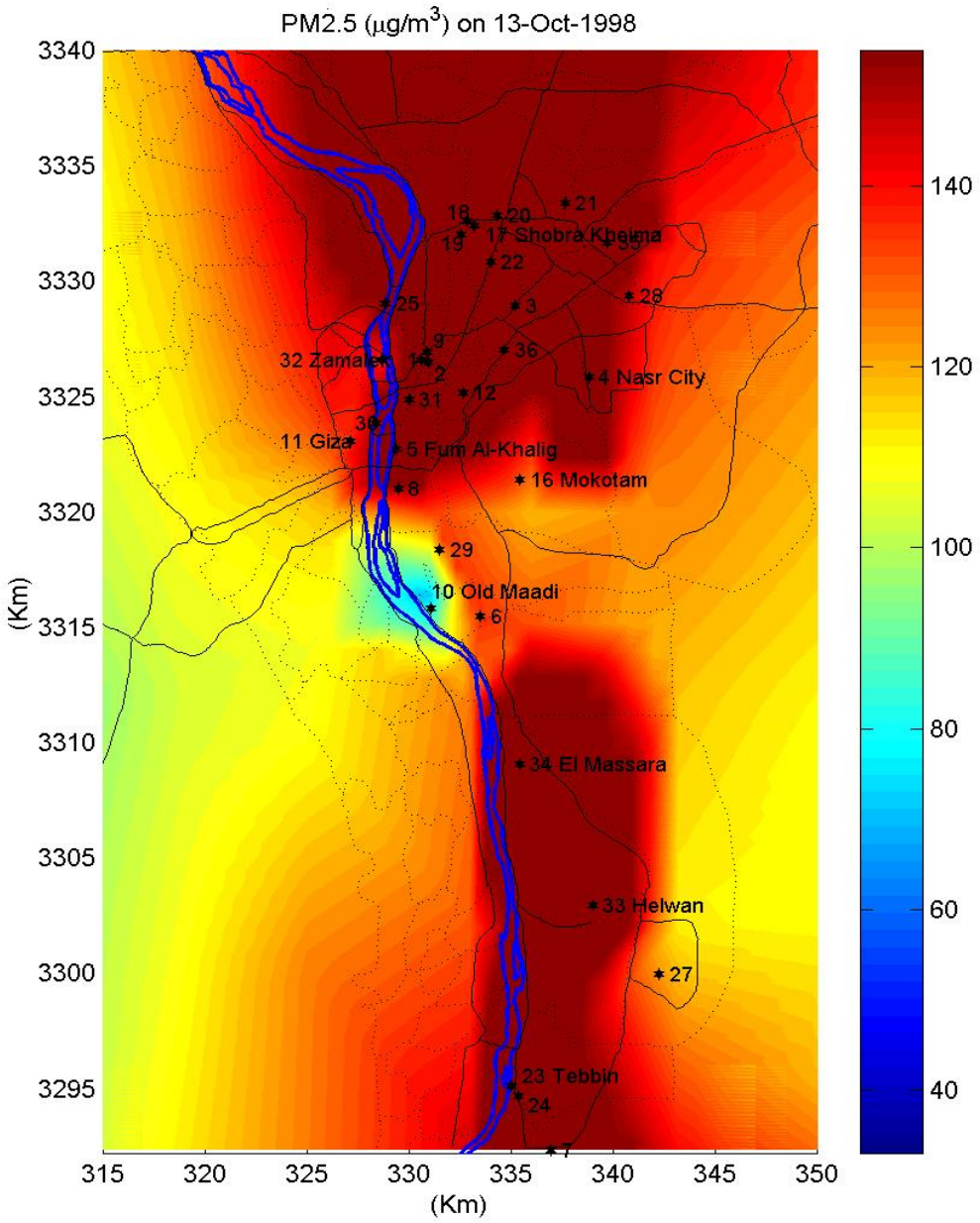

Figure 5-11: Estimated PM2.5 Concentrations on 13 October 1998 (Color Scale Indicates PM2.5 Concentration in μg/m³)

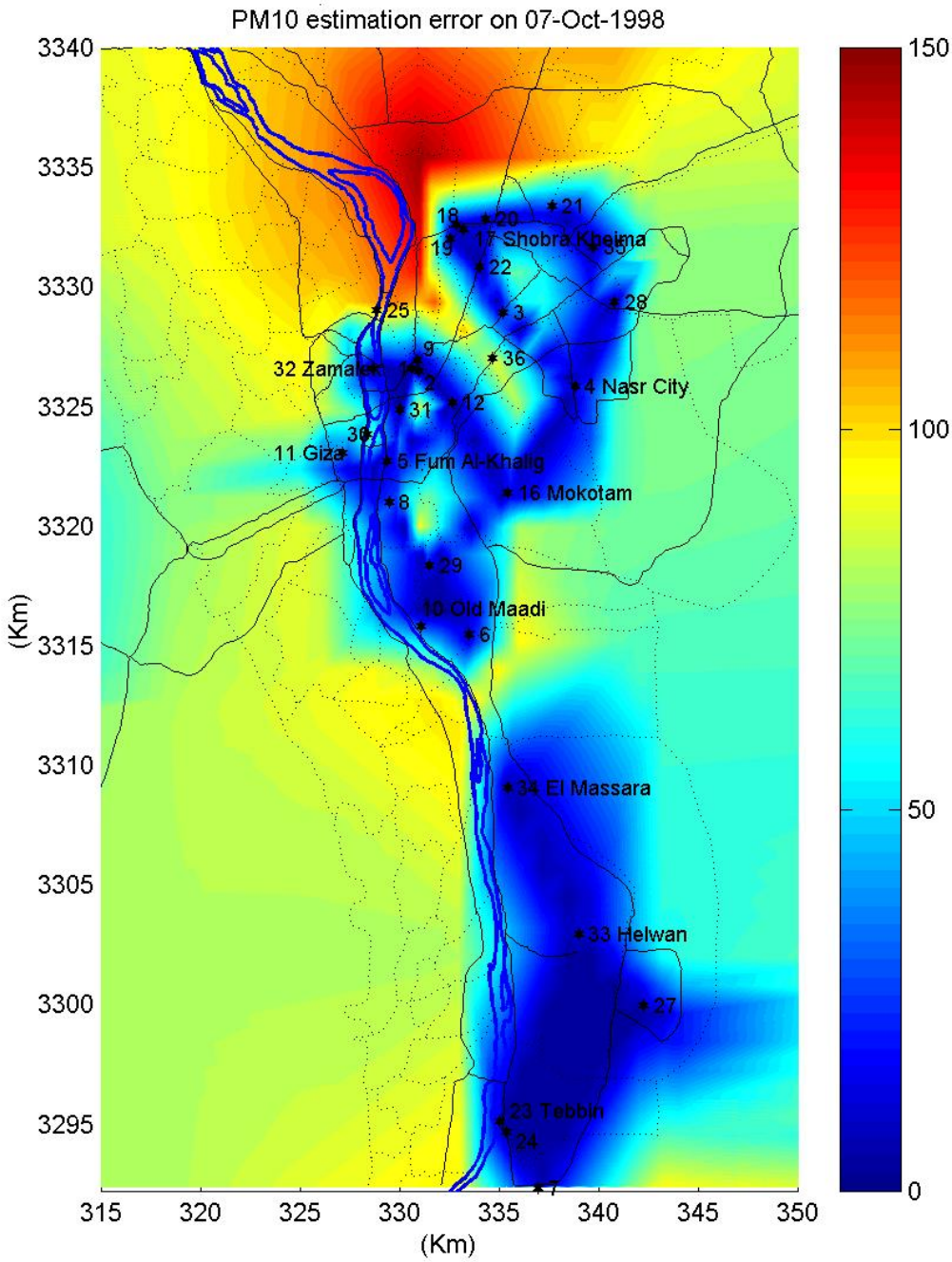

Figure 5-12: The 68% Confidence Interval for PM10 Concentration on 13 October 1998 (Uncertainty Color Scale in μg/m³)

Annual Average PM Concentrations

The arithmetic average of the daily PM concentrations at each estimation point can be used to construct a map of the annual PM average over the Greater Cairo area. The map of average PM10 distribution estimated for the baseline year is shown in Figure 5-13. Although Egypt does not have an annual ambient PM10 standard, this map is useful to show areas where high annual average PM10 concentrations prevail on a persistent basis. Note that, in Figure 5-13, most of the area along the Nile River, from downtown Cairo in the North to Tebbin in the South is generally exposed to the high PM10 concentrations. The highest annual average PM10 concentrations occur in the Shoubra El-Kheima area, which is just north of downtown Cairo. Note that the color scale is truncated at 250 $\mu g/m^3$, while the estimated maximum value for the annual PM10 concentration is 293 $\mu g/m^3$. The maximum annual PM10 concentration occurs in the Shoubra El-Kheima area.

The map of annual average PM2.5 concentration, presented in Figure 5-14, exhibits generally the same spatial distribution as that of PM10 shown in Figure 5-13. The area of high PM2.5 concentration likewise spreads along the Nile River from Shoubra in the North to Tebbin in the South. The area of the highest PM2.5 level encompasses Shoubra El-Kheima and extends into a large section of downtown Cairo. The color scale used for this map is truncated at 120 $\mu g/m^3$, while the maximum estimated annual-average value for PM2.5 is 171 $\mu g/m^3$. Similar to PM10, the estimated maximum PM2.5 concentration occurs in the Shoubra El-Kheima area.

While the PM2.5/PM10 ratio has an annual average value that is usually close to 0.5, the site-to-site variation in the ratio shows a slight spatial trend. The spatial trend can be seen in Figure 5-15, which shows the map of baseline year PM2.5/PM10 average. The ratio values displayed in the map are generally in the range 0.43 to 0.56, a relatively narrow range centered approximately at 0.5. The PM2.5/PM10 ratio is higher in the northern part of the map corresponding to the Shoubra El-Kheima and downtown Cairo areas, and, in a more localized fashion, in the Tebbin area to the south. The higher PM2.5/PM10 ratio in these areas indicates the presence of a higher proportion of fine particles, which normally are emitted from anthropogenic sources. In the downtown area, the higher proportion of fine particles may be due to the higher density of mobile sources. The higher PM2.5/PM10 ratio in Shoubra El-Kheima and Tebbin is most probably due to the numerous industries located in these areas. A lower PM2.5/PM10 ratio is shown for the area extending from Maadi to Helwan. Three major cement production plants are located in this area. It is surmised that the lower PM2.5/PM10 ratio is due to the impact of larger particles in the emissions (both fugitive and stack) from the cement plants.

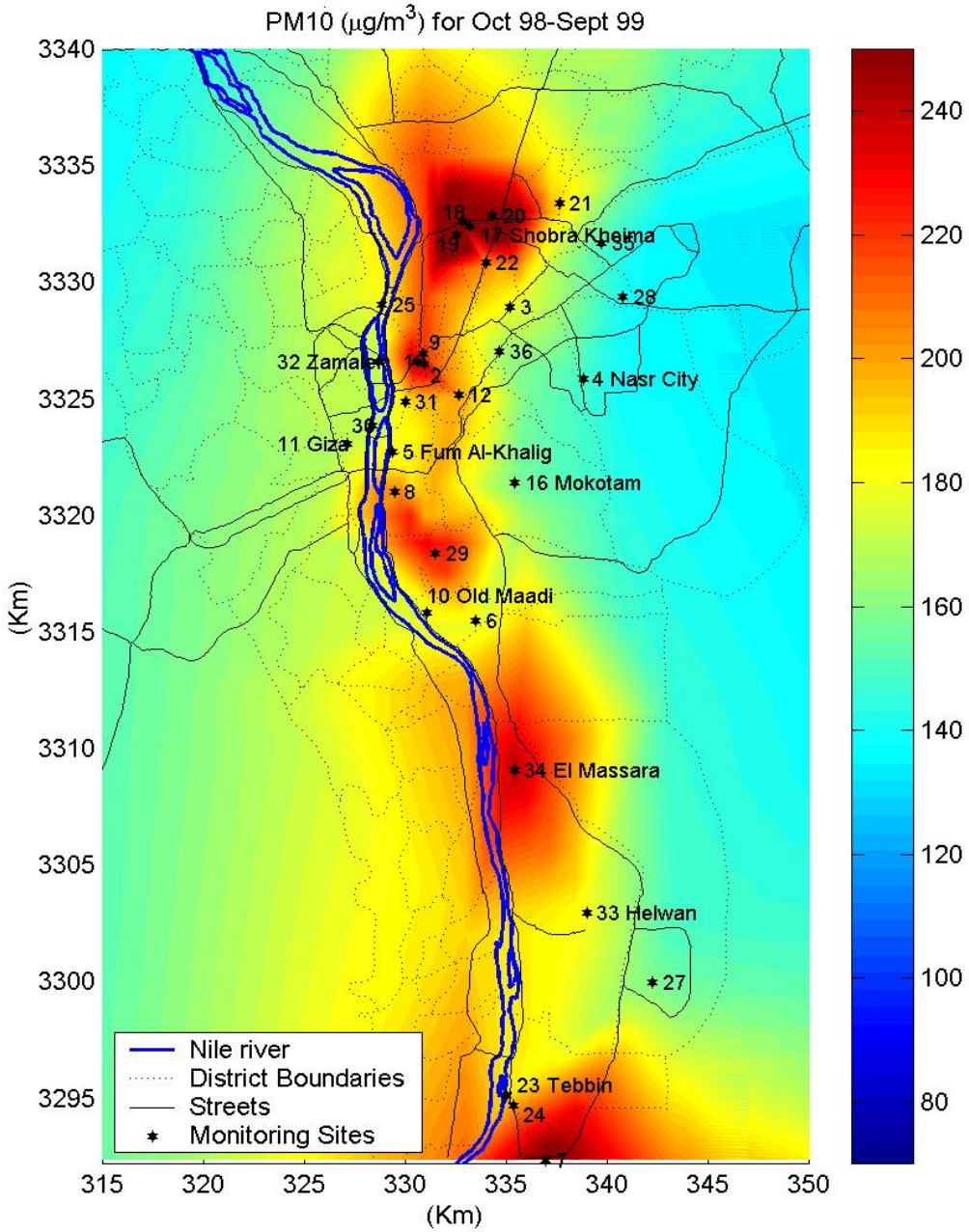

Figure 5-13: Estimated Average PM10 Concentrations for Baseline Year (Color Scale Indicates PM10 Concentration in μg/m³)

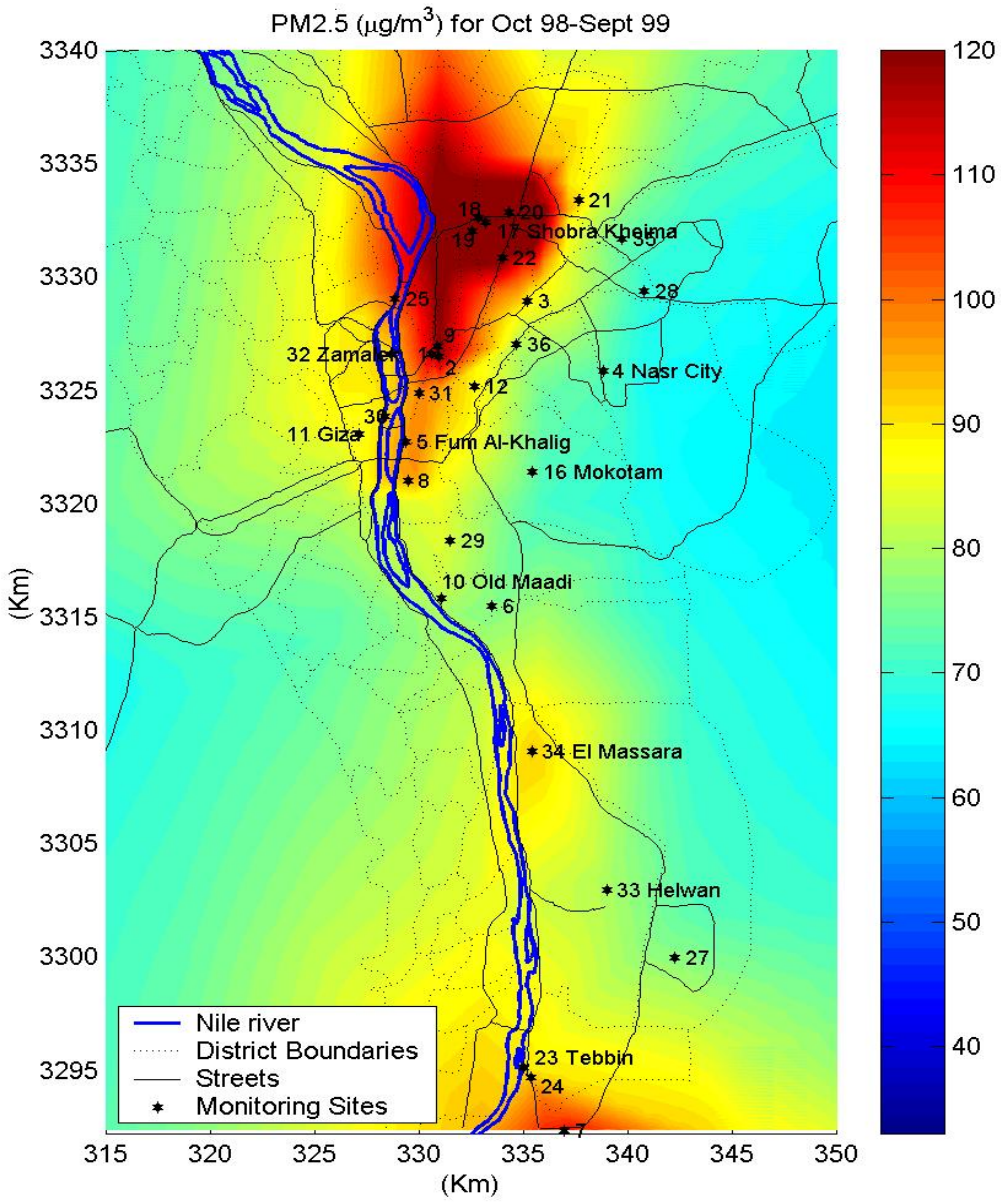

Figure 5-14: Estimated Average PM2.5 Concentrations during Baseline Year (Color Scale Indicates PM2.5 Concentration in μg/m³)

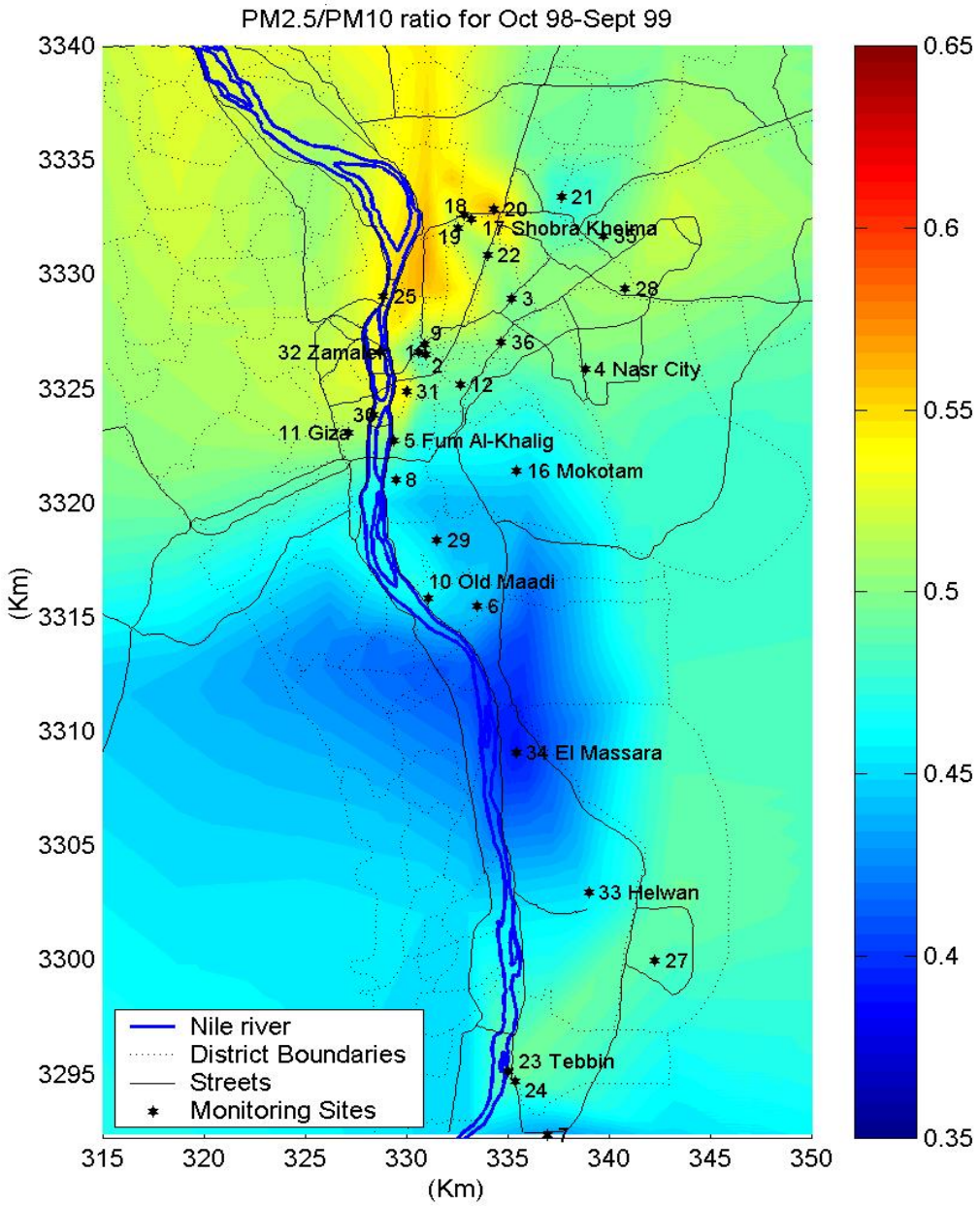

Figure 5-15: Estimated PM2.5/PM10 Average Ratio During Baseline Year (Color Scale Indicates PM2.5/PM10 Ratio Value)

5.3 Lead

5.3.1 Temporal Characteristics

Typical Estimated Profiles at a Selected Monitoring Station

The temporal plot of measured and estimated Pb10 concentrations for monitoring Site #6 is shown in Figure 5-16. This is the same site that was selected for a similar illustration of PM10 data (see Figure 5-4) and serves to show a typical lead concentration profile. As explained earlier, the estimated profile, shown as a dashed line, goes through the hard data points and is consistent with the soft data intervals representing the measurements below the lead MDL. A comparison of lead data in Figure 5-16 with PM10 data indicates a correlation between the two pollutants; however, Pb10 concentration varies significantly more than the PM10 levels. The higher Pb10 variability translates into a higher estimation error between measurement days, which can be seen from the large increase in the width of the 68% confidence interval between the data points.

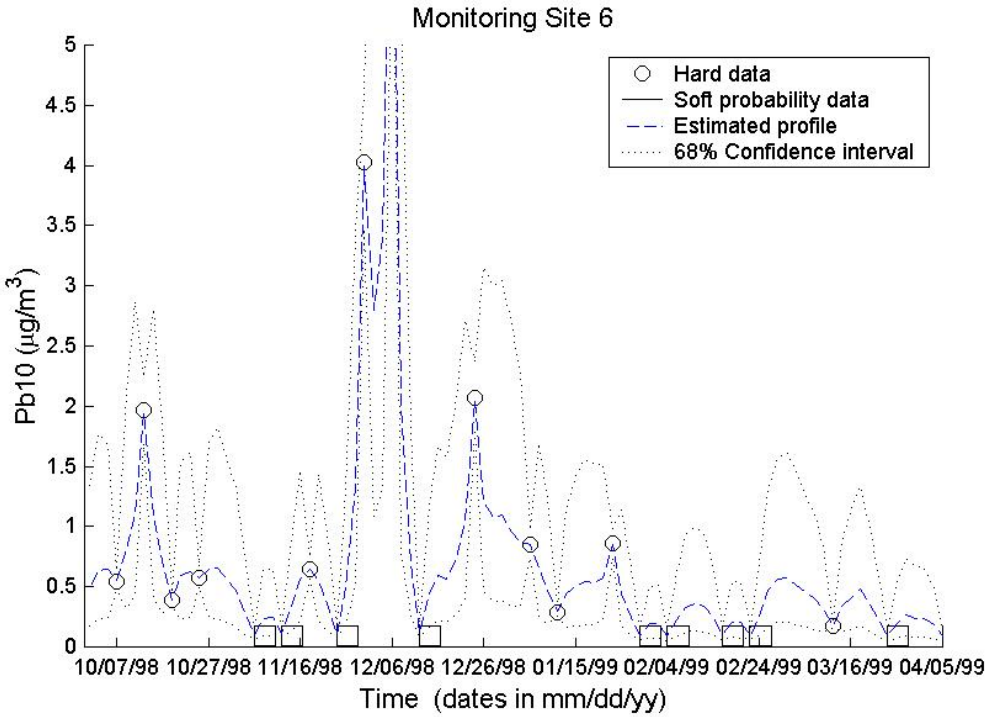

Figure 5-16: Estimated Lead Profile for Monitoring Site #6 in Maadi/Degla

Seasonal Trends in Lead Levels

A graph showing the logarithm of the average lead concentration for sampling events plotted versus days of the baseline year is presented in Figure 5-17. As for the PM trend analysis discussed earlier, the crosses and solid lines represent the measurement data. The smoothed curve of the logarithm of the lead concentration was estimated and is represented by a dotted line in Figure 5-17. The smoothed line is not constant over the year. Its shape is approximated by the cosine function used to model the space/time trend of PM (see Section 5.1.4). The parameters of the cosine function for the temporal trend of Pb10 are a=0.2 (amplitude of the variation of the log of Pb10, with Pb10 in $\mu g/m^3$) and t_0 = 7 October 1998 (date when the seasonal maximum for lead occurs).

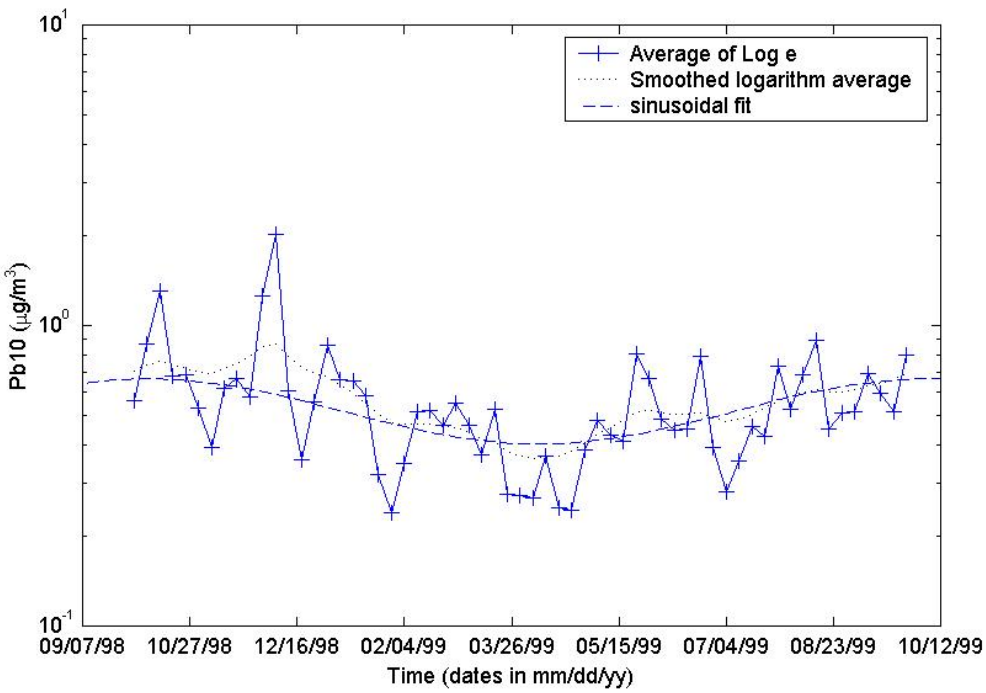

Figure 5-17: Temporal Plot of the Average of Logarithm of Lead over Greater Cairo

Although the cosine function, in Figure 5-17, seems to reproduce the shape of the smooth curve of average lead concentration for the baseline year, it is difficult to assess whether this is a reliable model. The difficulty arises from the high variability in the lead concentration, which is evident in percentile plots shown in Figure 5-18 (especially in the 95-percentile curve). Therefore, it is concluded that there is insufficient evidence to support that the cosine function is a reliable model for the seasonal trend of lead concentration. It is possible that the value of the parameter t_0 = October 07 (time when the seasonal maximum for lead occurs) is just an artifact of the variability of the lead data.

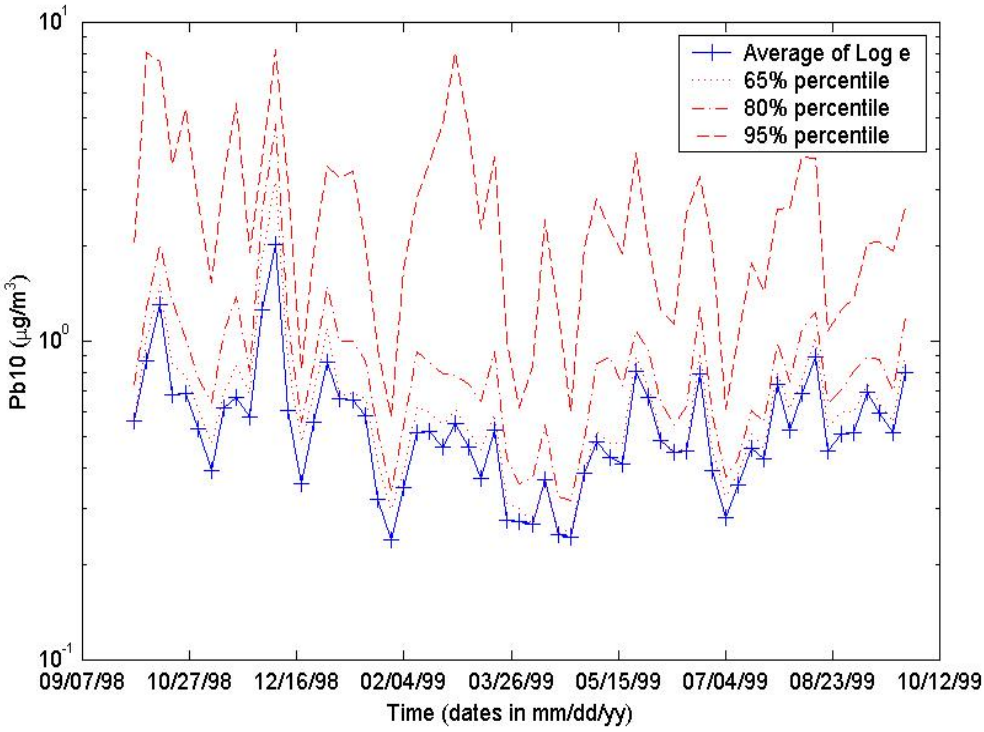

Figure 5-18: Temporal Plot of Different Percentiles for Lead Concentration

Day-of-the-Week Trend in Lead Levels

While there is not sufficient evidence to indicate a clear seasonal trend in the lead data, there is a very clear day-of-the-week trend in the lead concentration. The trend is obvious, as can be seen in Figure 5-19, which shows the median Pb10 concentration as a function of the day of the week. The lead concentrations were normalized to a value of 1 for Friday. For comparison purposes, the median PM10 concentration is also shown. Figure 5-19 clearly shows that the lowest lead concentration occurs on Fridays when the industries are closed, and that this concentration reaches a maximum during the working days. The median Pb10 concentration increases from the weekend to the mid-week period by a factor of approximately 2.7, which is substantially more than the factor of 1.14 for PM10. The strong day-of-the-week pattern in Pb10 concentration is due to the fact that, unlike PM10, the source of lead in the atmosphere is mostly anthropogenic. Therefore, the atmospheric concentration is strongly associated with the work schedule of lead processing industries.

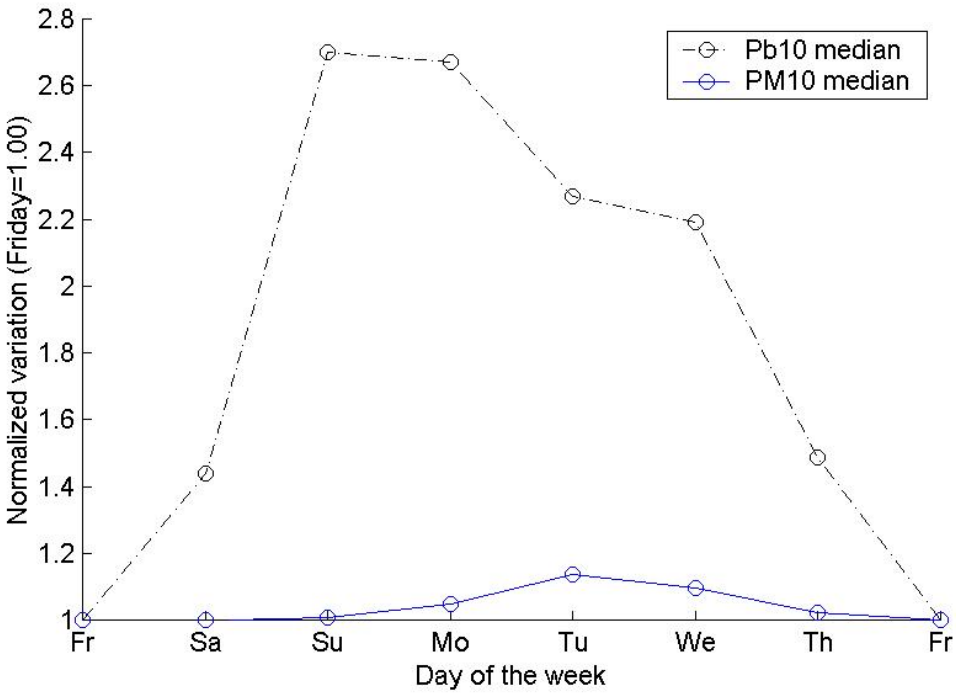

Figure 5-19: Median Lead & PM10 Concentrations over Days of the Week

5.3.2 Spatial Characteristics

Typical Lead Concentration Profile Maps for Selected Days

Maps showing the spatial distribution of lead in Greater Cairo were produced for each measuring days of the baseline year (60 maps in total). Three of these maps, shown in Figures 5-20 though 5-22, were selected to illustrate the typical features of the lead distribution in Cairo. The maps show estimated lead concentrations on 7 October 1998 (Figure 5-20), 13 October 1998 (Figure 5-21), and 29 January 1999 (Figure 5-22). The first two dates of October 7 and October 13 correspond to days when lead concentrations was relatively high. Estimated lead concentrations are generally much lower for 29 January 1999. The color scale used to represent the Lead concentration starts at 0 μg/m³ and is truncated at 5 μg/m³ in order to provide the same scale for each map. Note that the maximum concentration level reached for the two high days is greater than the 5-μg/m³ limit of the color range. The estimated maximum concentration of Lead is 79.2 μg/m³ on 7 October 1998 and is 22.8 μg/m³ on 13 October 1998; both occur in Shoubra.

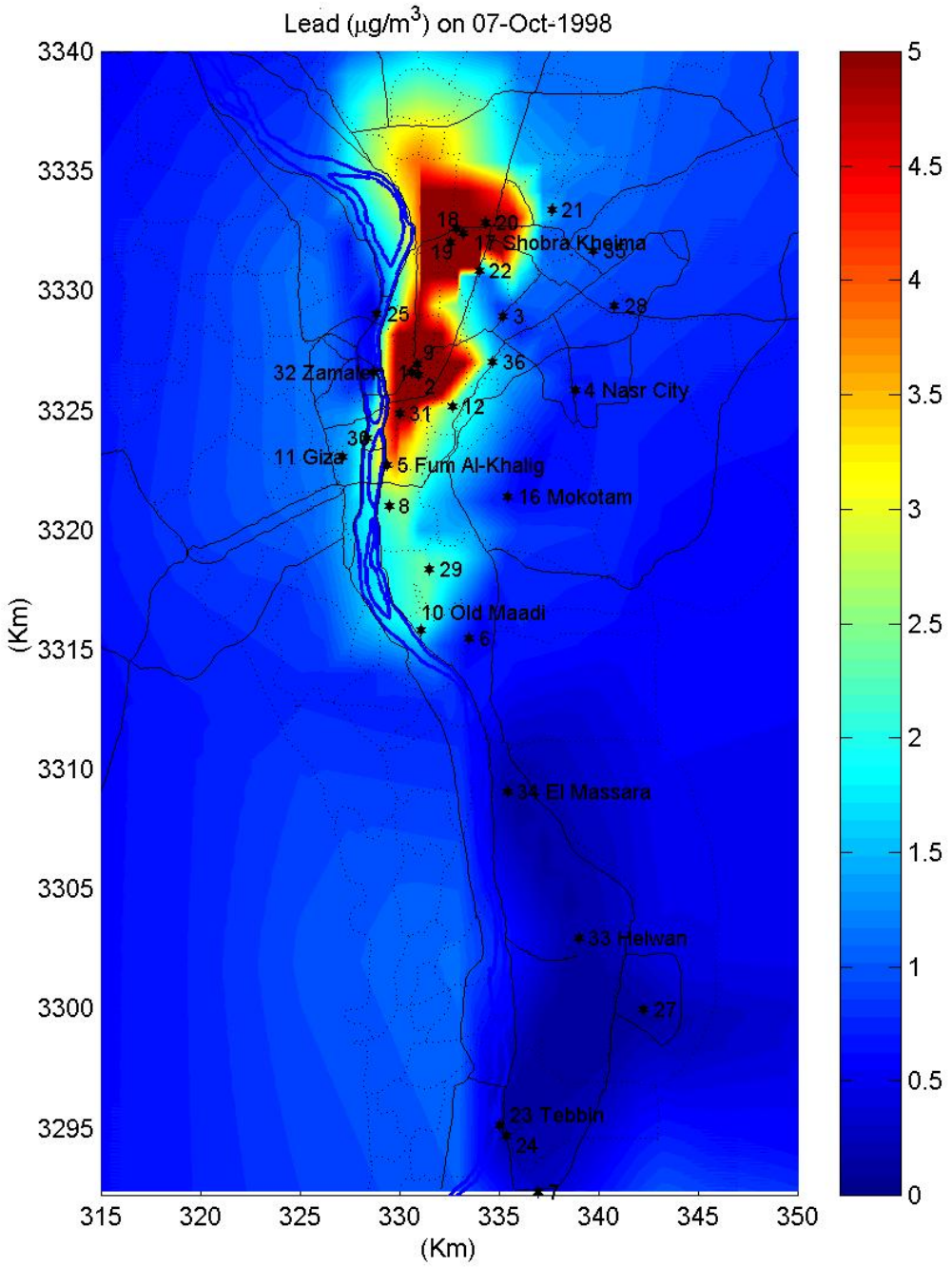

Figure 5-20: Estimated Pb10 Concentrations on 7 October 1998 (Color Scale Indicates Lead Concentration in μg/m³)

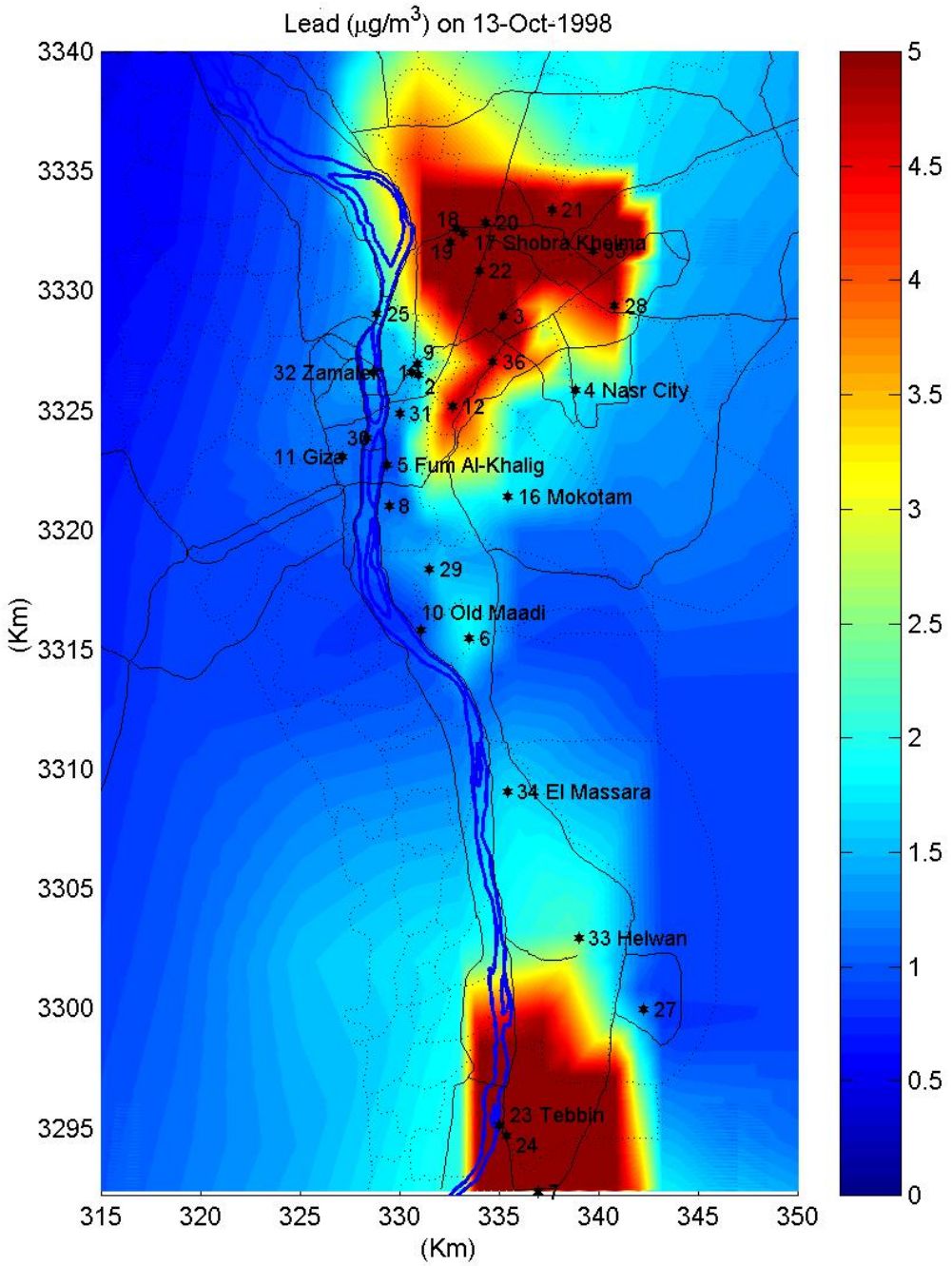

Figure 5-21: Estimated Pb10 Concentrations for 13 October 1998 (Color Scale Indicates Lead Concentration in μg/m³)

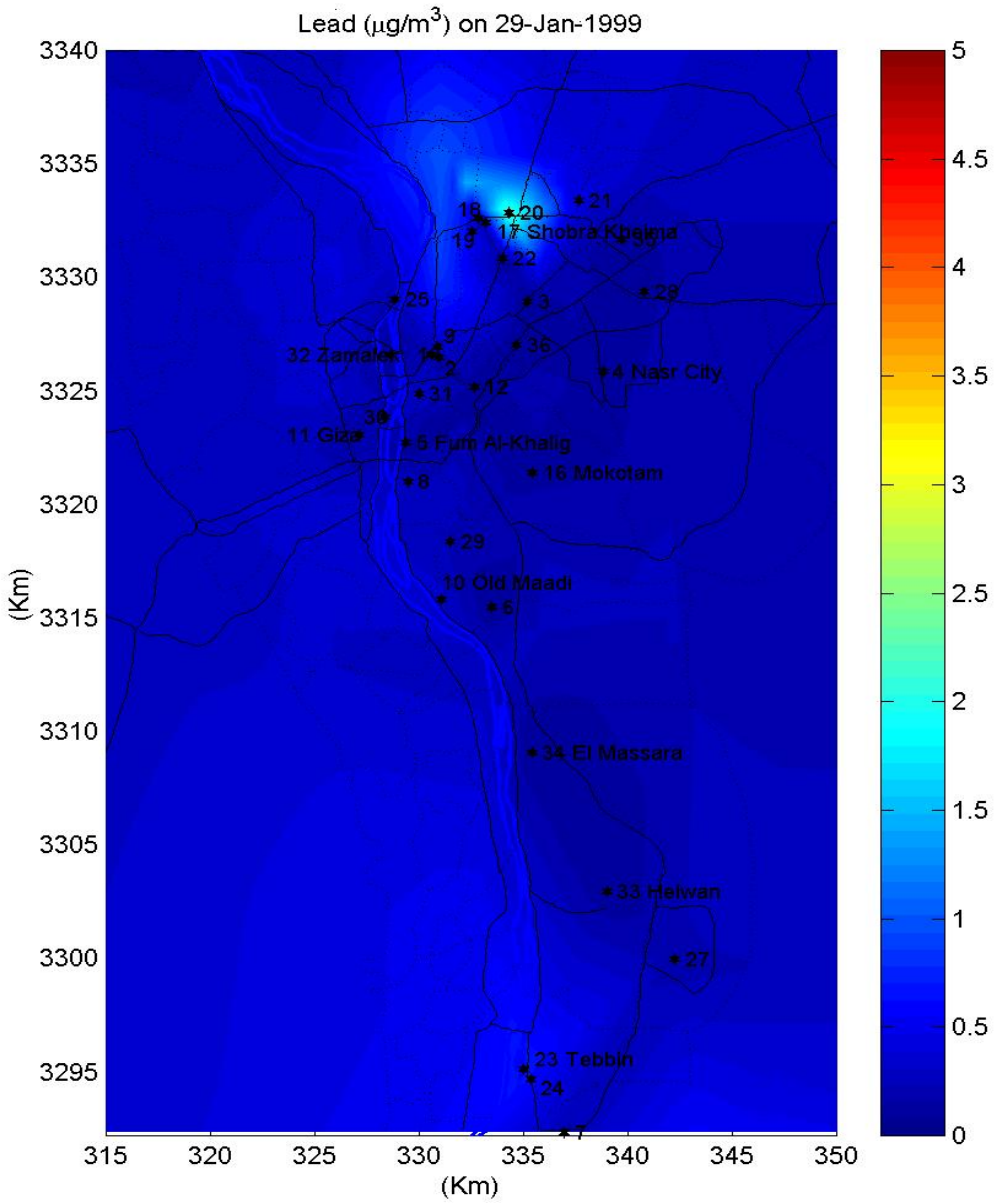

Figure 5-22: Estimated Pb10 Concentrations on 29 January 1999 (Color Scale Indicates Lead Concentration in μg/m³)

In contrast to PM10, the spatial distribution of lead indicated on the maps is characterized by a short-range distribution profile, as was predicted form the covariance analysis. The short-range profiles are due to the fact that the lead is emitted from point sources, primarily secondary lead smelters. On 13 October 1998, the day of the second highest lead concentrations for the baseline year (see Figure 5-17), the areas subjected to high lead levels are localized in two pockets of about 10–15 km in size. These two pockets encompass the highly industrialized areas of Shoubra El-Kheima and Tebbin.

As a result of the large temporal variability of the lead concentration and the short-range profiles in the spatial distribution, the maximum concentration value reached on a given day may be extremely high in one locality, while other areas of the city are exposed to relatively low lead levels. An example of this situation can be seen on the 7 October 1998 map, where most of the Greater Cairo area is exposed to relatively small lead concentration (less than 0.75 $\mu g/m^3$), while the maximum for that day is extremely high, with an estimated value of 79.2 $\mu g/m^3$. Finally, the lead distribution is also characterized by days with low lead levels throughout the city, as seen in the 29 January 1999 map (Figure 5-22). Since 29 January 1999 was a Friday, the low lead levels are most probably correlated with a suspension in the operations at lead processing industries.

As explained earlier, the map of estimated lead concentration depicts the most probable lead distribution given the measurements available for that day. However, one should be aware of the estimation error corresponding to each of these maps. The map of the width of the 68% confidence interval (corresponding approximately to twice the standard deviation of estimation error) offers a good assessment of the mapping accuracy. Such a map is shown in Figure 5-23 for lead on 7 October 1998. As expected, it may be noted from this figure that the estimation error for lead is lower closer to the monitoring sites, and increases gradually with increasing distance from the monitoring stations. The estimation error is also similar for all measurement days. The estimation errors shown in Figure 5-20 should be kept in mind when using any of the estimated lead concentration maps such as the one shown in Figures 5-20 through 5-22.

Annual Average Lead Levels and Law No. 4/1994 Non-Attainment Areas

By taking the arithmetic average of the daily lead concentrations at each estimation point, it is possible to construct a map of the annual lead average concentration over Greater Cairo. A map constructed in this manner is shown in Figure 5-24. The color scale for this map starts at 0 $\mu g/m^3$ and is truncated at 3 $\mu g/m^3$ in order to capture the spatial distribution of concentrations with values close to the annual lead standard of 1 $\mu g/m^3$.

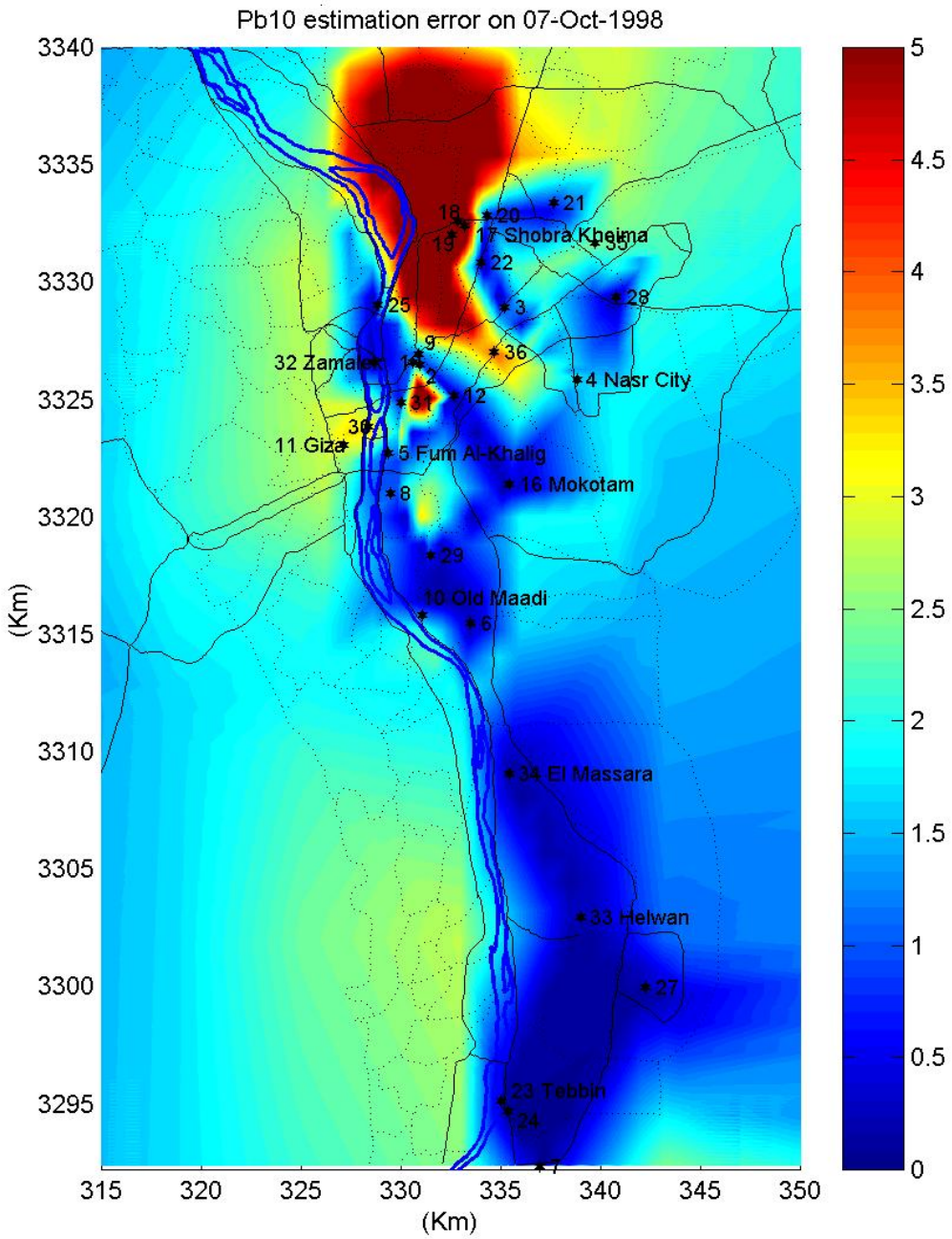

Figure 5-23: Map of the 68% Confidence Interval for Lead Concentrations on 13 October 1998

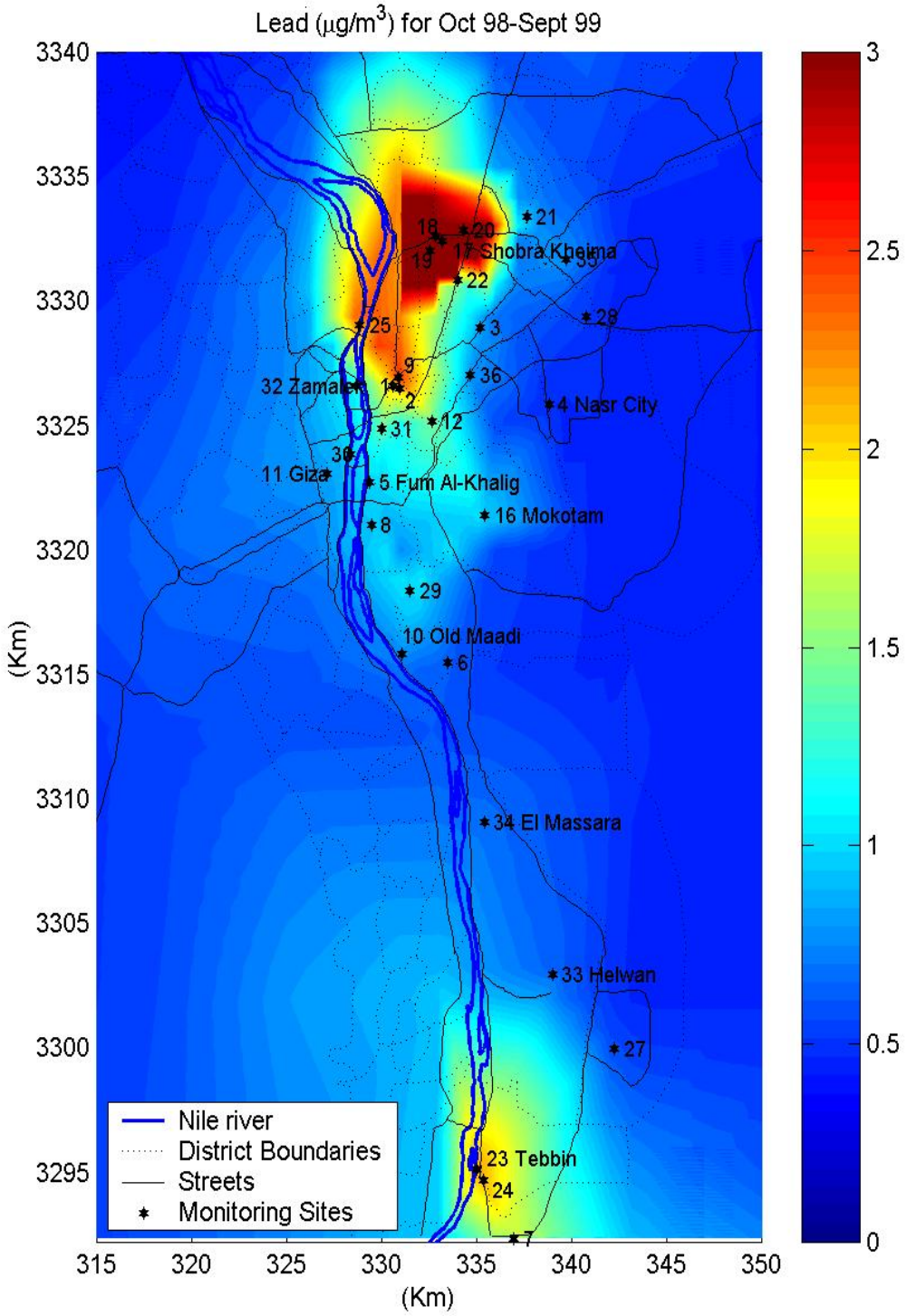

Figure 5-24: Estimated Average Lead Concentrations for Baseline Year (Color Scale Indicates Lead Concentration in μg/m³)

Although the value for the color scale is truncated at 3 μg/m³, it should be noted that, in the vicinity of monitoring Sites #18 and #19 (located in Shoubra), the annual lead concentration reaches values that are much greater than 3 μg/m³. The highest annual average Pb10 concentration recorded at CAIP monitoring network sites (26.2 μg/m³) was observed at Site #18 in Shoubra El-Kheima.

The map in Figure 5-25 provides an estimate, at the 50% confidence level, of the Law 4/1994 lead standard non-attainment areas. It is estimated that in these areas, shown in red on the map, the annual average lead concentration exceeded 1 μg/m³ during the baseline year. It is estimated that, at the 50% confidence level, annual average lead concentration was below the Law 4/1994 limit of 1 μg/m³ in the white areas of the map. The Law 4/1994 limit for lead is exceeded in two large areas about 10–15 kilometers in diameter. One of the areas encompasses Shoubra El-Kheima, where several lead smelters are located, and the other encompasses Tebbin, also the site of lead smelters. There are also some small areas in Basateen and Old Cairo where it is estimated that the Law 4/1994 limit was exceeded.

Population Exposure to Lead

Using a GIS platform, the areas exceeding the Law 4/1994 annual ambient lead limit (shown in Figure 5-25) were layered over a map of Cairo containing the boundaries of the Central Agency for Planning, Mobilization, and Statistics (CAPMAS) Districts. The percentage of each district that was in the non-attainment zone was determined by dividing the affected area of the district (determined with the GIS) by the total area of the district (determined either with the GIS or from CAPMAS data when available). The affected population in each district was determined by multiplying the affected area of the district by the CAPMAS 1996 population data for that district. Implicit in this calculation is the assumption that the population is uniformly distributed within the districts.

The estimation of the population exposed to a lead level above the Law 4/1994 limit is summarized in Table 5-3. The total population of Greater Cairo estimated to be exposed to a lead concentration exceeding the Law 4/1994 limit is nearly 4 million residents. The affected area shown in the table is the area of the district that is in the Law 4/1994 non-attainment zone. The affected population shown in Table 5-3 is the estimated number of people that reside in the Law 4/1994 non-attainment zone. The areal data for some districts is insufficient to estimate the exposed population.

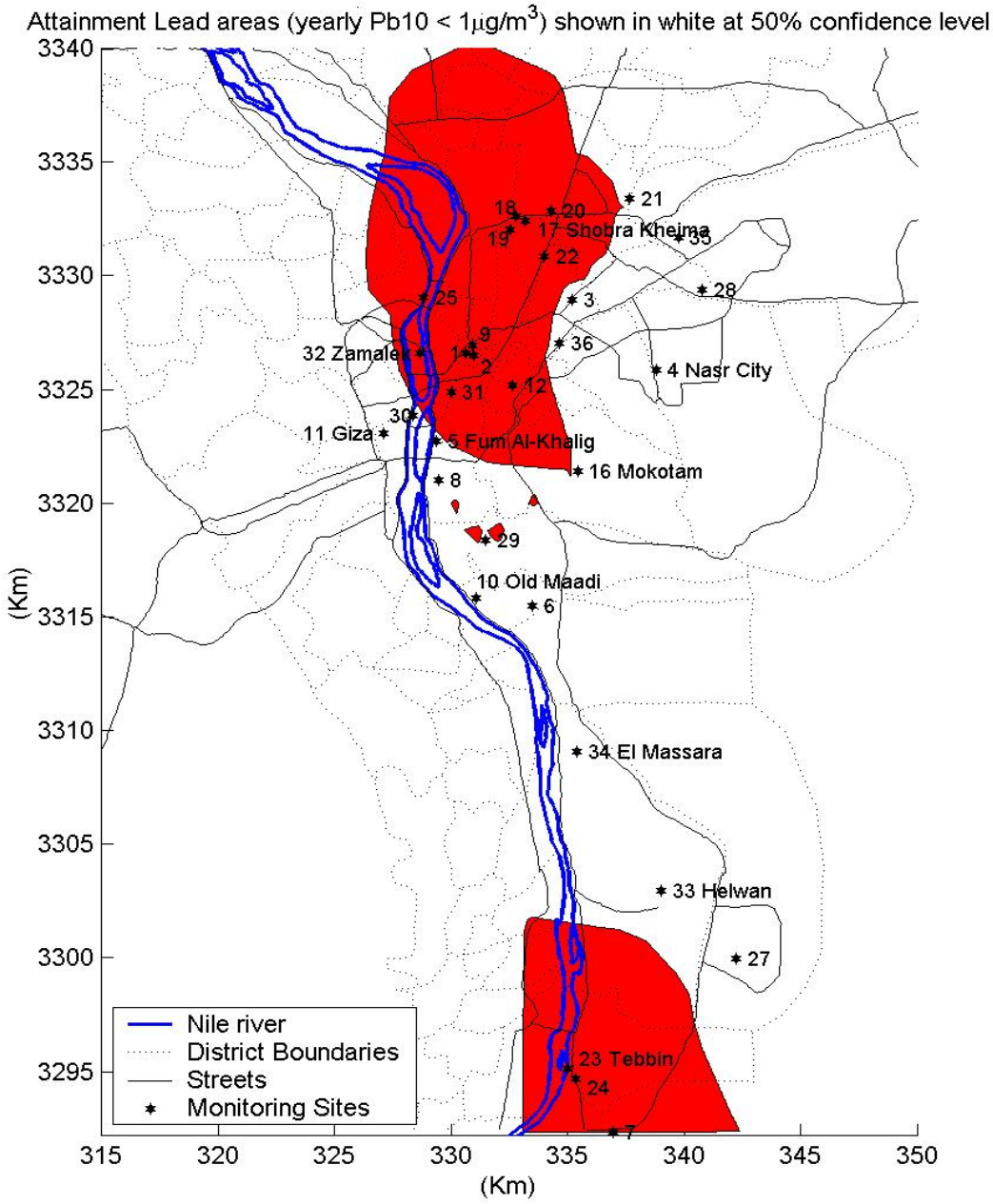

Figure 5-25: Estimated Law 4/1994 Lead Limit Non-attainment Areas (shown in red)

Table 5-3: Lead Exposure Estimation

Governorate	CAPMAS District	CAPMAS Population (a)	District Area, km² (b)	Affected Area		Affected Population
				km²	Percent	
Cairo	Tebbin	59352	24.64	18.44	74.9	44431
	Helwan					(c)
	Old Cairo	225256	10.10	0.74	7.3	16487
	El-Sayeda Zeinab	155558	4.02	3.83	95.3	148323
	Khalifa/Mokattam	186080	38.66	7.49	19.4	36067
	Abdeen	48792	1.60	1.47	92.0	44897
	Moski	28633	0.87	0.87	100.0	28633
	Bab El-Sheiriya	59687	0.95	0.95	100.0	59687
	Shoubra	83084	1.63	1.63	100.0	83084
	Rod El-Farag	178072	2.79	2.79	100.0	178072
	Zeitoon	322566	7.29	2.97	40.8	131495
	Hadayek El-Kobba	308274	4.62	3.61	78.2	240928
	El-Sahel	333198	6.50	6.50	100.0	333198
	El-Matariya	498434	5.99	2.63	43.9	218869
	El-Zawya El-Hamra	306983	4.83	4.83	100.0	306983
	Menshaat Nasser	169099	5.41	1.87	34.5	58399
	Basateen/Dar El-Salam	658877	30.85	0.65	2.1	13903
	El-Sharabia	246564	4.14	4.14	100.0	246564
	El-Wayli	89388	4.65	0.57	12.3	11018
	El-Darb El-Ahmar	78284	2.80	2.80	100.0	78284
	El-Gamaliya	58839	2.08	2.03	97.7	57501
	El-Dhaher	65062	2.02	1.68	83.1	54083
	Qasr El-Nil	12925	6.00	6.00	100.0	12925
	Boulaq	74631	2.70	2.70	100.0	74631
	El-Azbakeya	30427	1.70	1.70	100.0	30427
	Zamalek	15498	2.52	2.52	100.0	15498
Giza	El-Agouza	175131	12.66	1.20	9.5	16653
	El-Dokki	88519	4.75	0.23	4.9	4369
	El-Warrak	393992	22.46	6.18	27.5	108431
	Imbaba	523298	8.45	6.27	74.2	388204
	Abo Ragwan El-Bahary					(c)
	Abo Ragwan El-Qebly					(c)
	El-Shobak El-Gharby					(c)
Qalioubiya	Shoubra El Kheima 1	416526	19.25	19.13	99.4	413929
	Shoubra El Kheima 2	454190	19.26	13.41	69.6	316299
	Qalioub	362054	33.49	16.62	49.6	179642
	Totals	6707264	300	148		3951914

(a) Population data for 1996
(b) Determined either from CAPMAS data or GIS measurement
(c) Part of the district is in the lead limit non-attainment area, but there is not sufficient data to estimate affected population.

Chapter Six
Conclusions

6.1 Particulate Matter

- Particulate matter levels in the Greater Cairo area are characterized by long-range spatial and long-term temporal distributions, which are probably created by meteorological conditions.
- The PM concentrations during the baseline year were found to be consistently high throughout the Greater Cairo area. The consistently high level of PM is attributed to a combination of: (1) a high background from natural areal-type sources, (2) emissions from mobile and fixed sources, and (3) the large spatial scale of generation and spreading of particulate matter.
- It is believed that one of the components of PM in Cairo is the re-suspension of soil, sand, and dust from buildings, vegetation, etc. by the winds. The arid climate in Cairo is a significant factor in producing this "background" PM level. The "background" contribution to the PM levels varies temporally and spatially and is probably governed by wind conditions. This "background" PM component is nearly always at a level that precludes complying with the current Law 4/1994, 24-hour limit of 70 $\mu g/m^3$. This "background" PM component must be considered when evaluating the efficacy of PM mitigation measures.
- The PM data shows a seasonal trend. The highest PM levels during the baseline year occurred during the October–December period and the lowest PM levels occurred during June and July. PM levels exhibit a mild day-of-the-week trend, with lower PM levels on Fridays and Saturdays than the PM levels during workdays (Sundays through Thursdays).
- The fairly constant PM2.5/PM10 ratio at all sites and throughout the year indicates a strong, persistent source of particulate matter in the 2.5–10 μm size range. For example, nearly all the mass of PM emitted by mobile sources is in the PM2.5 size range. However, the PM2.5/PM10 ratios obtained at

sites in heavily trafficked areas, e.g. El-Qolaly Square and Gomhuriya Street, are essentially the same as ratios measured at all the other sites.

6.2 Lead

- The distribution of lead is characterized by relatively small-scale spatial and temporal structures. The scale indicates that lead enters the atmosphere primarily from anthropogenic point sources and that the major impact of the lead emissions is in the locality of the source.
- The recorded annual average of ambient lead concentration was highest in Shoubra El-Kheima, where several lead smelters are located. The highest annual average lead concentration in Cairo (26.2 mg/m^3) was recorded at Site #18 in Shoubra El-Kheima.
- The annual average lead concentration exceeded the Law 4/1994 limit of 1 mg/m^3 at 15 of the 34 CAIP ambient monitoring stations. The BME analysis permits delineation of the non-attainment areas, i.e. where the annual average lead concentration exceeded 1 mg/m^3. The major areas of non-attainment are centered in Shoubra El-Kheima in the North, and in Tebbin in the South. The sizes of the non-attainment areas are approximately 150 km^2 in Shoubra El-Kheima, and 80 km^2 in Tebbin.
- Using the non-attainment area data developed from the BME analysis, it is estimated that nearly 4 million Cairo residents may be exposed to lead levels exceeding the Law No. 4/1994 limit.
- A seasonal trend in lead concentrations is not evident for the baseline year data. However, a very distinct day-of-the-week trend was found. The median ambient lead concentration increased by a factor of 2.7 from Friday to mid-week. The observed day-of-the-week trend supports the contention that lead in the atmosphere comes from anthropogenic sources.

6.3 Quality of Data

- An intensive quality control (QC) effort was incorporated into CAIP's PM and lead monitoring program. The QC effort ensures that high quality monitoring data are collected, and provides an assessment of the accuracy and precision of the monitoring data.
- Data quality is important in all monitoring data applications. Poor data quality may lead to erroneous policy or regulatory decisions and may render

the data unusable for any trends' assessment. Consequently, it is recommended that the strong QC program initiated during the baseline year be maintained as part of the future PM and lead monitoring effort.

6.4 Space/Time Mapping using the BME Estimation Method

- The Bayesian Maximum Entropy (BME) is a powerful analysis method that enabled a comprehensive analysis of air quality data. The features of the BME method that are particularly useful for the mapping analysis of air quality data in Cairo are (1) the rigorous incorporation of both hard and soft data, (2) the space/time framework, and (3) the ability to incorporate physical-laws governing air transport.
- It is recommended that the BME method be used for future air quality and health analysis. The BME code is open and the authors are encouraging its use. Since a large part of the BME air quality analysis is available through this baseline year study, any additional analysis could fully take advantage of the work already completed and, therefore, would require a minimal incremental effort.
- Some of the direct extensions of the current BME-method analysis are: (1) incorporation of data from other monitoring stations, (2) incorporation of meteorological data, (3) health risk analysis, and (4) optimization of the current CAIP monitoring network.

6.5 PM and Lead Monitoring Network Optimization

- For the baseline year study, it was desirable to have a large monitoring network with numerous sites in order to study the spatial variability of PM and lead. Having obtained the spatial variability data for PM and lead during the baseline year, it is now possible to optimize the monitoring network for sustained operation. The optimization can be achieved in a manner that will reduce operating costs without compromising on the collection of essential data or on the usefulness of the monitoring data for policy and regulatory decisions and for trends analysis.
- The BME method provides an ideal platform to optimize the CAIP monitoring network. Using this method, it is possible to perform a sensitivity analysis to identify the number and location of sites required to adequately predict spatial trends. Optimization of the network using this approach

would maintain air pollution mapping accuracy, at the same time reducing the cost of the monitoring program.

References

1. Nasralla, M.M., 1994. Air Pollution in Greater Cairo. Proceeding of the Italian–Egyptian Study: Days on the Environment, Cairo, Egypt, October 9–20, 1994.
2. Rodes, C.E., M.M. Nasralla, and P.A. Lawless, 1996. An Assessment and Source Apportionment of Airborne Particulate Matter in Cairo, Egypt. Activity Report No. 22 prepared for the USAID Mission to Egypt under EHP activity No. 133-RCm delivery order No. 7.
3. Environmental Data Report, Third Edition, United Nations Environmental Programme, 1991/1992.
4. WHO and UNEP, Urban Air Pollution in Megacities of the World, Blackwell, Oxford, 1992.
5. Chappell, F., P. Billig, E. P. Brantly, S. Ault, and H. S. Ezzeldin. 1997. "Activity Report No. 32 - Lead Exposure Abatement Plan for Egypt, Results of Environmental Sampling for Lead," prepared for the USAID Egypt Mission under the Environmental Health Project (EHP) Activity No. 256-CC, Cairo, August 1997.
6. Environmental Studies Department, Institute of Graduate Studies and Research, University of Alexandria. "A Comparative Study on the Contribution of Lead Emission from Motor Vehicles to Atmospheric Pollution: A Consultancy Study for the Egyptian Ministry of Petroleum," Alexandria, April 1996.
7. Sessions, S. M. Gaffen, S. Moore, R. Efroymson, F. El-Gohary, M. Nasralla, A. El-Gamal, and A. Abdel Gawaad, 1994. "Comparing Environmental Health Risks in Cairo, Egypt," Volume 1: Final Report, prepared for USAID/NE/DR/ENR by Chemonics International and its Associates, Cairo, September 1994.
8. Christakos, G., and V. M. Vyas, 1998. A composite spatiotemporal study of ozone distribution over eastern United States, *Atmospheric Environment*, 32 (16), 2845-2857.

9. Christakos, G., and M. L. Serre, 1999b. Space/Time Analysis of PM10 in North Carolina, *Reviews in Geophysics*, in review.

10. Christakos, G., and M. L. Serre, 1999a. A Spatiotemporal Analysis of Environmental Exposure-Health Effect Associations. *Journal of Exposure Analysis and Environmental Epidemiology*, in press.

11. Choi, K., G. Christakos, and M. L. Serre, 1998. "Recent Developments in Vectorial and Multi-Point BME Analysis". *Proceedings of Fourth Annual Conference of the International Association for Mathematical Geology*, Ischia Island, Italy.

12. Bogaert, P., M. L. Serre, and G. Christakos, 1999. "Efficient Computational BME Analysis of non-Gaussian Data in Terms of Transformation Functions". *Proceedings of Fifth Annual Conference of the International Association for Mathematical Geology* , Norway.

13. Serre, M. L., P. Bogaert, and G. Christakos, 1998. "Latest Computational Results in Spatiotemporal Prediction Using the Bayesian Maximum Entropy Method". *Proceedings of Fourth Annual Conference of the International Association for Mathematical Geology*, Ischia Island, Italy.

14. Serre, M. L, 1999a. Mapping Atmospheric Pollutants and Analyzing Their Health Effect in the Face of Uncertain Information: A Relevant Framework for Developing Countries. *ESEnotes*, University of North Carolina at Chapel Hill, July.

15. Serre, M. L., 1999b. Modeling Particulate Matter Using Uncertain Measurements: Case Study of PM10 in North Carolina. *Computational Science Graduate Fellowship Conference*, July 15-17, Poster Presentation.

16. Serre, M. L., and G. Christakos, 1999a. Modern Geostatistics: Computational BME Analysis in the Light of Uncertain Physical Knowledge— the Equus Beds study. *Journal of Stochastic Environmental Research and Risk Analysis*, 13 (1), 1-26.

17. Christakos, G, D. Hristopulos, and M. L. Serre, 1999. "BME Studies of Stochastic Differential Equations Representing Physical Laws —Part I", *Proceedings of Fifth Annual Conference of the International Association for Mathematical Geology* , Norway.

18. Serre, M. L. and Christakos, 1999b. "BME Studies of Stochastic Differential Equations Representing Physical Laws - Part II". *Proceedings of Fifth Annual Conference of the International Association for Mathematical Geology*, Norway.

19. Howes Jr., J.E., N. Samaha, M. Labib, M. Sabry, and H. El-Araby, 1999. "Ambient PM2.5, PM10, and Lead Measurements in Cairo, Egypt". *Conference Proceedings*, Alexandria, Egypt.